AD

AMMRC TR 79-11

BRITTLE MATERIALS DESIGN, HIGH TEMPERATURE GAS TURBINE

CERAMIC TURBINE ROTOR TECHNOLOGY

13TH INTERIM REPORT FOR THE
PERIOD OCTOBER 1977 — MARCH 1978

Arthur F. McLean, Robert R. Baker

Date Published — February, 1979

Prepared for
ARMY MATERIALS AND MECHANICS RESEARCH CENTER
Watertown, Massachusetts 02172

Contract Number DAAG-46-71C-0162
Agency Accession Number DA-OD 4733

FORD MOTOR COMPANY
ENGINEERING AND RESEARCH STAFF
DEARBORN, MICHIGAN 48121

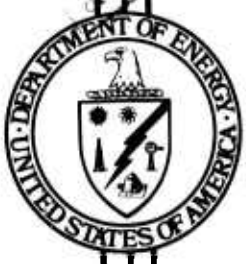

U. S. DEPARTMENT OF ENERGY

Division of Transportation Energy Conservation

The findings in this report are not to be construed as an official Department of the Army, or U.S. Government position, either expressed or implied, unless so designated by other authorized documents.

Mention of any trade names or manufacturers in this report shall not be construed as advertising nor as an official indorsement or approval of such products or companies by the United States Government.

DISPOSITION INSTRUCTIONS

Destroy this report when it is no longer needed.
Do not return it to the originator.

Printed in the United States of America

Available from

National Technical Information Service
U.S. Department of Commerce
5285 Port Royal Road
Springfield, Virginia 22161

Price: Printed Copy $6.50
Microfiche $3.00

DISCLAIMER NOTICE

THIS DOCUMENT IS THE BEST QUALITY AVAILABLE.

COPY FURNISHED CONTAINED A SIGNIFICANT NUMBER OF PAGES WHICH DO NOT REPRODUCE LEGIBLY.

UNCLASSIFIED

SECURITY CLASSIFICATION OF THIS PAGE (When Data Entered)

REPORT DOCUMENTATION PAGE

READ INSTRUCTIONS BEFORE COMPLETING FORM

(13) 1. REPORT NUMBER: AMMRC TR79-11

(19) 2. GOVT ACCESSION NO.: TR-79-11

3. RECIPIENT'S CATALOG NUMBER:

4. TITLE (and Subtitle):

(6) Brittle Materials Design, High Temperature Gas Turbine. Ceramic Turbine Rotor Technology

5. TYPE OF REPORT & PERIOD COVERED: Interim Report Number 13, 10-1-77 to 3-31-78

6. PERFORMING ORG. REPORT NUMBER: DAAG 46-71-C-0162

7. AUTHOR(s):

A. F. McLean, Ford Motor Company
R. R. Baker, Ford Motor Company

8. CONTRACT OR GRANT NUMBER(s):

9. PERFORMING ORGANIZATION NAME AND ADDRESS:

Ford Motor Company, Dearborn MI 48121

10. PROGRAM ELEMENT, PROJECT, TASK AREA & WORK UNIT NUMBERS: D/A Project: ARPA Order 1849, AMCMS Code: Agency Accession: DA OD4733

11. CONTROLLING OFFICE NAME AND ADDRESS:

Army Materials and Mechanics Research Center
Watertown, Massachusetts 02172

(1) 12. REPORT DATE: February, 1979

13. NUMBER OF PAGES: 94

14. MONITORING AGENCY NAME & ADDRESS (if different from Controlling Office):

(12) 86 p.

15. SECURITY CLASS. (of this report): Unclassified

15a. DECLASSIFICATION/DOWNGRADING SCHEDULE:

16. DISTRIBUTION STATEMENT (of this Report):

(9) Interim rept. no. 13. 1 Oct 77-31 Mar 78.

Approved for public release; distribution unlimited.

17. DISTRIBUTION STATEMENT (of the abstract entered in Block 20, if different from Report)

(10) Arthur F./McLean Robert R./Baker

18. SUPPLEMENTARY NOTES

(15) DAAG 46-71-C-0162, ARPA Order-1849

19. KEY WORDS (Continue on reverse side if necessary and identify by block number)

Gas Turbine Engine	Silicon Nitride
Brittle Design	Silicon Carbide
Ceramics	Non-Destructive Test
High Temperature Materials	Mechanical Properties

20. ABSTRACT (Continue on reverse side if necessary and identify by block number)

(See reverse side)

DD FORM 1 JAN 73 1473 EDITION OF 1 NOV 65 IS OBSOLETE

UNCLASSIFIED

SECURITY CLASSIFICATION OF THIS PAGE (When Data Entered)

141 250

ABSTRACT

This report contains progress during the last six months and a summary of earlier progress on the DOE supported programs within the joint DARPA/DOE "Brittle Materials Design, High Temperature Gas Turbine" Program and constitutes the final report of work under DOE funds. A separate report will cover the progress on the DARPA supported Ceramic Turbine Testing Program.

The summary of previous work supported by DOE includes progress on reaction bonded and hot pressed silicon nitride materials technology. Several NDE techniques were considered for the detection of flaws in complex-shaped silicon nitride components. Improvements to the hot press bonding process resulted in a significant improvement in the yield of flaw-free hot press bonded rotors. M.O.R. and cold spin tests of rotor blade rings revealed the presence of undetected subsurface flaws in both the blades and the rim. Blade bend testing indicated that blade strength degraded during hot press bonding.

During this reporting period, an investigation of hot press bonding temperatures and time at temperature defined a region of zero microstructural and strength degradation. This study involved 19 hot press bondings from which curves were generated defining the changes in color, porosity, hardness, phase and strength as a function of time and temperature.

Improvements in injection molding of rotor blade rings were made utilizing an adaptive process control unit which controlled and monitored the injection velocity and die cavity pressure during the injection and hold portions of the molding cycle. Five parametric studies were conducted with systematically varied injection profiles and hold pressures. Microfocus X-ray results indicated that high injection flow rates combined with low holding pressures in the die cavity reduced the number of subsurface void-type blade flaws.

The detection of planar flaws in both green as-molded and nitrided blade rings revealed that this type flaw was only detectable after nitriding, indicating that it may only occur after burn out and/or nitriding. Void-type flaws were detected in the rim of blade rings using a panoramic microfocus X-ray technique.

Approximately 30 experiments were conducted utilizing glass and/or metals as isostatic hot pressing media. A grafoil seal system was developed which contained the molten pressurized glasses. Decomposition of the glass was minimized with vycor utilizing boron nitride as a barrier material. A sliding seal for molten metals employed a grafoil-glass hybrid system; however, the metals were extruded through the porosity of the graphite.

A reliability analysis was conducted for individual loading conditions and the cumulative reliability estimated for Rotor #1195 which was previously engine tested. The cumulative time-dependent reliability for the 36.5 hour run was 0.838. Reliability estimates were also made for 0.40 and 0.48 inch thick throat rotors operating in the hot spin rig at a rim temperature of 1800°F at 50,000 rpm.

An assessment of where the technologies addressed in this report now stand and recommendations for follow on work are presented.

FOREWORD

This report is the thirteenth technical report of the "Brittle Materials Design, High Temperature Gas Turbine" program initiated by the Defense Advanced Projects Agency, DARPA Order Number 1849, (Contract Number DAAG-46-71-C-0162).

In fiscal year 1977, the Energy Research and Development Administration (ERDA), now Department of Energy (DOE), joined with DARPA to support this project and this constitutes the final report of the DOE funded work.

This report is also the final report on materials development in the iterative design and materials development portion of the DOE funded portion of the Brittle Materials Design Program, as such it represents the state of the art in materials processing developed as of the end of the program. However, this does not Imply that further processes improvements are not desirable.

The ERDA Division of Transportation (TEC), started to support process development to improve the quality of duo-density silicon nitride turbine rotors, and ERDA's Division of Conservation Research and Technology (CONRT), supported some of the work on non-destructive evaluation of ceramics and ceramic materials characterization. DOE has delegated project management responsibility to the NASA Lewis Research Center for the TEC Heat Engine Highway Vehicle Systems Program. This includes work under the TEC/AMMRC Heat Engine Systems Materials and Components Technology Program. The Army Materials and Mechanics Research Center continued to function as the technical monitor of the overall program.

The principal investigator of this program is Mr. A. F. McLean, Ford Motor Company, and the technical monitor is Dr. E. S. Wright, AMMRC. The authors would like to acknowledge the valuable contributions in the performance of this work by the following people.

Ford Motor Company

N. Arnon, R. J. Baer, J. H. Buechel, D. J. Cassidy, J. C. Caverly, G. C. DeBell, R. C. Elder, A. Ezis, E. A. Fisher, R. K. Govilla, M. N. Gross, D. L. Hartsock, P. H. Havstad, J. A. Herman, R. A. Jeryan, C. F. Johnson, J. A. Mangels, W. E. Meyer, J. T. Neil, A. Paluszny, G. Pelisch, J. R.. Secord, L. R. Swank, W. Trela, T. J. Whalen, R. M. Williams, W. Wu

Army Material and Mechanics Research Center

G. E. Gazza, R. N. Katz, E. M. Lenoe, D. R. Messier, H. Priest

DOE-TEC Project Officer — R. B. Schulz

DOE-CONRT Project Officer — J. Neal

DOE-NASA Lewis Project Officer — C. P. Blankenship

TABLE OF CONTENTS

TABLE OF CONTENTS

LIST OF FIGURES

LIST OF FIGURES

LIST OF FIGURES

LIST OF TABLES

1.0 INTRODUCTION

In July, 1971, the Defense Advanced Research Projects Agency of the Department of Defense jointly sponsored a program with Ford Motor Company to develop and encourage the use of brittle materials for engineering applications. The major program goal of the "Brittle Materials Design — High Temperature Gas Turbine" program was to prove by a practical demonstration that efforts in ceramic design, materials, fabrication, testing and evaluation could be drawn together and developed to establish the usefulness of brittle materials in demanding high temperature structural applications.

The replacement of high cost nickel-chrome superalloys in gas turbines with low cost, higher temperature capability ceramics offers significant advances in efficiency, materials utilization and power per unit weight. The vehicular turbine project was organized to design and develop an entire ceramic hot flow path for a high temperature (2500°F) vehicular gas turbine engine (Figure 1.1).

The progress of the gas turbine engine has been and continues to be closely related to the development of materials capable of withstanding the engine's environment at high operating temperature. Since the early days of the jet engine, new metals have been developed which allowed a gradual increase in operating temperatures. Today's nickel-chrome superalloys are in use, without cooling, at turbine inlet gas temperatures of 1800°F. However, there is considerable incentive to further increase turbine inlet temperature in order to improve specific air and fuel consumptions. The use of ceramics in the gas turbine engine promises to make a major step in increasing turbine inlet temperature to 2500°F. Such an engine offers significant advances in efficiency, power per unit weight, cost, exhaust emissions, materials utilization and fuel utilization. Successful application of ceramics to the gas turbine would therefore not only have military significance, but would also greatly influence our national concerns of air pollution, utilization of material resources, and the energy crisis.

Therefore the goals of this program were considered to be congruent with the goals of the emerging ERDA (now DOE) Highway Vehicle Systems Program. It was also apparent that ceramic component processing developments and life prediction methodologies being developed under the DARPA program would be directly transferable to future ERDA (DOE) programs in the heat engine area. Accordingly in FY77, ERDA joined with DARPA to support the program and to carry the materials development portions of the program. The ERDA Division of Transportation, working closely with NASA-Lewis, started to support process development to improve the quality of duo-density silicon nitride

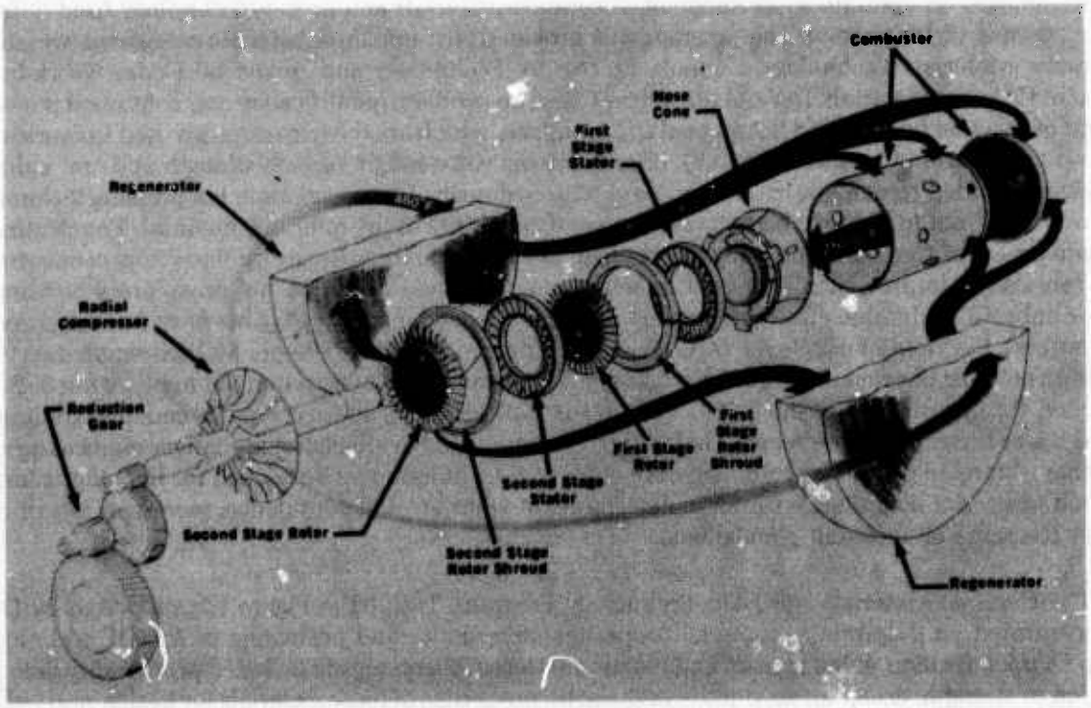

Figure 1.1 Schematic View of the Vehicular Gas Turbine Engine Flowpath

turbine rotors, and ERDA's Division of Convservation Research and Technology supported some of the work on non-destructive evaluation of ceramics and ceramic materials characterization (Figure 1.2). The Army Materials and Mechanics Research Center continued to function as the technical monitor of the overall program.

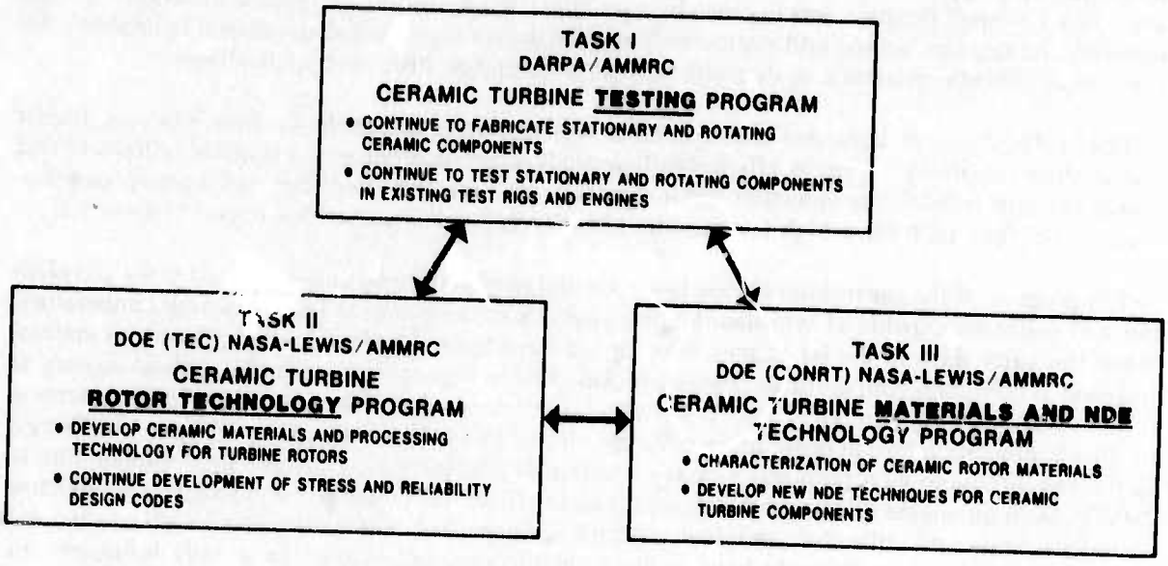

Figure 1.2 DARPA/DOE Supported Tasks in the "Brittle Materials Design, High Temperature Gas Turbine" Program

The DARPA portion of the fiscal year 1978 program, Task I in Figure 1.2, was specifically oriented toward the evaluation of the reliability of state-of-the-art ceramic components which were developed over the previous five and one half years. The progress made on the DARPA Ceramic Turbine Testing Program will be reported in a separate document.

The Turbine Rotor Technology Program, of fiscal year 1978, Task II in Figure 1.2, supported by DOE, focused on continued development of ceramic materials and process technology used to fabricate ceramic turbine rotors. The program was broken down into three separate categories, which are Ceramic Materials Technology, Ceramic Processing Technology and Analytical Codes. Work in the area of Ceramic Materials Technology concentrated on problem identification and continued development of reaction bonded and hot pressed silicon nitride which are the two materials used in fabricating duo-density turbine rotors (Figure 1.3). Improvements were sought in both strength and "m" value of injection molded rotor blade ring materials of 2.7g/cc density. Investigations in hot pressing technology were carried out to improve both the strength and reliability of the rotor hub material. The continued development of Ceramic Processing Technology as applied to duo-density turbine rotors concentrated on fabrication improvements on both injection molded blade rings and hot press/press bonding of rotor hubs. Considerable effort was needed and was spent on modifying the hot press bonding process to increase the yield of usable rotors. Cold spin testing and room temperature MOR strength tests were used to monitor improvements in the processes. The Analytical Codes continued to be developed and applied through the use of the statistical and 3-D finite element stress computer codes for reliability analysis of ceramic turbine rotors. This analysis was required to effect design changes made as a result of data generated on material strengths. An analytical technique was developed for hypothesis testing which utilized a computer program to determine, at what level of confidence, were two sets of data from the same or different populations.

The Ceramic Materials and NDE Technology Program, Task III in Figure 1.2, supported by DOE, concentrated on determining material properties of ceramics and evaluating new NDE techniques. The characterization of hot pressed and reaction sintered silicon nitride included preliminary determination of strength, creep, stress rupture and elastic properties of these materials for design purposes. A study was also initiated on the relationship of material composition and processing variables on the

fracture mechanisms, microstructure and strength of these two forms of silicon nitride. New ceramic NDE techniques were evaluated and applied to duo-density turbine rotors. The primary emphasis was on the reaction sintered silicon nitride rotor blade ring utilizing microfocus x-ray radiography.

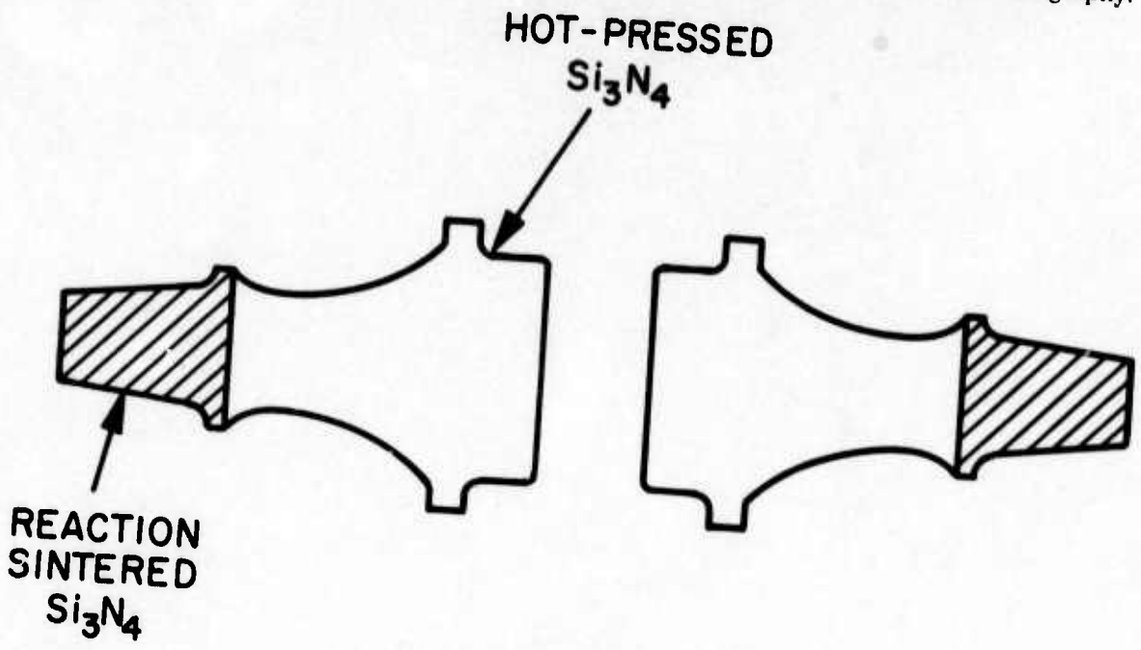

Figure 1.3 Duo-Density Ceramic Turbine Rotor

The progress made on the Ceramic Turbine Rotor Technology Program and the Ceramic Turbine Materials and NDE Technology Program, up to September 1977, was covered in detail in references 11 and 13. A summary of the results is presented in Section 2.0 of this report.

Work during this reporting period under the DOE(ERDA)-sponsored portion of the program and reported herein focused on development of ceramic processing technology used to fabricated duo-density silicon nitride turbine rotors. During the previous reporting period(13) several areas were identified which limited the rotor materials from achieving their strength potential. For example, cold spin testing revealed that blades which failed in the lower-speed range had internal flaws not detected by NDE. Also, it was shown that the bend strength of blades after hot press bonding was lower than before; this material degradation was confirmed by microstructure analyses. These problems formed the basis for work during this reporting period aimed at improving the duo-density silicon nitride rotor.

In the past, efforts to improve rotor quality have been closely coordinated with the need to fabricate rotors for material and spin testing. During this reporting period, the need to make rotors for testing was relaxed and emphasis was placed on quantifying and resolving rotor material degradation. As a result, fabricated rotors were disected to help make flaws more accessible to NDE and blades were fractured to assess material degradation. The primary objective of this was not to make rotors, but to define the process for making improved rotors.

Under plans to improve the quality of injection molded rotor blade rings, recently acquired microfocus X-ray equipment was used to examine separate, cut-off parts of blade rings in an effort to detect the type of internal voids previously revealed in cold spin testing. Parallel efforts in the injection molding process continued with emphasis on utilization of the Hunkar adaptive process control unit to maintain a programmed flow rate of mold material into the die cavity during injection.

In the area of hot press bonding, experiments were conducted to quantify blade strength degradation as a function of hot press bonding conditions and to develop the conditions for minimum blade degradation. Special attention was paid to the sensing of parameters (particularly temperature) and the control of the hot press bonding process.

2.0 SUMMARY OF PREVIOUS DOE SPONSORED WORK

Introduction

The duo-density silicon nitride rotor concept utilizes creep resistant reaction bonded silicon nitride for the complex shaped blades and hot pressed silicon nitride for the high strength rotor hub. The blades are formed by injection molding a one piece blade ring consisting of all 36 blades and the blade ring rim. The green preform, made of silicon particles and an organic binder, is subsequently burned out, to removed the binder, and then heated in a nitrogen atmosphere to convert the silicon to silicon nitride. The silicon nitride blade ring, after blade encapsulation in a blade fill, is placed in a hot press. Silicon nitride powder is then hot pressed to form the hub while simultaneously hot press bonding the hub to the blade ring.

Table 2.1 presents a summary of all DOE sponsored work. Improvements in ceramic materials technology (Section 2.1) in addition to improvements in both the injection molding and hot press bonding processes (Section 2.2) were sought in order to improve the quality of duo-density silicon nitride turbine rotors.

TABLE 2.1

DOE PROGRAM ACCOMPLISHMENTS

Status at Start of Program	Status at Program Termination
I. CERAMIC MATERIALS TECHNOLOGY	
1. Reaction Bonded Silicon Nitride	
— Strength variability exhibited by 2.7 g/cc Injection Molded RBSN.	— Iron and chromium contaminant identified as source of strength variability.
	— Magnetic separator equipment ordered for powder cleaning.
2. Hot Pressed Silicon Nitride	
— Limited coefficient of expansion data available.	— Coefficient of expansions determined for varying concentrations of MgO over the 100-900°C temperature range.
— Parametric study needed to identify the best combination of starting powder, w/o MgO, milling conditions and hot pressing pressure.	— Best material produced with 5 w/o MgO, wet WC milling in methanol, even at low pressure.
3. Non-Destructive Evaluation	
— Standard X-ray techniques failed to detect subsurface voids in blades and blade ring rim.	— Microfocus X-ray set up and evaluated for detection of subsurface voids, 0.010 inch and larger, in blades and rim.
	— Panoramic X-ray of rim with magnification achieved.

TABLE 2.1 — Continued

DOE PROGRAM ACCOMPLISHMENTS

Status at Start of Program	Status at Program Termination
II. CERAMIC ROTOR FABRICATION TECHNOLOGY	
1. Injection Molding of Rotor Blade Ring	
— Poor surface finish of molded blade rings.	— Mold release/air blast distribution system noticeably improved surface finish.
— Low yield (10-15%) of good blade rings due to blade cracks.	— Yield increased to 75% with automated system controlling molding parameters.
— Subsurface molding voids present.	— Hunkar flow control equipment procured and set up, and shown to greatly reduce the number of subsurface voids in highly stressed portions of blades.
2. Hot Press Bonding	
— 3-piece rotor configuration had inadequate hot pressed to hot pressed bond joint strength.	— Simplified 2-piece configuration eliminated this bond joint.
— 2-piece contoured rotor processing cracked blades resulting in a low yield of usable rotors.	— Yield of flaw-free hot pressings increased to 70% with improved process controls.
— Blade fill/graphite wedge support system limited hot pressing pressure.	— Molten glass media identified as a suitable support system and sealing configuration developed.
— Blade rings exhibited varying color and microstructure after press bonding.	— Blade strength degradation identified as occurring during hot press bonding. Region of hot pressing time and temperature defined to eliminate material and strength degradation.
III. ANALYTICAL DESIGN CODES	
— Standardized method needed to estimate Weibull parameters.	— Maximum Likelihood Method selected and automated with computer program.
— Standardized analytical test needed to check differences in sets of data.	— Hypothesis testing computer program developed.
— Fast fracture reliability analysis developed resulting in thin throat rotor design.	— Analytical procedure developed to compute time-dependent reliability of ceramic structures. Rotor throat thickness increased to increase time-dependent life.

2.1 CERAMIC MATERIAL TECHNOLOGY

Introduction

The development of ceramic material technology for reaction bonded and hot pressed silicon nitride has been an ongoing activity since the beginning of the Ford/DARPA program, and continued under the DOE sponsored portion of the FORD/DARPA/DOE Program. This technology is a very important portion of the systems approach employed in this project for the development of high temperature gas turbine engines. Improvements in materials have been made and characterized so that components could be designed, fabricated and evaluated.

2.1.1 REACTION BONDED SILICON NITRIDE

The mixing of silicon powder and organics, prior to injection molding, was improved with the addition of vacuum capability to the equipment. This, combined with better temperature control during mixing, produced a more homogeneous mix which should result in fewer macroscopic flaws in molded components[13].

The starting silicon powder, used to injection mold rotor blade rings, was found to contain contaminant in the form of iron and chromium. Microstructural examination of both test bars and rotor blades indicated a definite correlation between strength and the size of microscopic flaws due to contamination (Figures 2.1 and 2.2). Magnetic separator equipment was ordered and received so that all starting silicon powder can be cleaned in-house[13].

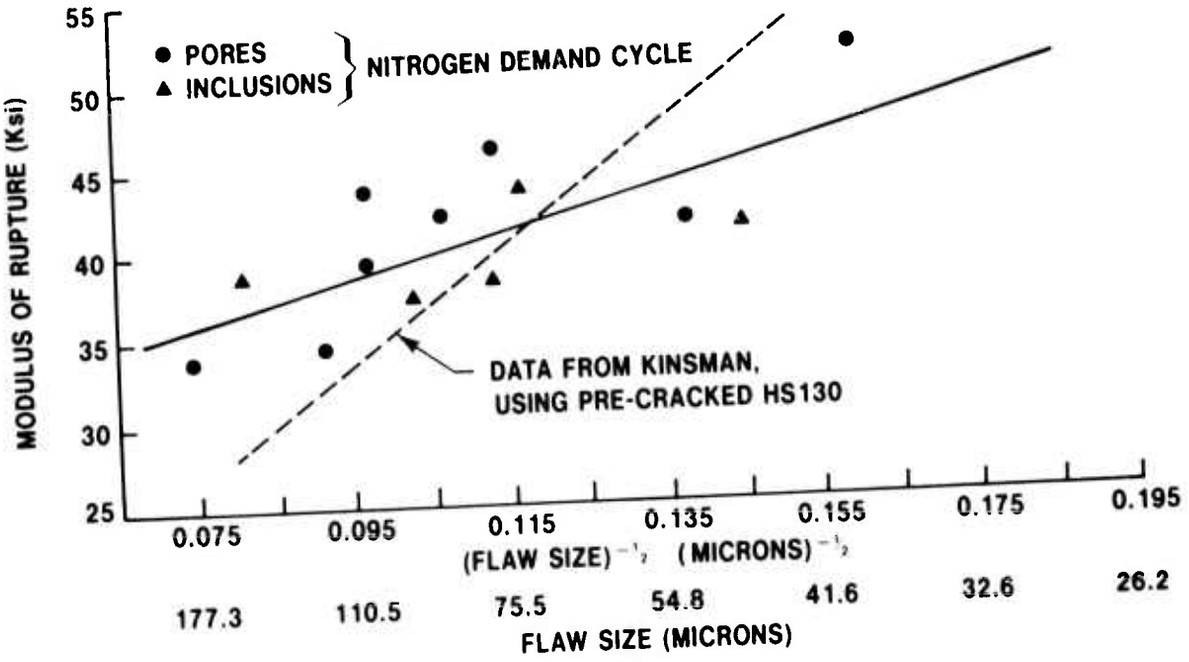

Figure 2.1 Test Bar MOR Versus Flaw Size

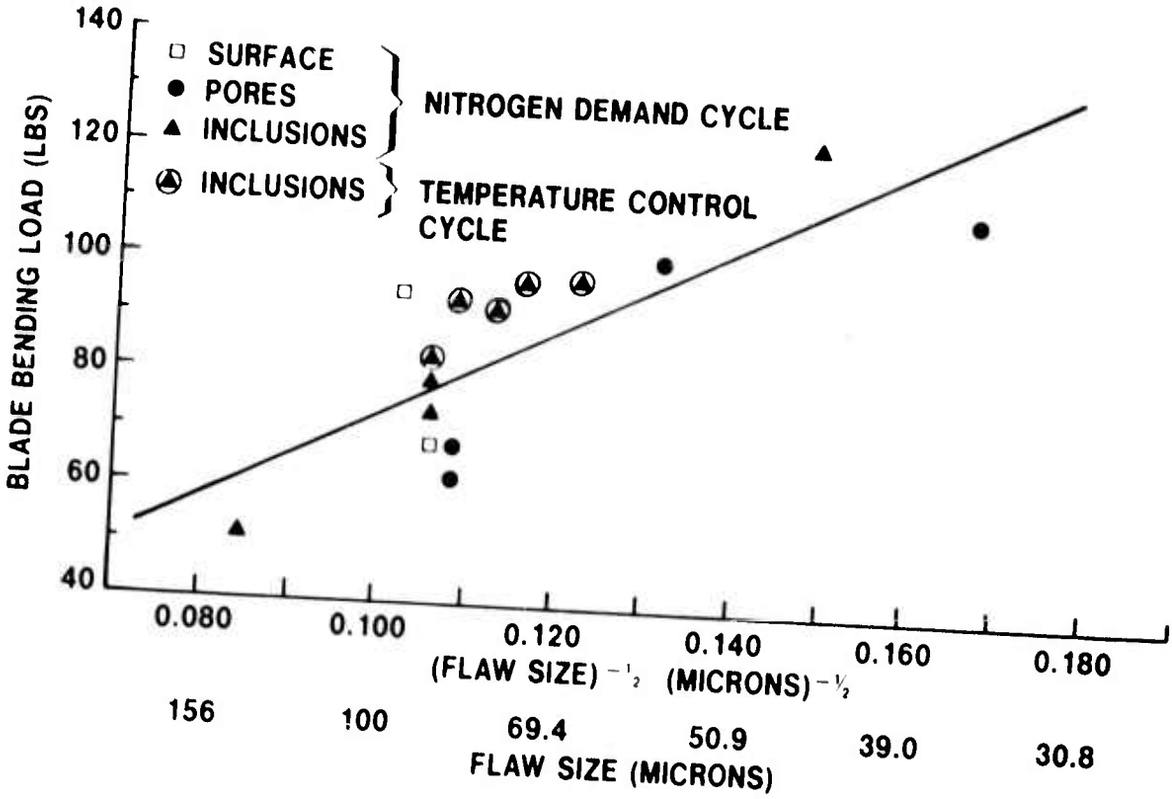

Figure 2.2 Rotor Blade Bend Load Versus Flaw Size

2.1.2 HOT PRESSED SILICON NITRIDE

A parametric study on hot pressed silicon nitride included such variables as starting powders (CP-85,KBI), MgO content (2-7w/o), powder milling (wet, dry, WC, Al_2O_3, 24-72 hours) and pressing pressure (500-5000 psi). The best material was produced by WC milling and contained 5w/o MgO densification additive(11).

This study was continued with fabrication of twenty-two hot pressed samples with systematically varied hot pressing temperature (1500-1750°C), time (1 to 7 hours) and pressure (1000-5000 psi). The optimum hot pressing conditions would then be determined once strength data had been generated. Approximately 30 hot pressings were made with various purity level starting powders and a variety of hot pressing aids shown in Table 2.2. The high temperature strength would then be determined to identify the best candidates for further study(13).

Comparative thermal expansion measurements were made on twenty-two samples of hot pressed silicon nitride to evaluate the effects of MgO content, powder milling conditions, powder source, and hot pressing pressures.

The ranges of variables investigated are shown below:

Weight % MgO	1, 2, 3½, 5, or 7
Milling Balls:	WC or Al_2O_3
Milling Fluid:	Methanol or none
Milling Time:	48, 72, or 144 hours
Powder Type:	CP85, CP85 after KBI cleaning, or new CP85
Pressing Pressure:	1500 or 5000 psi (1715°C, 3 hours)

The MgO content was found to be the only significant variable affecting thermal expansion (Figure 2.3)(13).

TABLE 2.2

Chemistry of Commercial Grade Silicon Nitride Powder and Hot Pressing Additives

	AME CP-85B	AME Hi-Purity	Starck	Annawerk	Sylvania SN 402	Sylvania SN 502	Zyttrite (Δ)	Cerium Oxide (CeO_2)	Yttria ($Y_2O_3$3)	Magnesium Oxide (MgO)
α-Si_3N_4*	84.7	~70	93.4	~80	0.5-1	~90				
β-Si_3N_4*	14.3	~30	6.6	~20	Amorphous	~10				
Si_2N_2O*	0.7	0.5-1	<0.5	0.5-1	0	0				
Si(free)*	0.3	0.5-1	0	0.5-1	0	<0.5				
Oxygen**	1.44	1.89	1.10	2.15	2.61	1.84				
SiO_2*	0	0	<0.5	0	0	0				
Fe***	0.88	0.35	0.02	1.40	<0.01	0.04	0.05	0.01	0.01	0.05
Al***	0.63	0.17	0.05	0.15	0.01	0.01	0.02	0.01	<0.01	0.51
Mg***	0.01	0.01	0.02	0.10	<0.01	<0.01	<0.01	<0.01	<0.01	Base
Ca***	0.20	0.01	0.05	0.20	<0.01	<0.01	0.10	<0.01	<0.01	0.10
Ni***	0.03	<0.01	<0.01	0.02	<0.01	<0.01	<0.01	<0.01	<0.01	<0.01
Cr***	0.01	<0.01	0.02	0.01	<0.01	<0.01	0.01	<0.01	<0.01	<0.01
Ti***	0.08	0.05	0.02	0.05	<0.005	<0.005	0.05	<0.005	<0.005	<0.005
B***	0005	0.0005	<0.002	0.008	<0.0002	<0.0002	<0.0005	0.01	<0.0002	0.05
Si***					Base		0.03	<0.01	0.03	0.10

* By X-ray Analysis — weight percent
** By Neutron Activation Analysis (AMMRC)
*** By Emission Spectrographic Analysis — weight percent
Δ — 12% w/o Y_2O_3 stabilized ZrO_2

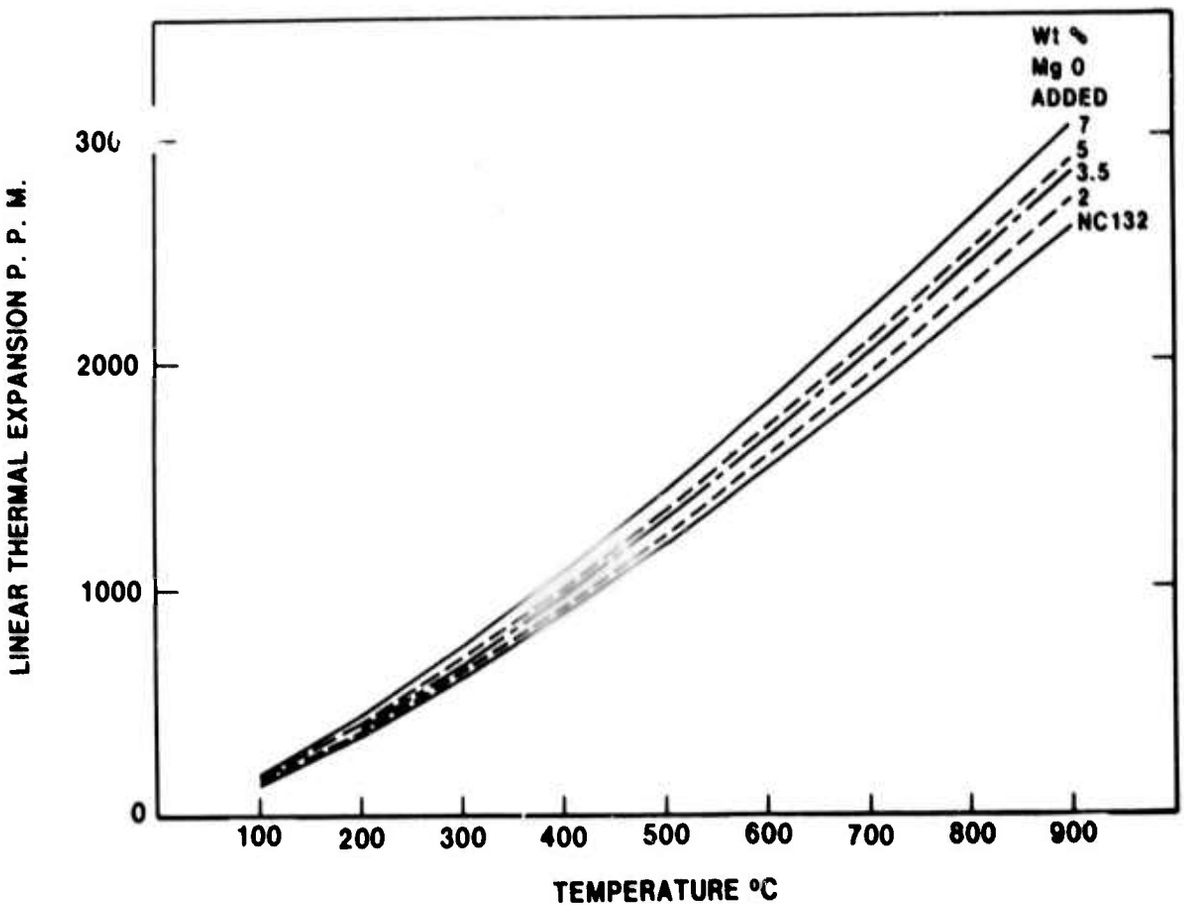

Figure 2.3 Linear Thermal Expansion of HPSN

2.2 CERAMIC ROTOR FABRICATION TECHNOLOGY

Introduction

Improvements were sought in the injection molding process which is utilized to fabricate a one piece blade ring consisting of all 36 blades and the blade ring rim. Improvements were also sought in the subsequent hot press bonding process used to form and bond the dense hot pressed silicon nitride hub to the blade ring.

2.2.1 INJECTION MOLDING OF ROTOR BLADE RINGS

The injection molding process was improved by optimizing the molding parameters with the automated control system. The installation of nozzles to apply mold release and air blast jets, to clean the die and evenly distribute the mold release, resulted in a noticeable improvement in the surface finish of blade rings. The improved part yield as reflected in cracks detected in the as-molded components is shown in Figure 2.4. The bottom curve represents blade rings having no visible defects, in the as-molded state, under 70x microscopic inspection. The top curve represents usable test blade rings and includes those molded with no cracks or other functional defects and less than two minor surface imperfections. The number of parts refers to the total number of blade rings molded during a particular stage of control development[13].

In an effort to further improve the quality of molded blade rings, an adaptive process control unit manufactured by Hunkar Laboratories Inc. was installed on the Reed Prentice injection molder. This system interfaced with the Ford automatic control system and controlled machine operation from the time the inject command was given until the plunger retract command was received[13]. Section 4.1 of this report describes the initial experiments with this adaptive process control unit.

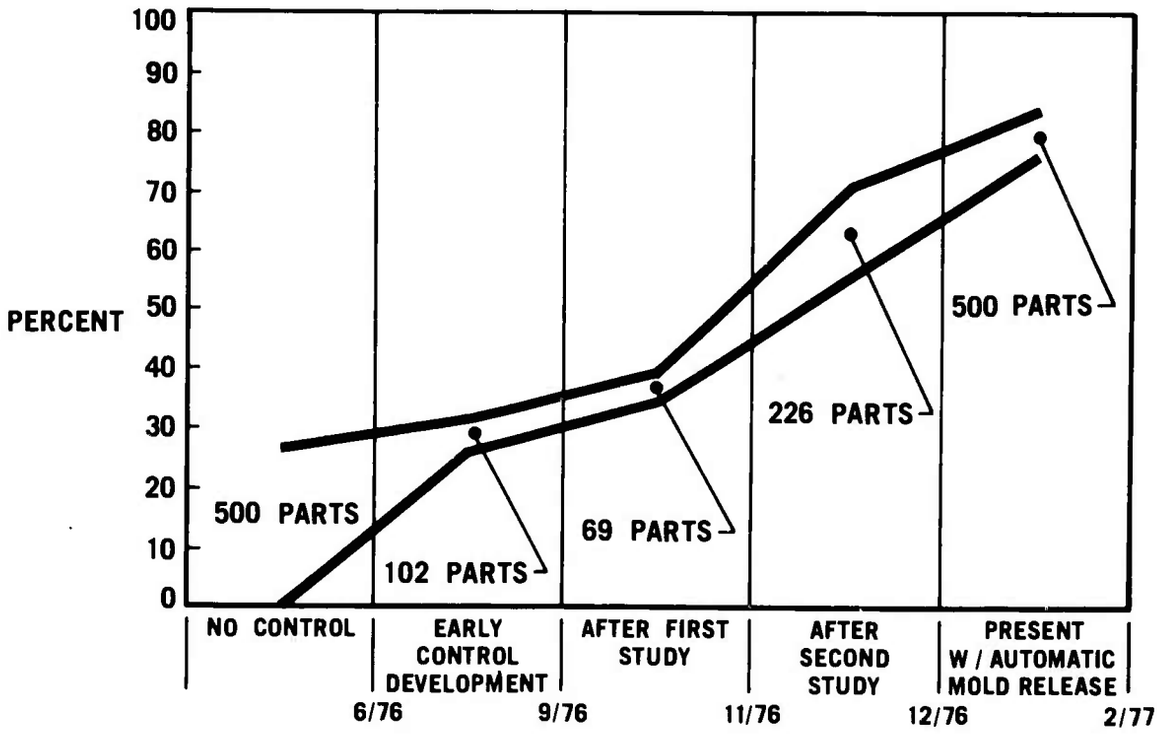

Figure 2.4 Yield of Good As-Molded Blade Rings Versus Process Development

2.2.2 HOT PRESS BONDING OF DUO-DENSITY ROTORS

The three-piece approach to fabricating duo-density rotors was developed earlier[10] in order to circumvent blade cracking problems. Figure 2.5 shows this concept. An investigation was made of the bond strength between the pre-formed hot pressed hub and the hot pressed bond ring. Test bars were cut from the bond region of six rotors representing six different compositional or forming conditions and tested at 2200°F. The results showed the hot pressed-to-hot pressed silicon nitride bond strength to vary from 18 to 98% of the parent material[11]. The fabrication concept was changed to a two-piece design involving hot pressing and simultaneous bonding of a simplified, flatter hub to a reaction bonded blade ring as shown in Figure 2.6[11]. Several rotors were fabricated using pressures of 500 to 1500 psi with 3½w/o magnesium oxide added to the silicon nitride powder which was milled with tungsten carbide balls in methanol. Blade cracking was minimized at 1000 psi pressure, 1000 lbs. wedge restraining load and three hours at temperatures of 1700 to 1775°C[11].

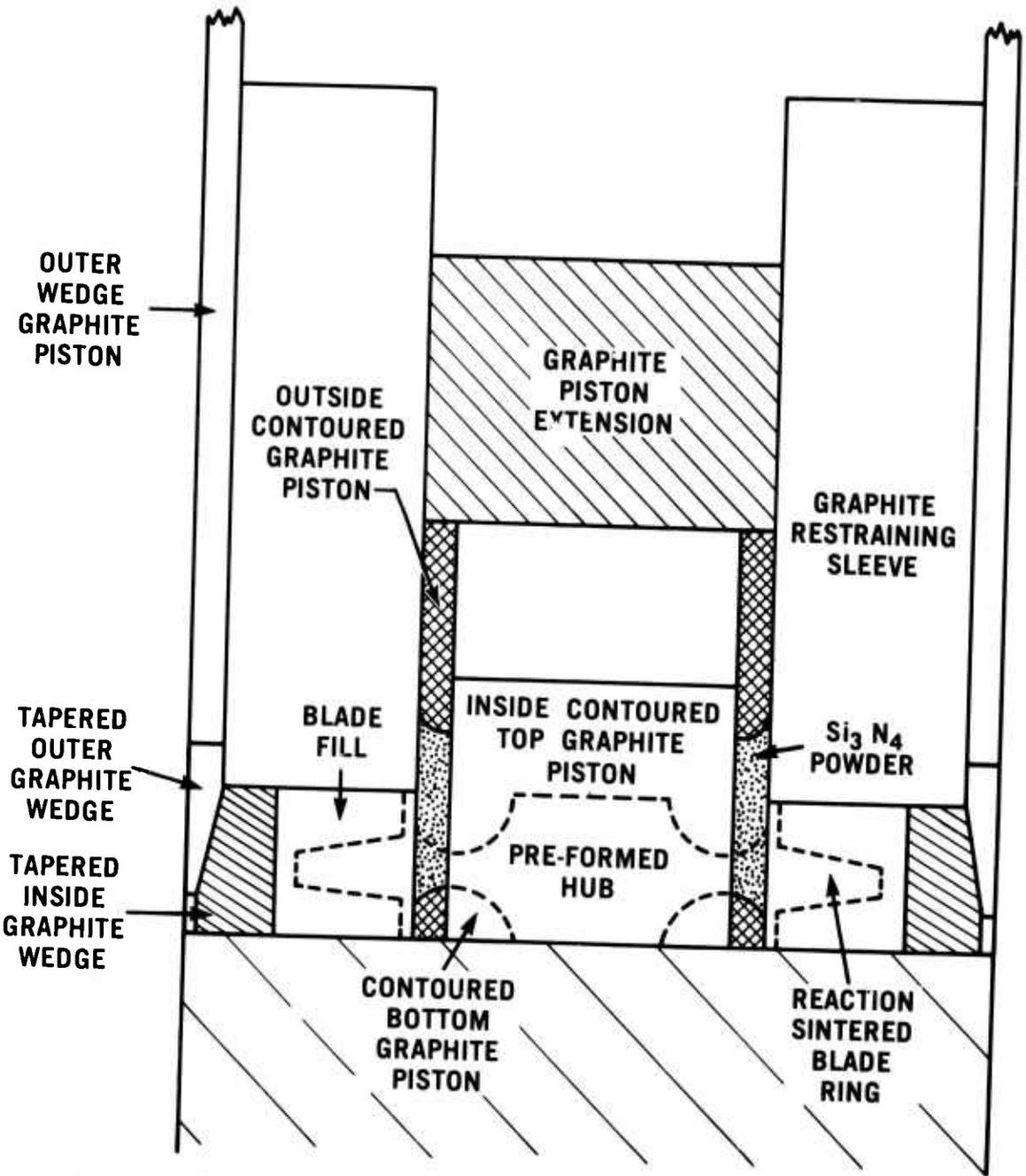

Figure 2.5 Hot Press Bonding Assembly — Three Piece Duo-Density Concept

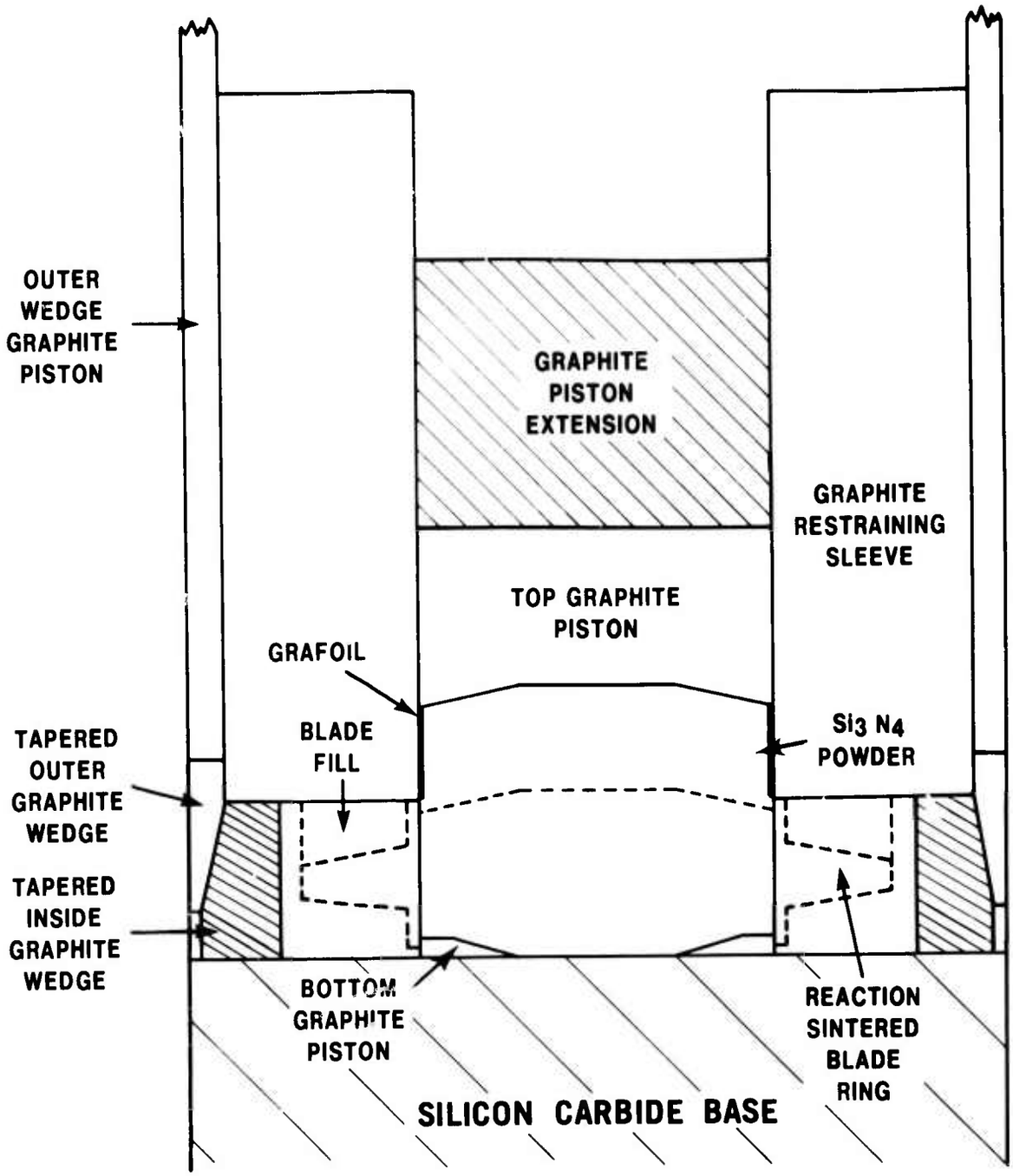

Figure 2.6 Simplified Two-Piece Configuration

Control of the hot pressing load was refined by modifying the hydraulic pressure regulating system. Initial experiments conducted with a radiation pyrometer coupled to an automatic temperature control unit were successful and this system was used during this reporting period (Section 3.0). The graphite tooling was redesigned to provide more consistent action of the blade ring restraining wedges. The blade filling process was modified to more accurately control the thickness of boron nitride used as a barrier material. These last two changes resulted in a significant improvement in hot press bonding as 70% of the rotors fabricated were free of flaws induced by hot pressing[13].

3.0 CERAMIC MATERIAL TECHNOLOGY (ROTOR IMPROVEMENT)

3.1 INTRODUCTION

Rotors produced during the development of the simplified two-piece hot press bonding concept were sectioned to examine the bond joint between the blade ring and the hot pressed hub. During these examinations, it was observed that the reaction bonded blade ring material usually had changed color, from a shiny black to a dull gray. Several rotors were then selected for an investigation into the color changes and possible microstructural changes. In addition, a few rotors were subjected to blade bend testing to determine if the strength of the blades was affected by hot press bonding. Several blade rings were also bend tested to establish the blade bend strength prior to hot press bonding. The results, in Table 3.1, show the characteristic loads after hot press bonding were 14 to 38% lower than those for the "as-nitrided" or before hot press bonding state.[13]

TABLE 3.1

Summary of Blade Bend Test Results

Nitriding Number	As Nitrided		After Hot Pressing		% Change	
	Weibull Slope	Characteristic Load* (Pounds)	Weibull Slope	Characteristic Load* (Pounds)	Weibull Slope	Characteristic Load*
48	9.1	89.9	6.9	77.0	−24	−14
67	11.2	85.7	6.8	53.0	−39	−38
78	9.2	79.1	15.1	61.6	+64	−22

*Load at 63.2% failure rate

Analysis of the microstructure of the blades indicated they had changed from a shiny black to a gray color after hot pressing with a corresponding increase in non-uniform porosity as shown in Figure 3.1. X-ray analysis showed the phase composition of the silicon nitride had changed from an average of 70% α, 29% β before press bonding to an average of 22% α, 75% β and 3% silicon oxynitride after press bonding (Table 3.2). Also shown in this table is data on two blade rings at an intermediate processing step, (after blade fill nitriding), which indicated that the degradation was occurring during hot press bonding.[13]

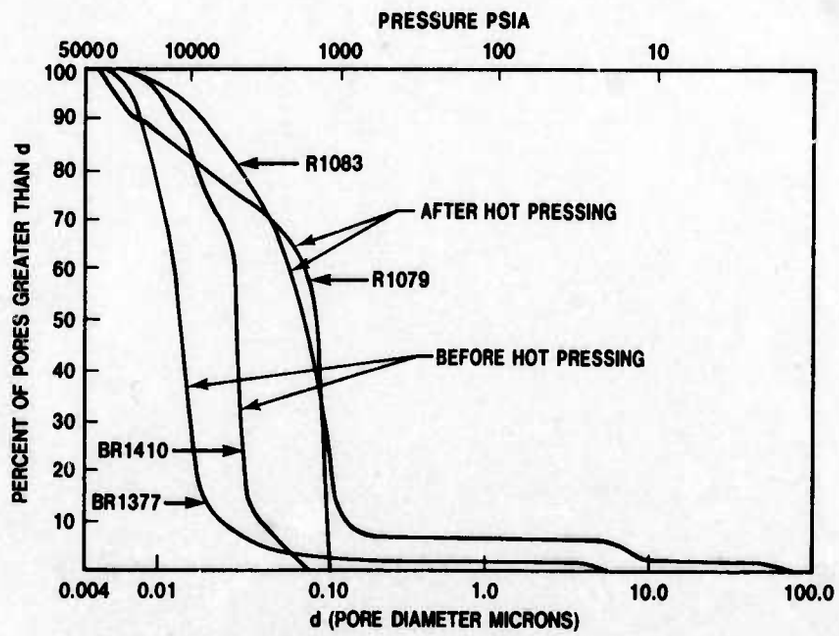

Figure 3.1 Pore Size Distribution Before and After Hot Press Bonding

Table 3.2

Blade Ring Degradation Characteristics at Various Process Steps

	NO. OF SAMPLES	BLADE DENSITY	COLOR	MICROSTRUCTURE	% PHASE COMPOSITION			
					α	β	Si	Si_2ON_2
AFTER NITRIDING	16	2.70	SHINY BLACK	UNIFORM POROSITY, METALLIC PHASE, MOLDING FLAWS	70	29	0.3	0.4
AFTER BLADE FILL NITRIDING	2	2.69	SHINY BLACK	UNIFORM POROSITY, METALLIC PHASE	72	29	0	0.15
AFTER HOT PRESS BONDING	8	2.68	GRAY/ LIGHT GRAY CASE	NON-UNIFORM FINE POROSITY, 2ND PHASE	22	75	0	2.7

It was hypothesized that the reaction bonded silicon nitride blade rings were subjected to a high enough temperature, during press bonding, to result in dissociation of the silicon nitride which produced non-uniform porosity resulting in a reduction in strength.[13]

During this reporting period data in support of this hypothesis was collected on rotors previously fabricated and in some cases tested. In addition, a comprehensive study of the reaction bonded silicon nitride degradation was conducted and is presented in Section 3.3.

3.2 SUPPORTING DATA

The first two lines of data in Table 3.3 are from reference 13 with the exception of the hardness data which was generated during this reporting period to determine if hardness could be related to degradation. During the development of the hot press bonding fabrication process several rotors were fabricated at lower temperatures than the finalized standard of 1715°C. Two rotors, 1344 and 1365, were hot press bonded at 1600°C, approximately 100°C lower temperature than standardized. The data, lines 3 and 4 of Table 3.3, shows that little or no change had occurred in the microstructure, phase composition and hardness during hot press bonding. This indicated that a reduction in the hot press bonding temperature of 100°C or less, should result in eliminating the degradation of the reaction bonded silicon nitride blade ring. The next section of this report covers the experiments conducted to establish the required changes in hot press bonding parameters to eliminate degradation.

TABLE 3.3
Characterization of Rotor Blade Rings

Comments	Rotor S.N.	Density g/cc	Color	Microstructure	% Phase Composition α	β	Si_2ON_2	SiO_2	Hardness Vickers 30 Kg
Average As Nitrided[13]	—	2.7	SB	UP,SMP, MF	70	29	0.4	0.1	1110
Average After Hot Press Bonding[13]	—	2.68	G,LGC	NUP, 2P	22	75	2.7	0	938
Low Hot Press Bonding Temperature	1344	2.83	B	LP, SC	69	30	1.1	0	1076
Low Hot Press Bonding Temperature	1365	2.81	B	LP, C	60	37	3.6	0	1037
Cold Spin Tested	1246	—	G	NUP,MP,2P	3	91	3.2	0	717
Cold Spin Tested	1280	—	B	NC	61	37	1.7	0	928
Engine Tested Rotor	1195	—	G	NUP	0	~100	0	0	679

LEGEND

Color: SB = Shiny Black; B = Black; G = Gray; LGC = Light Gray Case

Microstructure: UP = Uniform Porosity; LP = Larger Porosity; NUP = Non Uniform Porosity; SMP = Some Metallic Phase; MP = Metallic Phase; 2P = 2nd Phase; NC = N. Change; SC = Slight Change; MF = Molding Flaws

Several rotors which had been tested previously were also analyzed during this reporting period. The blade fragments from rotors 1246, and 1280, which were cold spin tested were examined and the data presented in Table 3.3 (lines 5 & 6). The data shows the blades of rotor 1246 were severely degraded (gray color, non-uniform porosity and 3% α). Failure speeds of unflawed blades ranged from 70,900 to 86,950 rpm with a characteristic failure speed of 83,500 rpm[14]. Rotor 1280 was not degraded (black, uniform porosity, 61% α) and unflawed blades failed in the 87,140 to 96,900 rpm range with a characteristic failure speed of 96,200 rpm[14]. This 15% increase in characteristic failure speed, or therefore 32% increase in centrifugal stress confirms the previously seen strength degradation which was observed during blade bend testing[13]. More importantly however, rotor 1280 demonstrated that a rotor could be fabricated with a strong bond joint (150% speed, no bond joint failure) and with minimal or no degradation in blade strength.

Fragments of blades from rotor 1195 were recovered from the engine test described previously [12] and analyzed. The results, shown in the last line of Table 3.3, showed this to be one of the most severely degraded rotors analyzed. The gray blades were approximately 100% β, and had a lot of non-uniform porosity. This rotor had operated in the modified 820 engine for over 37 hours, all but a few minutes at a Turbine Inlet Temperature (T.I.T.) of 2200°F or higher, at speeds of 45,000 to 50,000 rpm, including 1-1/2 hours at 50,000 rpm and over 2500°F T.I.T.[12]. This unprecedented test demonstrated the capability of severely degraded blade rings indicating improved rotors with no blade strength degradation should be capable of higher speeds.

3.3 REACTION BONDED SILICON NITRIDE DEGRADATION STUDY

As mentioned in the previous section, a study was conducted to determine the parameters causing the strength degradation of the injection molded blade ring during the hot press processing. This section presents the details of that study.

The hot pressing process consists of two distinct operations — blade filling and hot pressing.

The blade filling operation[13] occurs prior to hot pressing and encapsulates the blade ring in an envelope of silicon nitride. This encapsulation was accomplished by coating the blade ring with a barrier layer of boron nitride (0.001-0.010" thick) and then slip casting an envelope of silicon around the coated blade ring. This slip cast assembly was then nitrided to convert the slip material to silicon nitride.

At this point, the blade ring was ready for the second operation, hot pressing[13] (see Figure 3.2). In this operation, silicon nitride powder was placed inside the encapsulated blade ring and subjected to temperature and pressure sufficient to cause the Si_3N_4 powder to densify and bond to the blade ring. In order to prevent deformation of the blade ring during this operation, a radially inward load was applied to the outer diameter of the blade fill assembly by means of a wedge system[13].

The technique employed in this study was such that the effect of each of these operations on blade ring degradation could be identified.

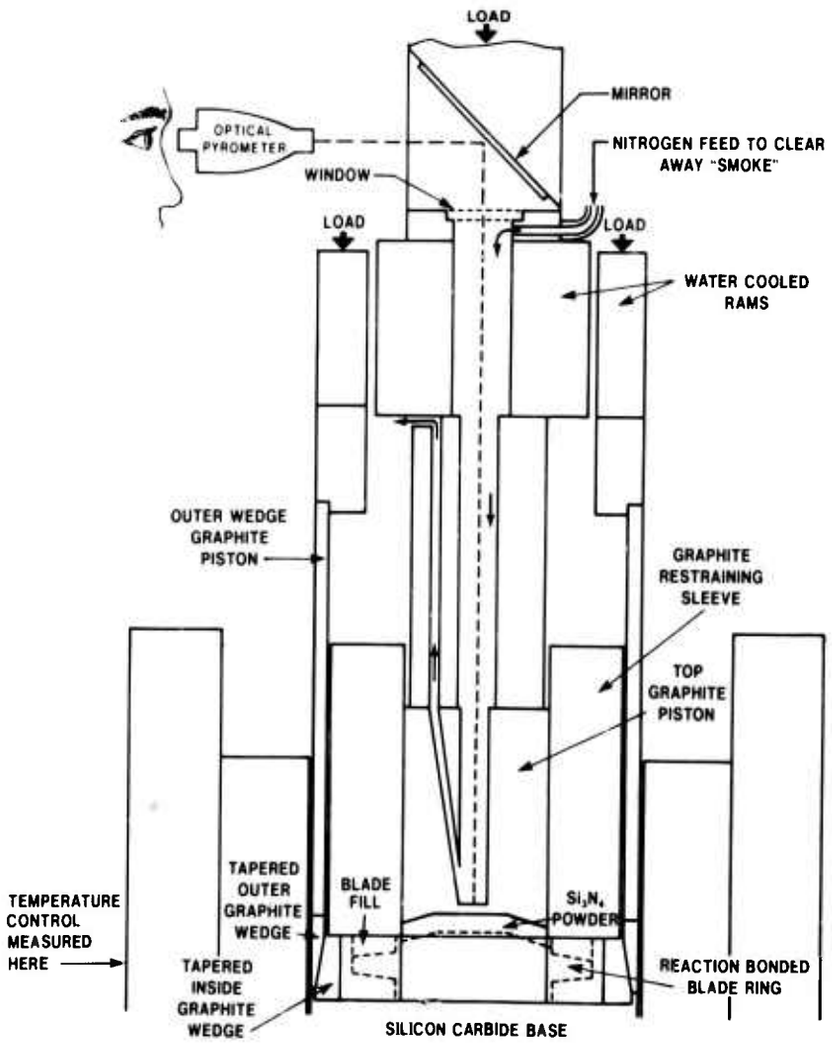

Figure 3.2 Graphite Tooling for Inside Temperature Measurement

3.3.1 TECHNIQUE FOR ASSESSING DEGRADATION

Data which was gathered outside this study and which, in essence, identified the presence of degradation contained a major variability. Comparisons between the "as nitrided" and the "after" hot pressing operations were made utilizing different blade rings. Such variability between blade rings was not desired in this study. To eliminate the variability, the following technique for determining before and after comparisons was established:

(a) First, the odd numbered blades of a blade ring were loaded to failure in the load test fixture[11] (Figure 3.3) resulting in a blade ring as shown in the top right of Figure 3.4.

(b) The blade ring with remaining even blades was then processed through the blade filling operation.

(c) If an "after blade filling comparison" was required, the blade fill was removed and the even blades were loaded to failure.

(d) If an "after hot pressing comparison" was required, the encapsulated blade ring was processed through the hot pressing operation, then the blade fill was removed and finally the even blades were loaded to failure.

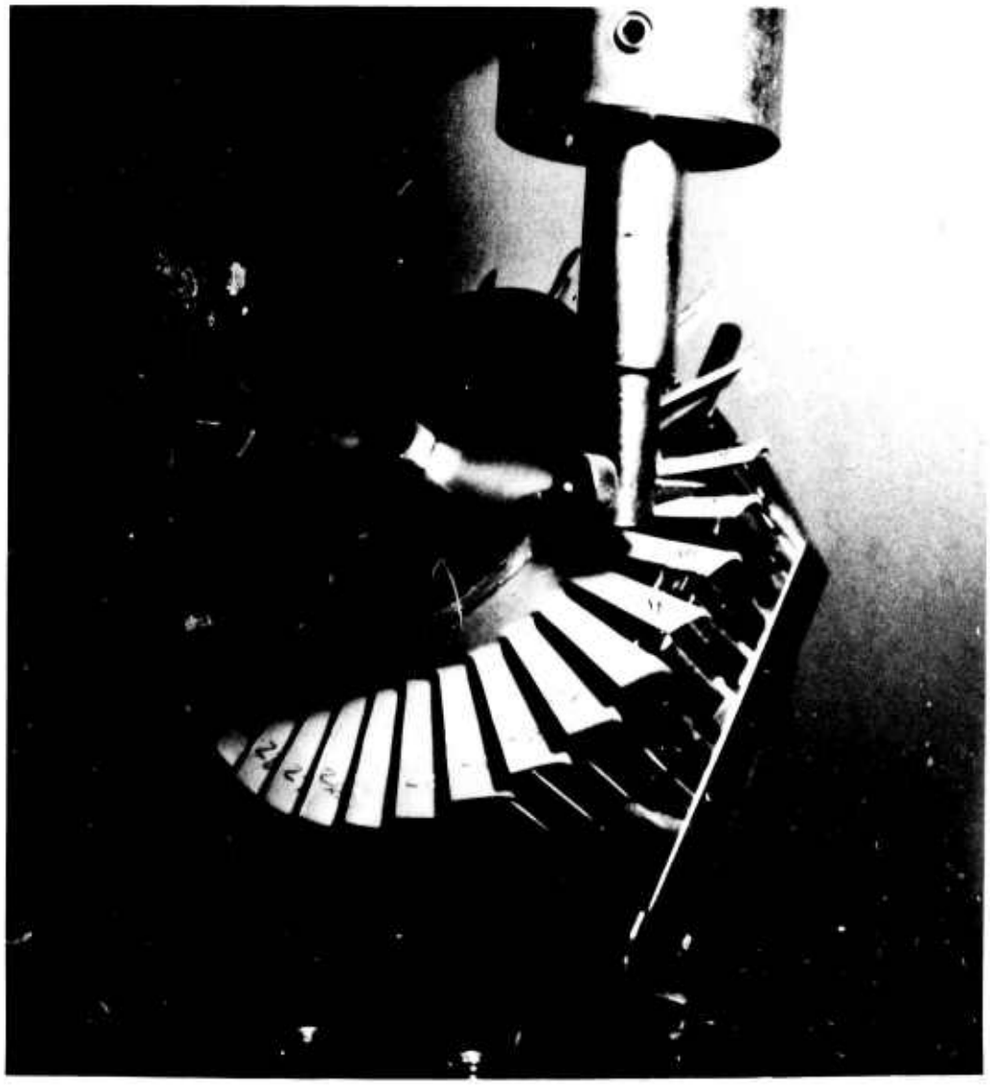

Figure 3.3 Rotor Blade Bend Test Set-Up

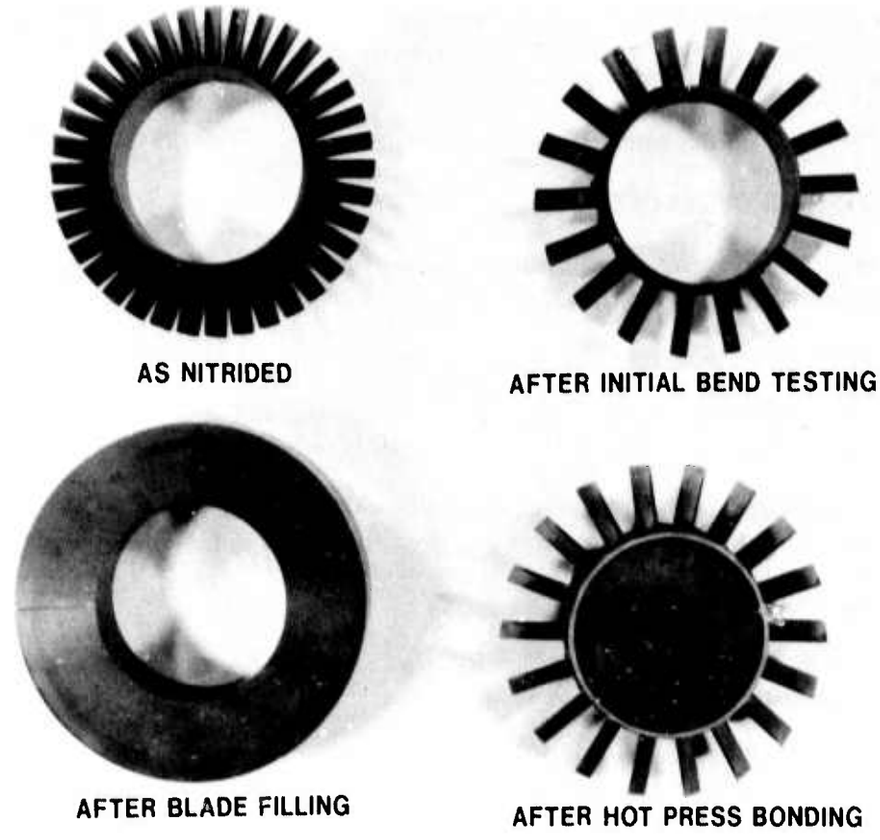

Figure 3.4 Processing Steps for Degradation Study

After completing either cycle [(a), (b) & (c) or (a), (b) & (d)], a comparison was made between properties of the before and after blades. Of concern were load, color, microstructure, hardness and phase composition. In addition, functional relationships between the independent and dependent variables were checked using a multiple regression computer program.

3.3.2 STUDY RESULTS

3.3.2.1 BLADE FILLING OPERATION

Although prior data indicated that the blade filling operation of the hot pressing process did not contribute significantly to the blade ring degradation[13], a number of blade rings were processed through the [(a), (b), (c)] sequence to verify this indication. One blade filled blade ring from each of five blade fill nitridings was evaluated. The results of these tests are shown in Table 3.4.

TABLE 3.4
Blade Ring Data Before and After Blade Fill Processing

	Before/After Blade Fill	Weibull Sample Size *	Characteristic Load Ubs P_{63}**	Statistical Difference	Weibull Slope m	Statistical Difference	Color	Vickers Hardness	Microstructure Porosity	Metallic Phase	2nd Phase	% Phase Composition α	β	Si_2ON_2	SiO_2	Si
2641	1 Before	5	60		6		SB***	905	Normal	Some	None	67.7	3.2	0	3	3
	1 After	8	66	No	8	No	SB	905	Some	None	None	76.9	23.1	0	0	0
2680	2 Before	10	75		11		SB	905	Normal	Some	None	79.1	19.7	1.2	0	0
	2 After	9	78	No	10	No	SB	1020	Normal	None	None	79.5	19.8	.7	0	0
2619	3 Before	10	87		8		SB	890	Normal	Some		78.9	19.2	1.3	0	6
	3 After	8	81	No	9	No	SB	970	Normal	None		80.3	19.7	0	0	0
2618	4 Before	14	91		13		SB	942	Normal	Some		80.9	18.5	0	0	6
	4 After	12	82	No	12	No	SB	890	Normal	None		76.7	22.8	0	0	5
2561	5 Before	9	78		24		SB	1075	Normal	Slight		74.9	23.9	1.2	0	0
	5 After	10	80	No	11	[illegible]	SB	965	Normal	None		74.7	24.2	1.1	0	0

* Number of unflawed blades
** Load at 63.2% failure rate
*** SB = Shiny Black

None of the parameters used to characterize a material demonstrated any significant change. The metallic phase present in "as nitrided" blade rings (probably silicon) was not detectable in blade rings after the blade filling operation. It was assumed that the free silicon was nitrided to form Si_3N_4.

The conclusion was that the blade filling operation did not contribute to blade ring degradation.

3.3.2.2 HOT PRESSING OPERATION

Based on the previously mentioned hypothesis, the hot pressing study concentrated on identifying the effects of two pressing parameters — temperature and time at temperature.

The temperature parameter was defined as the maximum pressing temperature as observed by optical pyrometer measurements on the top graphite piston t/4" from the hub (see Figure 3.2.). This study examined a range of temperature from t790°C to t670°C. Below this lower limit, adequate bonding between the rotor blade ring and hub could not be achieved.

The time at temperature parameter was varied between 1/2 hour and 4-t/2 hours. Shorter times do not allow the hot pressed hub to reach maximum strength[t5]. The upper time at temperature limit approaches a maximum as far as practical scheduling is concerned. Figure 3.5 shows a typical pressure and temperature versus time schedule.

The actual time-temperature matrix is shown in Figure 3.6. The points on this matrix were chosen to yield results which could be analyzed statistically.

The parameters of hub and wedge pressures were kept constant throughout these tests. These were 1000 psi hub pressure and 1000 lbs. wedge load.

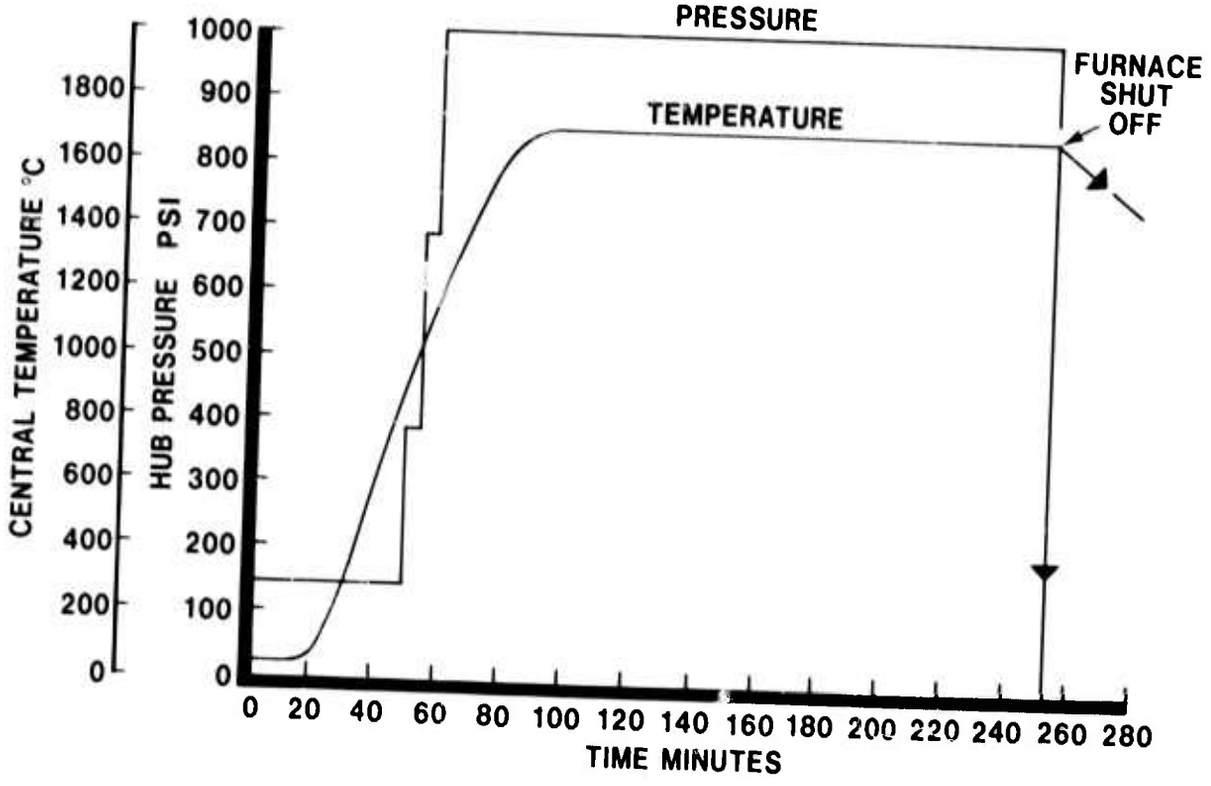

Figure 3.5 Typical Hot Pressing Schedule

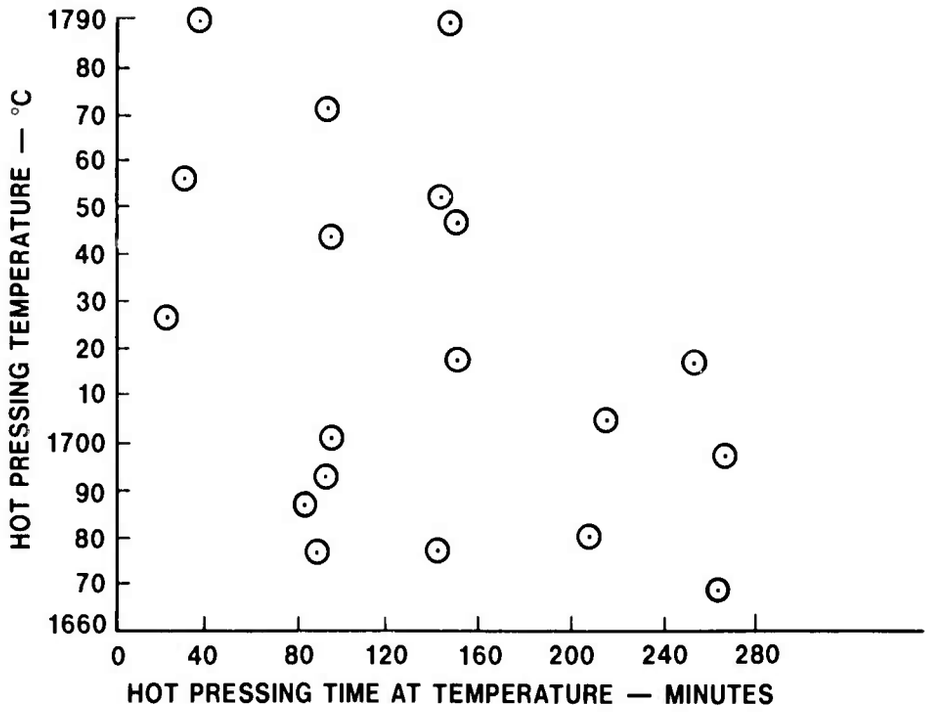

Figure 3.6 Times and Temperatures for Experimental Hot Pressings

Blade Bend Load

At the initiation of this study, it was assumed that the primary method to determine strength degradation was to compare failure loads of before and after hot pressing blades tested in the fixture shown in Figure 3.3. This before/after comparison was not successful for reasons discussed below.

Initial blade rings were available in the machined configuration shown on the left in Figure 3.7. When blade rings of this configuration were mounted on the blade load fixture and blade loaded, an occasional rim failure would occur. These rim failures were undesirable. A blade ring configuration with a center rib (shown on the right in Figure 3.7) was successful in eliminating rim failures.

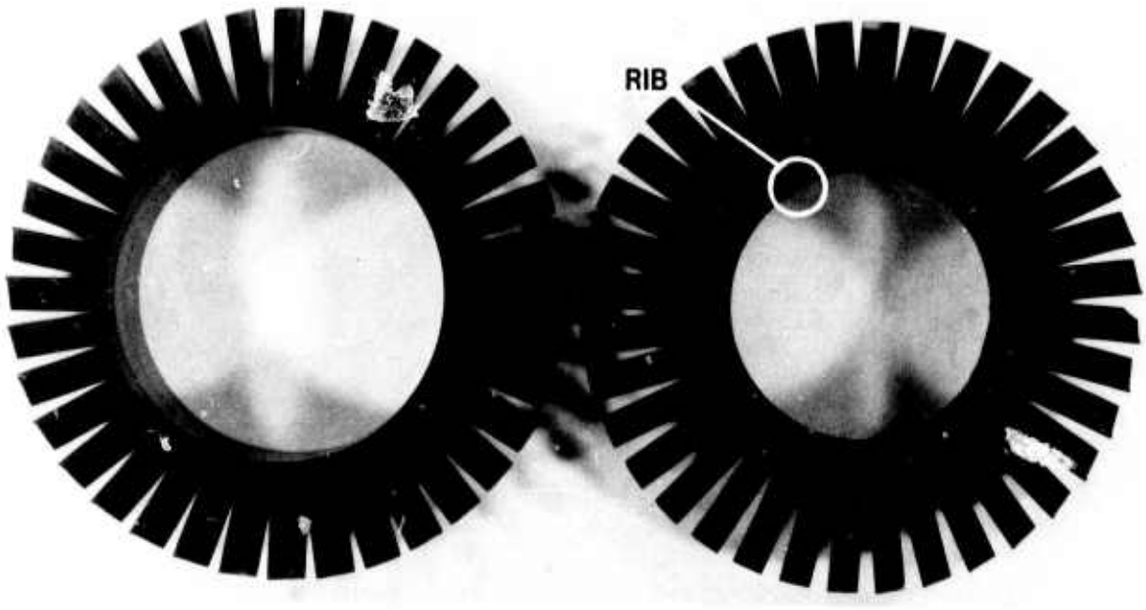

Figure 3.7 Blade Rings with and without Center Rib

As a check to determine if the rib had an effect on the measured blade failure load, two blade rings were tested in the following manner. Half of the blades were loaded to failure with the rib in place. After removal of the rib, the remaining blades were loaded to failure. In both cases, the blade loads with the center rib intact were significantly higher than with the center rib removed. These results are summarized in Table 3.5.

TABLE 3.5
Effect of Rib On Blade Bend Load

Blade Ring #	No. of Blades	Weibull Characteristic Load (lbs.)	Hub Configuration
2249	12	80	Rib in
2249	9	69	No Rib
2637	14	87	Rib in
2637	14	76	No Rib

The final hot pressed configuration introduced yet another blade ring support. In this configuration the blade ring is supported over its full width by the solid hub. It was anticipated that the failure loads would be effected and thus negate the usefulness of the before/after comparisons.

Failure of the before/after blade bend test to provide a satisfactory measure of blade ring degradation led to the evaluation of four material characteristics or properties (color, microstructure, hardness and phase composition).

To evaluate color, microstructure, and hardness, polished cross sections of before and after blades were made. The polishing was performed using a series of SiC grinding discs followed by polishing with 1 micron Linde C Al_2O_3 followed by 0.3 micron Linde A Al_2O_3 on a hard-backed polishing cloth.

Color

The color of the polished blade cross section was determined by visual examination. The results are summarized in Figure 3.8. In general, as hot pressing temperature and/or time at temperature increases, a color change occurs. The noted color change from black to light gray correlated well with strength degradation.

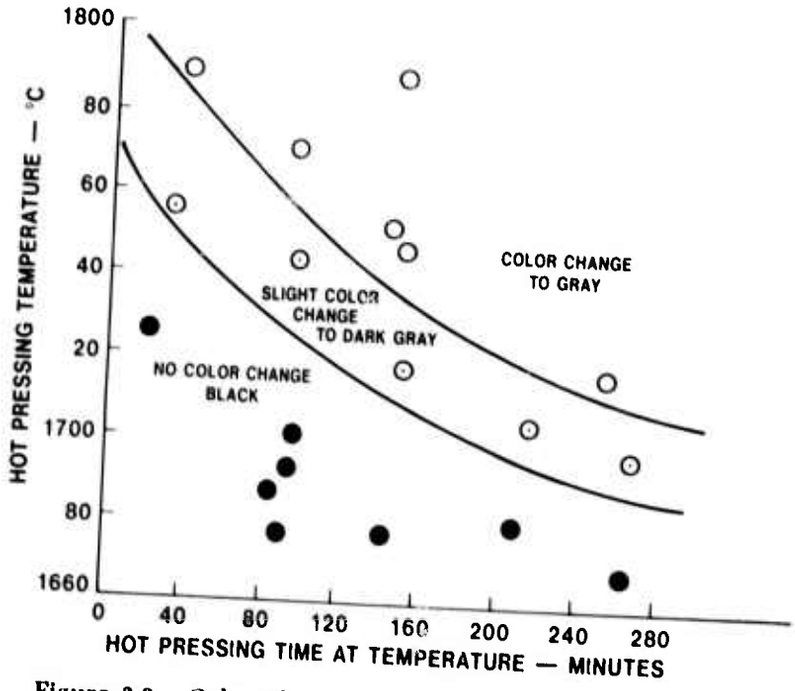

Figure 3.8 Color Change Versus Hot Pressing Parameters

Microstructure

A comparison of typical before and after microstructures of reaction bonded silicon nitride (Figure 3.9) showed two important results. The after microstructure contained much more fine, interconnected porosity. Hence the gray color. The presence of this increased porosity can be related to hot press bending conditions as shown in Figure 3.10. Also noted was the large clusters of second phase material. This second phase was usually, but not always, associated with a metallic phase. Figure 3.11 shows that below 1700°C no second phase formed while above this temperature the results were mixed.

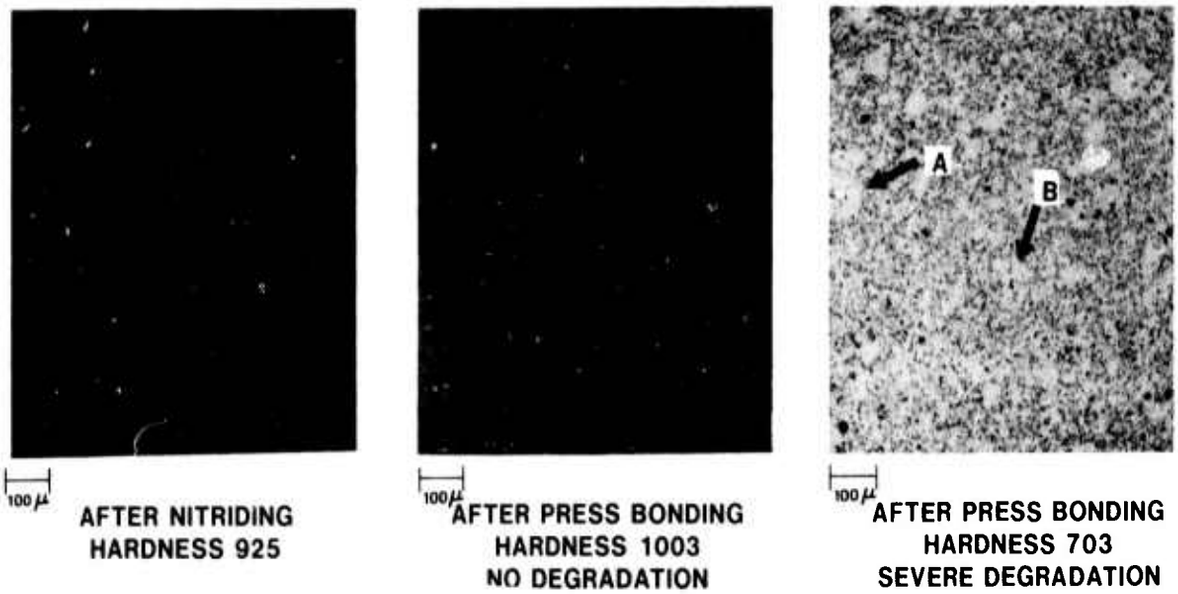

Figure 3.9 Typical Micrographs of Rotor Blades

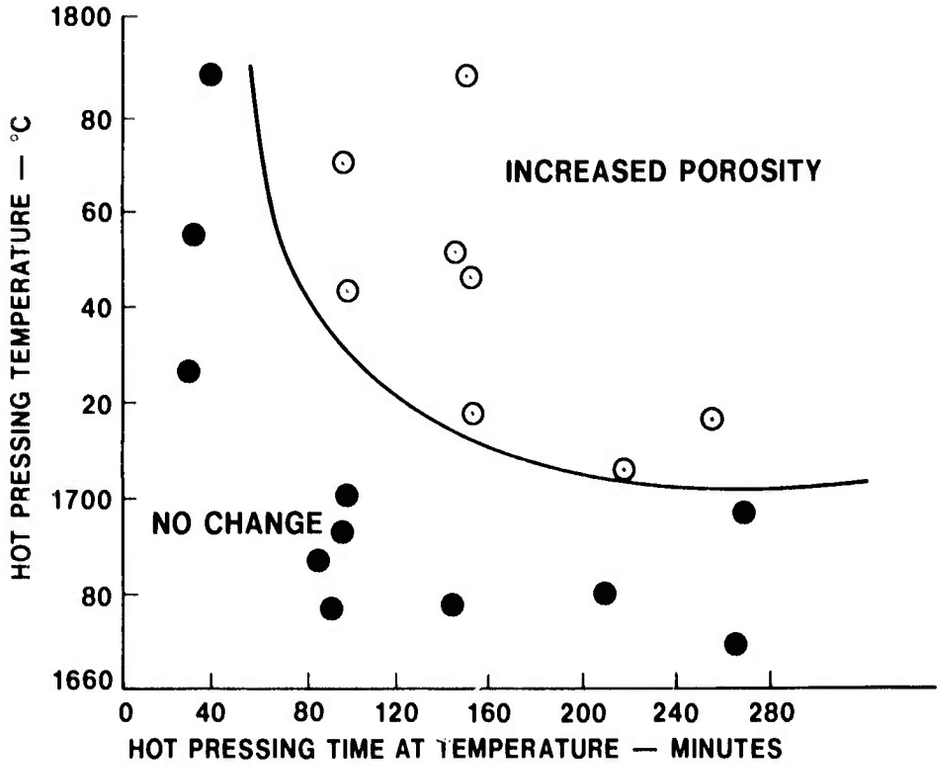

Figure 3.10 Change in Porosity Versus Hot Pressing Parameters

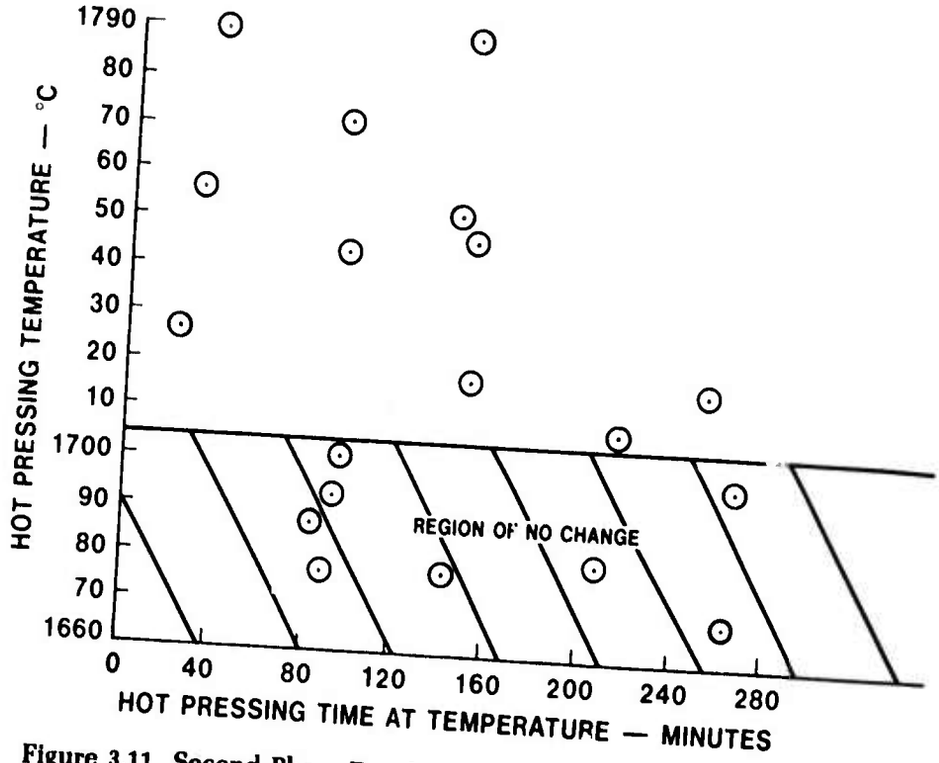

Figure 3.11 Second Phase Development Versus Hot Pressing Parameters

Hardness

The hardness of the blade ring material appeared to be a possible method to quantitatively describe the general microstructural appearance. Hot pressed silicon nitride has a hardness of 1700 kg/mm^2 while reaction bonded silicon nitride exhibits hardnesses of 900 to 1300 kg/mm^2[16]. It was assumed that changes in the microstructure (especially the porosity) would effect the hardness value. This was shown to be true for the samples shown in Figure 3.9. However, the hardness data in general only yielded a rough correlation to porosity. It was further assumed that hardness should show a correlation with the strength of reaction bonded silicon nitride. Figure 3.12 shows the relationship between hardness and characteristic blade bend load.

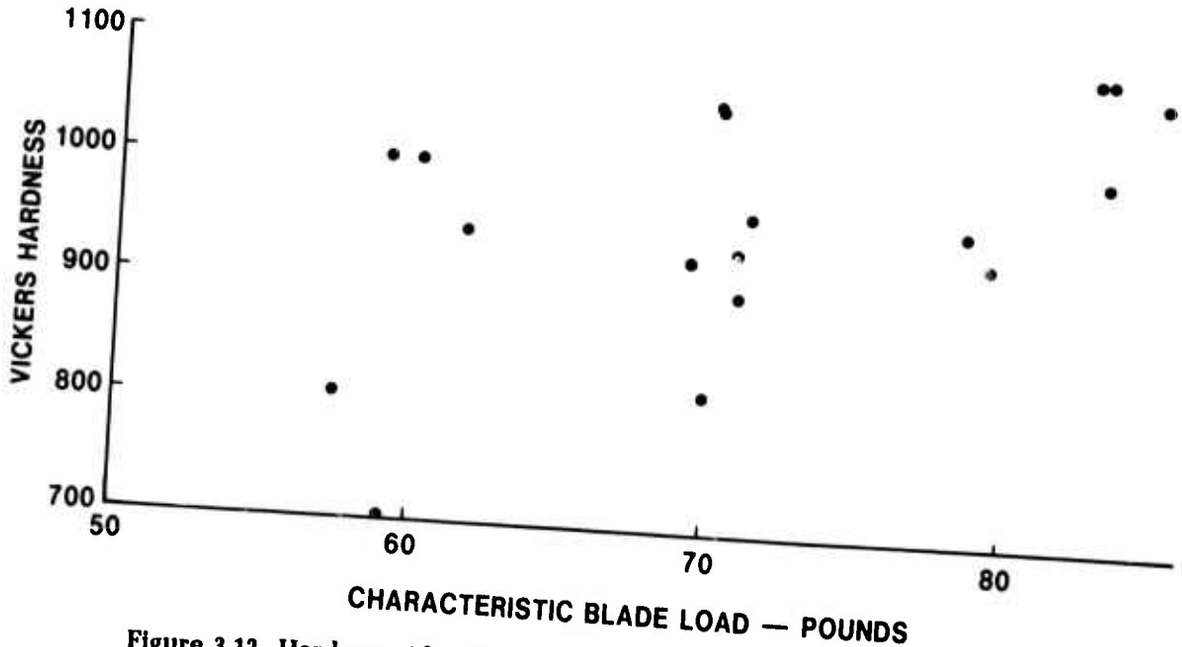

Figure 3.12 Hardness After Hot Pressing Versus Characteristic Blade Load

Phase Composition

The phase composition of the blade ring material was determined using an x-ray diffraction technique described by Mencik and Short[17]. The major observation was that the α silicon nitride transformed to β silicon nitride with increasing hot pressing times and temperatures as shown in Figure 3.13.

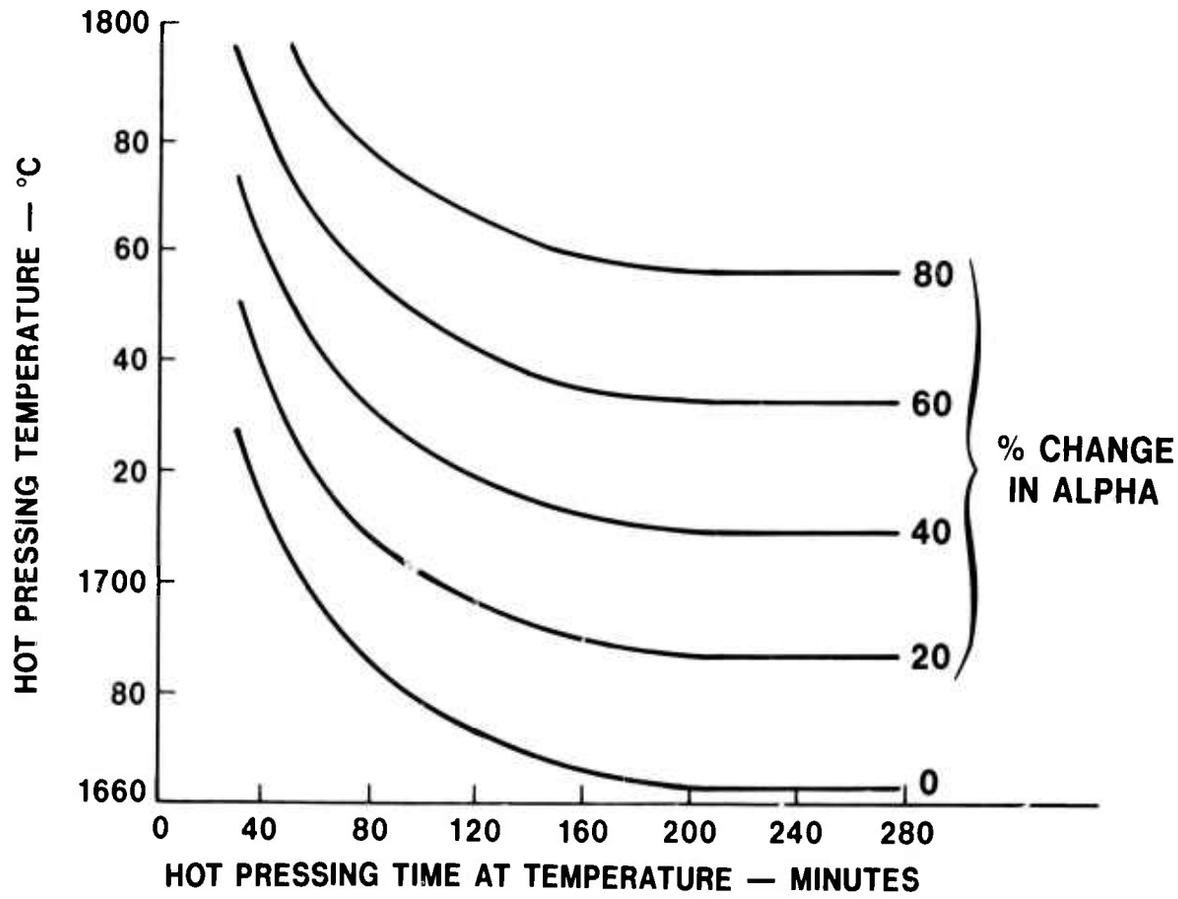

Figure 3.13 Percent Change in Alpha Versus Hot Pressing Parameters

A linear regression analysis of the data showed that the percent change in the α silicon nitride ($\%\Delta\alpha$) can be expressed as a function of the initial α silicon nitride composition and the hot pressing time and temperature. The derived relation was:

$$\%\Delta\alpha = -1604 - .196t + 47 \ln t + .846\,T - .156\alpha_I$$

$$\%\Delta\alpha = \frac{\%\alpha_I - \%\alpha_F \times 100}{\%\alpha_I}$$

where t = hot pressing time
T = hot pressing temperature
α_I = initial α Si_3N_4 composition
$\%\alpha_F$ = final αSi_3N_4 concentration

A correlation coefficient of 0.94 was achieved with this empirical relation.

3.3.2.3 DETERMINATION OF PERCENT STRENGTH DEGRADATION

The study results showed that changes occur in the reaction bonded silicon nitride as a result of hot press bonding.

Of prime concern was a degradation in strength. The study, however, did not yield before and after hot pressing strength values which could directly quantify the experienced degradation. Less direct quantification was attempted by evaluation of four other before/after parameters – color, hardness, microstructure and % phase composition.

The percent phase composition parameter (%αSi_3N_4) was of particular interest in the quantification attempt. Figure 3.14 presents a plot of blade bend load versus %αSi_3N_4 after hot pressing.

It can be seen that for any %αSi_3N_4, a maximum blade bend load was obtained and this maximum load increased as the %αSi_3N_4 increased. If it is assumed that this is an upper bound for the plot of blade bend load versus %αSi_3N_4 and that data points below this upper bound represent the effect of increased flaw size, then the upper bound defines the maximum load obtainable for a component with minimum flaw size.

Since the blade bend load reflects strength capability, a relationship for determining degradation was established. For example, if the %αSi_3N_4 before hot pressing is 80% and after hot pressing is 60%, then a 9% strength degradation is predicted (Figure 3.14).

Converting the data in Figure 3.13 utilizing the relationship established in Figure 3.14 resulted in the strength degradation versus hot pressing parameters (time and temperature) presented in Figure 3.15.

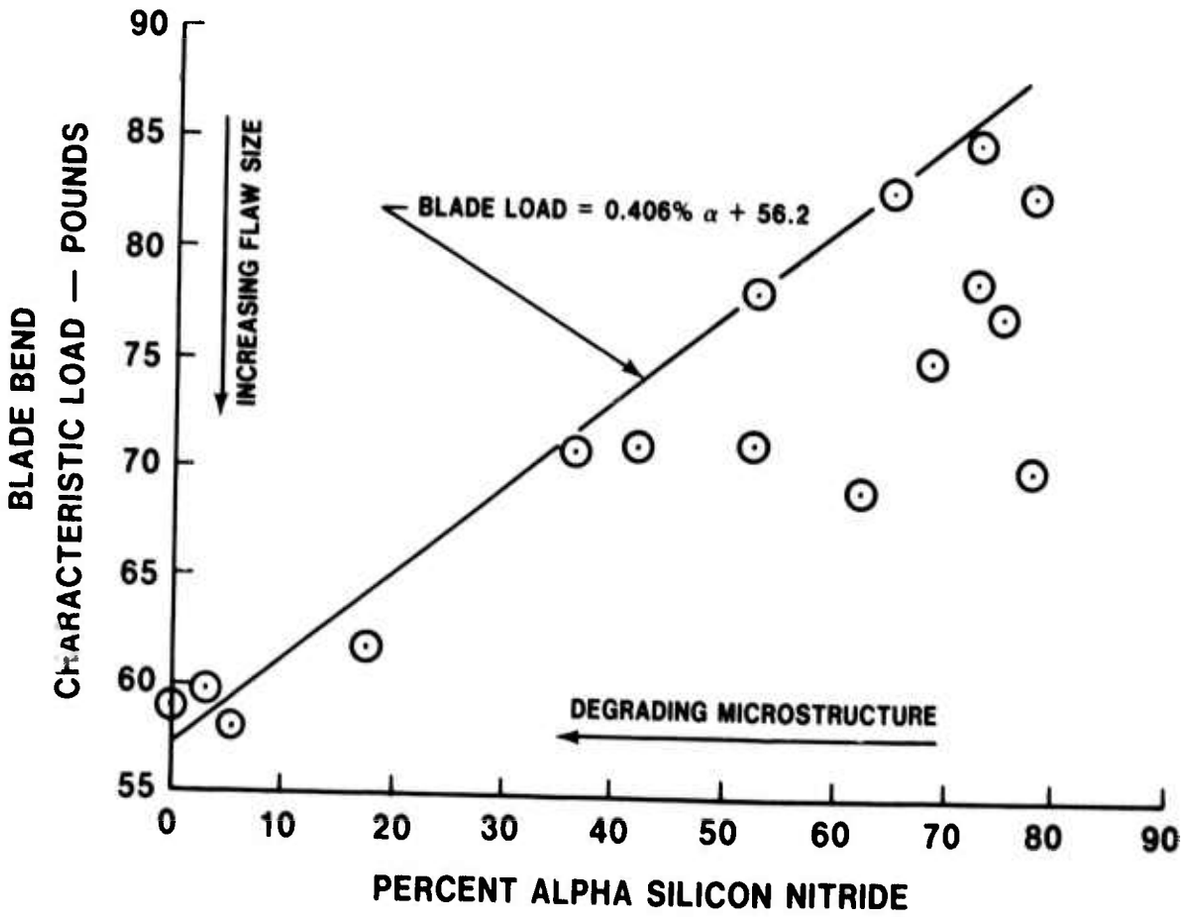

Figure 3.14 Blade Bend Load Versus Percent Alpha Silicon Nitride After Hot Pressing

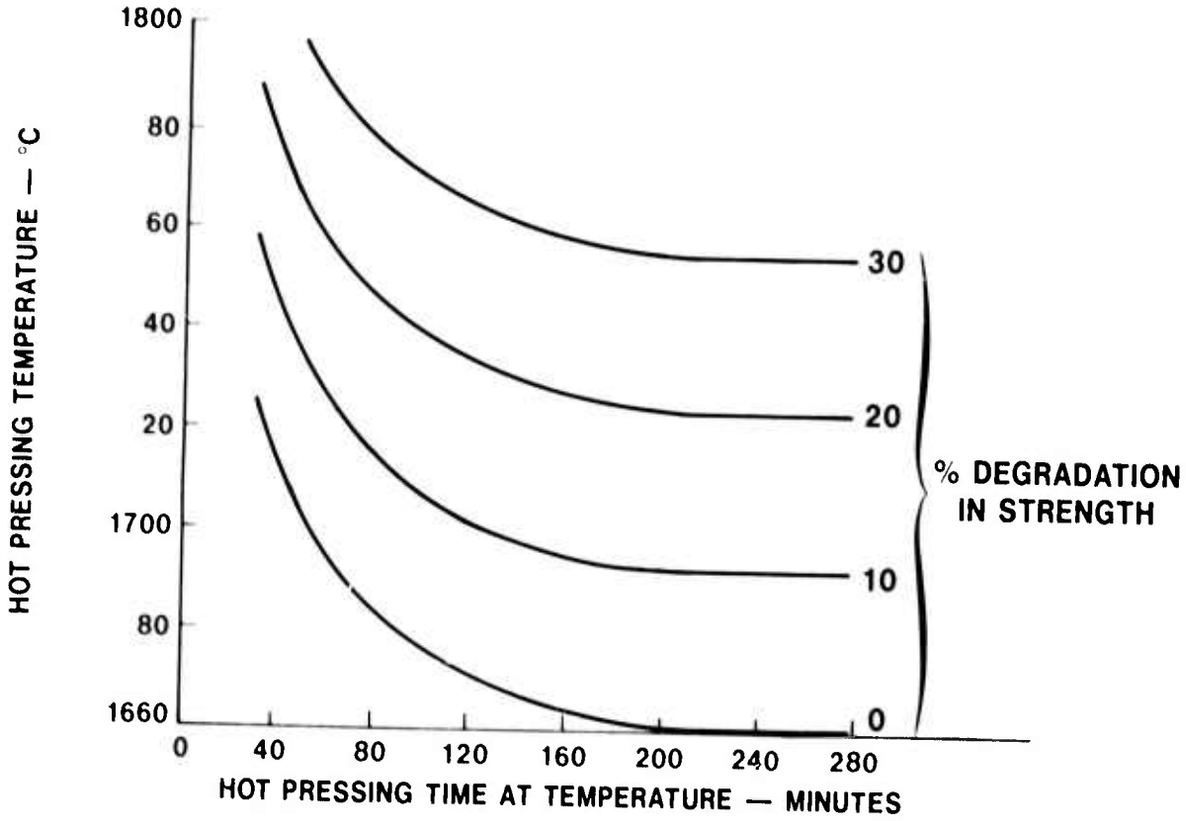

Figure 3.15 Percent Degradation in Strength Versus Hot Pressing Parameters

Of particular importance is the area under the zero percent strength degradation curve which now defines a region in which hot pressing can be conducted with no expected degradation.

3.4 SUMMARY AND CONCLUSIONS

The last interim report[13] hypothesized that the mechanism for the degradation of the reaction bonded silicon nitride during hot press bonding was silicon nitride dissociation. During this reporting period it was determined that the α to β conversion of silicon nitride was a good measure of the time/temperature seen during hot pressing which resulted in a degradation of the microstructure which in turn resulted in degraded strength. Since dissociation was the controlling degradation mechanism, it would be expected that a minimum temperature/time at temperature condition would exist where no degradation occurs. The study has defined a region of zero degradation. In addition, the study results provide for the determination of the amount of degradation for any chosen set of hot pressing parameters.

4.0 CERAMIC PROCESSING TECHNOLOGY

Introduction

Two major areas of improvements in ceramic processing technology were addressed in this portion of the program. These were (1) improvements in the quality of injection molded blade rings for the duo-density rotor by the application of additional process controls intended to reduce or eliminate the evidence of molding flaws and (2) improvements in the press bonding of duo-density rotors by replacing the wedge/blade-fill system with a hot isostatic media.

The blade ring molding program was based upon molding a matrix of blade rings in several experimental phases. Each phase was designed to explore molding variables available through the use of new adaptive process control equipment. This equipment is used to control the flow of material into the molding die cavity. A closed loop system of electronic control, high response (120 Hz) Hydro valve, hydraulic pressure sensors and ram position indicator are utilized to vary the injection velocity and hold pressure of the injection molding machine. Closer control of injection velocity and hold pressure may reduce trapped gas bubbles, knit lines and "molded-in" stress in injection molded blade rings. Since the relatively short time available under this project would not permit the completion of many phases if the blade rings were to be completely processed (i.e., burn-out, nitriding, post-nitriding inspection), blade ring quality was evaluated entirely using as-molded components. Microfocus X-ray equipment was utilized to assist this evaluation and to help locate subsurface defects in the blade rings.

The press-bonding program was based upon the use of materials which would be fluid at hot pressing temperatures (i.e., glasses, metals) and could then be mechanically loaded to apply isostatic pressure upon the blade ring in a radial, inward direction, thus counteracting the outward force used to densify the hub material. Potential advantages of such a system include simplified tooling, reduced in-process time now needed for blade filling, and more uniform inward pressure on the blade ring.

4.1 ROTOR BLADE RINGS

Background

The Ceramic Turbine Rotor Technology Program developed ceramic material and process technology and included both destructive and non-destructive tests to identify problem areas and evaluate process improvements. Two investigations conducted on injection molded blade rings during the previous reporting period[13] were cold spin testing to destruction and room temperature MOR testing of the rim material.

Room temperature MOR tests of bars cut from the rim area of four reaction bonded silicon nitride blade rings gave characteristic strengths of 25.4 to 33.8 ksi with Weibull slopes ranging from 2.6 to 6.8. Subsurface flaws were responsible for the low Weibull slope which was improved if the flawed test bar data was excluded from the analysis as shown in Table 4.1[13].

TABLE 4-1

Weibull Parameters

Blade Ring No.		All Bars	Flaw-Free Bars
2047	$\sigma\theta$	30.1 (27.8-32.7)	30.1 (27.8-32.7)
	m	6.8 (4.2-8.9)	6.8 (4.2-8.9)
	n	13	13
2155	$\sigma\theta$	33.5 (30.6-36.8)	33.8 (30.7-37.3)
	m	5.7 (3.6-7.5)	6.7 (3.7-9.1)
	n	14	10
2251	$\sigma\theta$	27.0 (23.4-31.1)	—*
	m	3.7 (2.3-3.1)	
	n	14	4
2256	$\sigma\theta$	25.4 (21.2-30.4)	31.1 (24.0-41.8)
	m	2.6 (1.7-3.3)	4.2 (1.5-6.2)
	n	17	5
Combined Values	$\sigma\theta$	29.1 (27.4-30.8)	31.6 (30.1-33.1)
	m	4.0 (3.3-4.6)	6.7 (5.1-8.2)
	n	58	32

$\sigma\theta$ = Characteristic M.O.R. (ksi) — strength at 63.2% failure rate
m = Weibull Modulus
n = Number of bars
Numbers in parenthesis represent the 90% confidence band.
* Too few specimens to permit Weibull analysis.

Four duo-density turbine rotors were tested in the cold spin pit to evaluate the hot pressed to reaction bonded bond joints and the effect of I.D. voids in the blade ring on blade failure speeds. Neither the I.D. voids nor the bond joints failed up to speeds of 96,900 rpm. However, blade failures which occurred from 38,440 rpm to 89,070 rpm were related to surface and internal flaws in the airfoils of the type shown in Figure 4.1. Blades which were free of obvious flaws failed in the 90,060 to 96,900 rpm range as shown in Figure 4.2. Flawed and unflawed failure distributions of the best and the worst rotor are shown in Figure 4.3 along with a failure distribution representing the state-of-the-art in 1975. All four distributions show significant improvements in rotor processing, however, it is also apparent that substantial improvement would be recognized with the elimination of large, process induced blade flaws[13][14]. Section 4.1.1 of this report presents the results of work during this reporting period directed towards this goal.

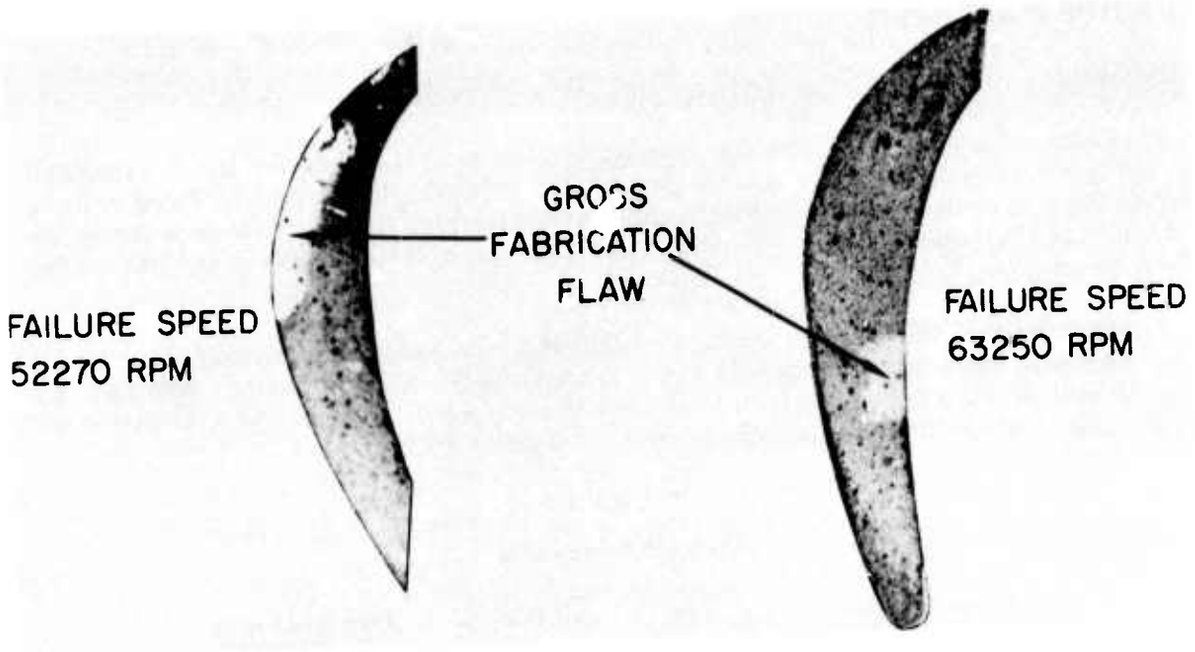

Figure 4.1 Typical Fracture Surfaces with Gross Fabrication Flaws

Figure 4.2 Typical Fracture Surfaces without Gross Fabrication Flaws

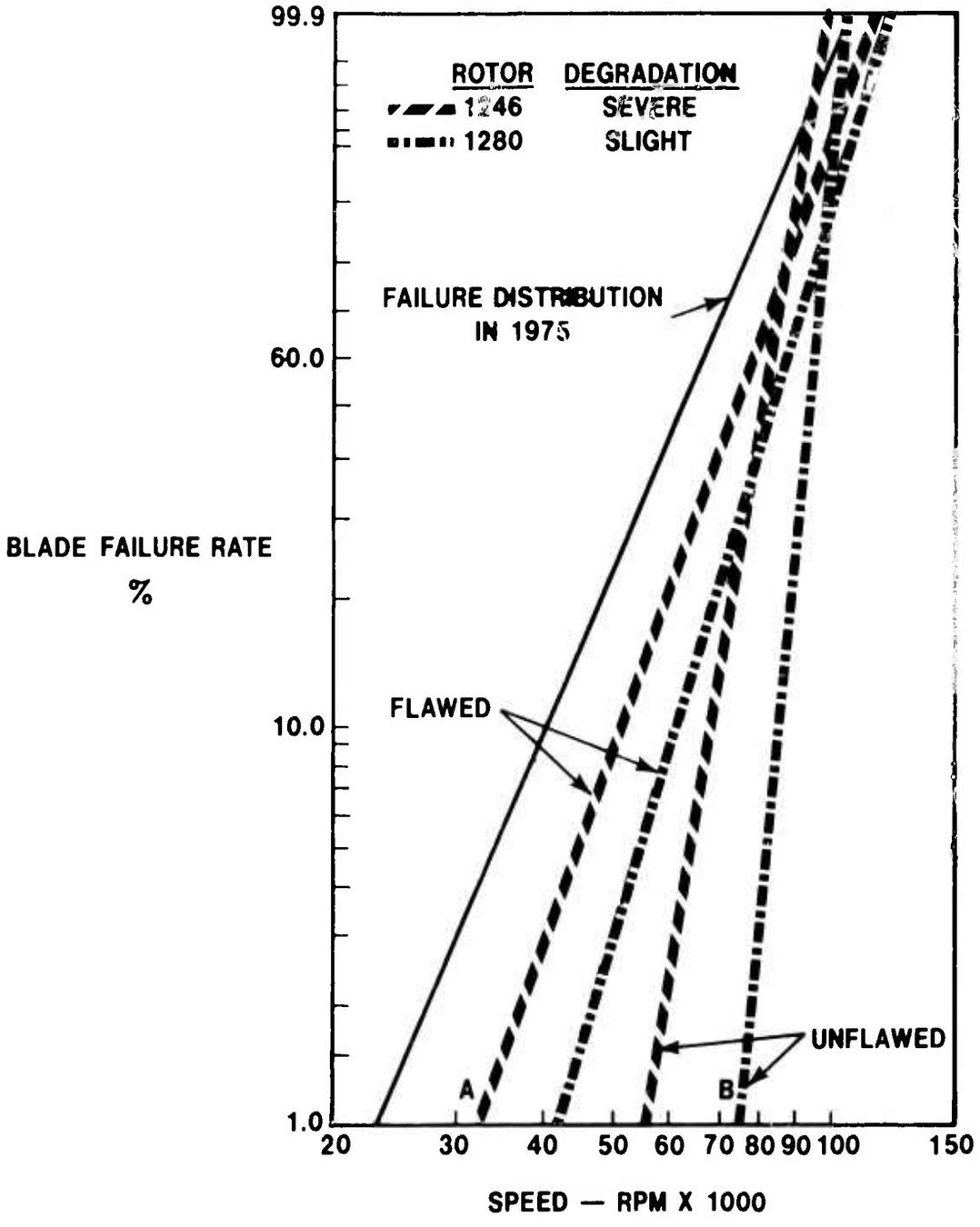

Figure 4.3 Weibull Distributions of Blade Failures

4.1.1 INJECTION MOLDING STUDIES

A Reed Prentice 450 TC plunger type injection molder was used for the injection molding of rotor blade rings. Control of the molding process was accomplished by a solid state machine function control unit, shown in Figure 4.4. This unit controls all machine timing and sequencing functions. Tooling utilized to mold the rotor blade rings is semi-automated and is shown in Figure 4.5. The operation of the molder, control, and tooling have been previously discussed[10, 11, 12].

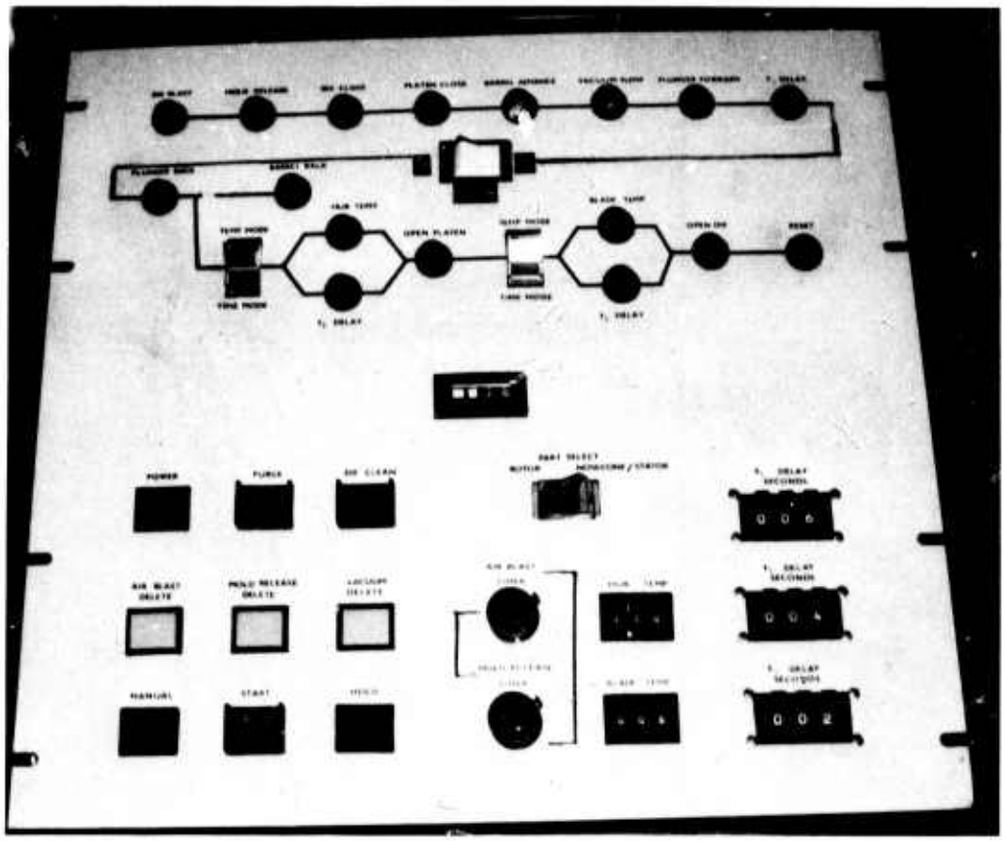

Figure 4.4 Control Console for Automated Injection Molding System

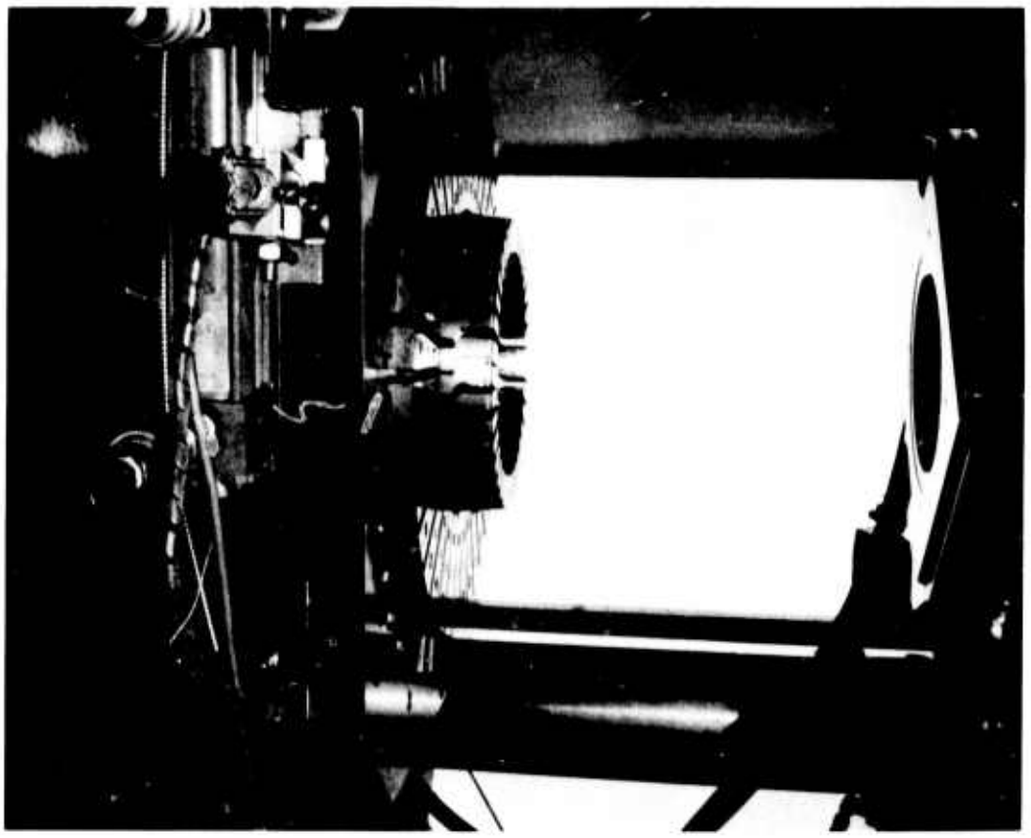

Figure 4.5 Tooling for Injection Molding Blade Rings

In order to study the effect of additional control during the injection portion of the molding cycle, an adaptive process control unit was added to the system. This unit, shown in Figure 4.6, consists of four control modules. The first module controls cushion, shot size, hold time, pressure limit, shot size correction and decompression. This module also selects the mode of flow control operation based upon type of material injected and injection cycle (i.e. thermoplastic or thermoset).

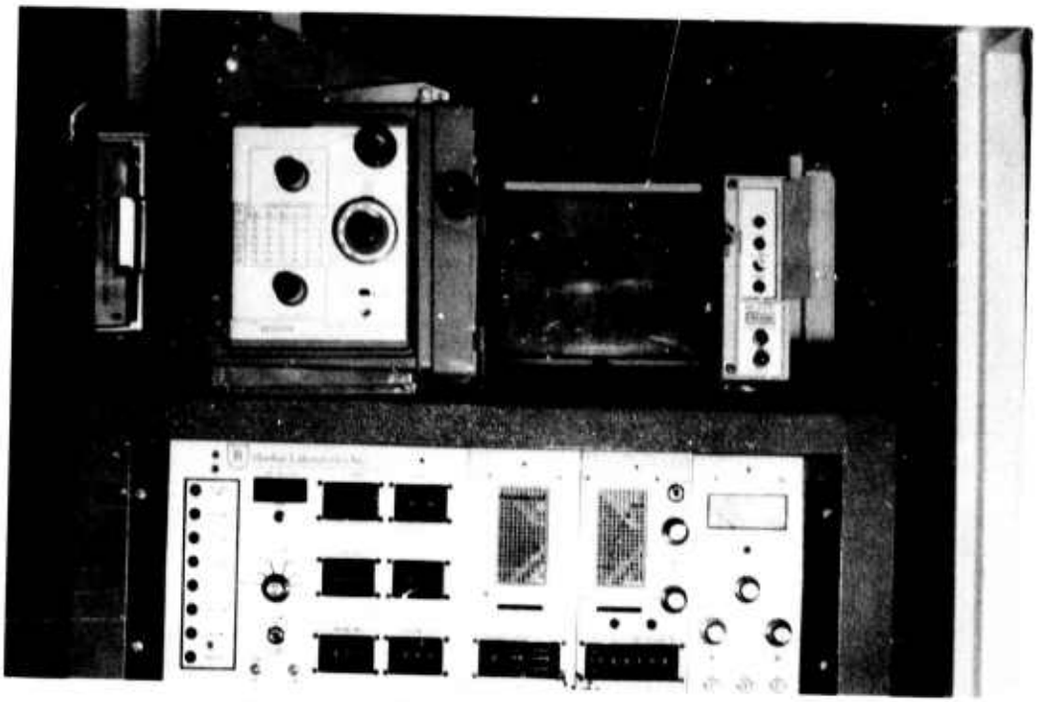

Figure 4.6 Hunkar Flow Control Equipment

The second module controls the material injection velocity. Injection velocity will determine the type of flow front formed in the die cavity. Low velocity is desired in areas where the material must change direction to maintain a uniform front. Velocities which are too high will cause non-uniform flow, i.e., jetting with its' associated knit lines and entrapped gas. Excess velocity will also lead to shear heating and its associated shrinkage cracks and part sticking problems. Velocity as controlled by the Hunkar unit varies as a function of ram position with the maximum velocity (100%) being equal to 10 inches/second. A 10 position pin panel can be set up to produce varied injection rate vs. ram position values. Each of the 10 injection profile increments can range in size from 1 inch to 0.01 inch. As the injection ram enters the zone defined by each pin, the hydraulic flow is modulated to achieve the flow rate set for that zone. Figure 4.7 shows the pin vs. ram position relationship.

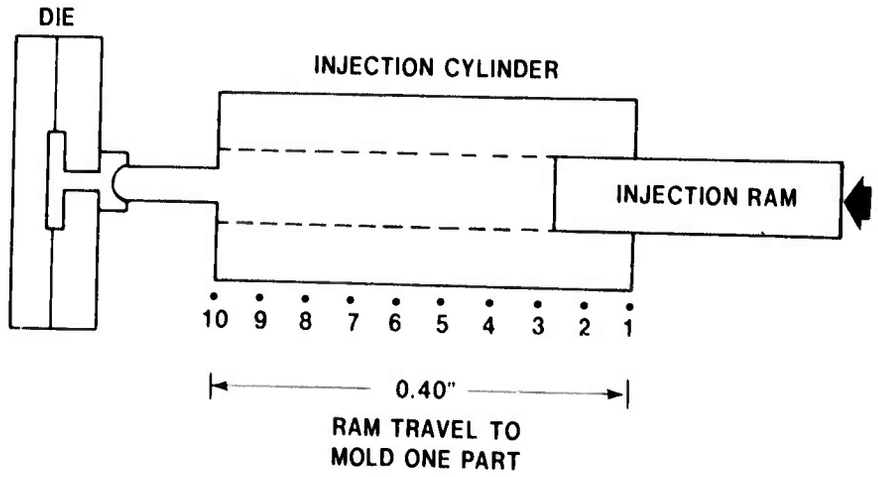

Figure 4.7 Relationship of Injection Patch Panel to Ram Position

The third module controls holding pressure exerted on the material in the cavity after injection is complete. The pin panel in this module is based upon 10 increments of time, whereas the injection panel is related to 10 increments of ram position. The overall hold time is selected and each increment is equal to t/10 of the selected value. The pins are arranged to yield a percentage of maximum machine hydraulic pressure during each increment. The point at which injection profile is complete and hold profile is initiated is determined by either a preset cavity pressure or a predetermined ram position. When this value or position is achieved, injection ends and hold begins. Once the hold expires, control is returned to the machine function control system for machine movement required to open the tool and prepare for the next shot.

The fourth module monitors the process and provides controlled outputs for cavity pressure, hydraulic pressure, or ram velocity. An oscilloscope is used to generate cavity pressure vs. ram position, hydraulic pressure vs. ram position or ram velocity vs. position curves.

A theoretical ram position vs. cavity pressure plot is shown in Figure 4.8. Note that as the ram moves through the filling of the sprue and runner, the pressure in the cavity is zero until material enters the tool. The cavity pressure then builds slowly until the tool is nearly full, at which point a rapid pressure rise is seen (packing). At the peak cavity pressure level the transition is made to hold pressure and the cavity pressure falls as the material shrinks. The ram continues to advance in the after-feed mode which replenishes volume lost to shrinkage. When the pressure is removed, the cavity pressure returns to zero and the part is removed from the tool.

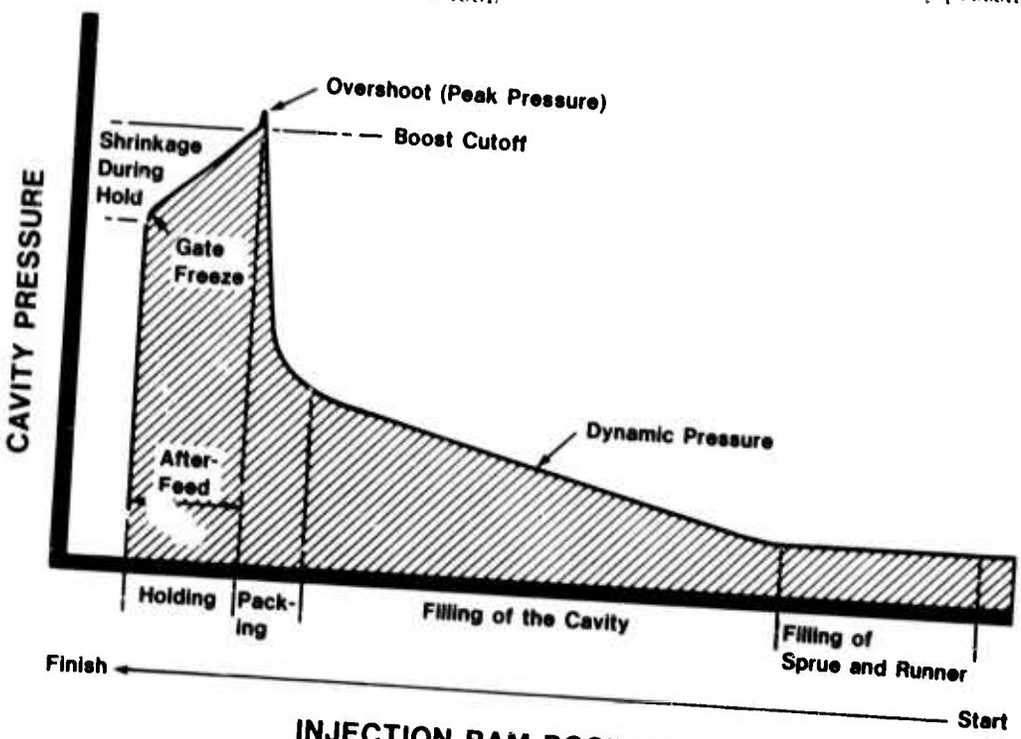

Figure 4.8 Schematic of Cavity Pressure Versus Ram Position

In theory, flow control of molding is desirable for several reasons. The injection molding process has many variables which affect part quality. The control of these interrelated variables such as temperature, pressure, volume and material viscosity variation is complex and virtually impossible to control manually. A relationship between variables is expressed by Spencer and Gilmore[18] in the following equation: $(P + \Pi)(V - w) = RT$.

P = external pressure (applied force)
Π = internal pressure of material being molded (material constant)
V = volume of material pressurized
w = absolute volume (material constant)
R = gas constant
T = temperature constant } From Van der Waals' equation

It can be seen that volume adjustments can be used to compensate for temperature and viscosity changes in the molding compound. Control and variation of flow and hold pressure make precise metering of volume possible.

In previous rotor blade ring molding runs, several types of flaws were noted during subsequent inspection and testing. Rim voids, blade voids, and planar crack-like flaws in blades were observed. One source of voids was deemed to be caused by uncontrolled flow and holding pressure on the material during injection. Controlling material flow into the tool reduces turbulence which tends to cause areas of poor fill, knit lines, and entrapped gas pockets. Proper holding pressure tends to "squeeze" voids from the part and also after-feeds the thicker portions of the part to eliminate shrinkage voids. Holding pressure may also be critical in eliminating the hard-to-detect planar defect. One possible cause of this type of defect is a stress build-up caused by uncontrolled hold pressure. If the outer skin of the blade solidifies at a high holding pressure and the inner skin solidifies at a lower pressure, the resulting density gradient will cause differential shrinkage and result in internal blade stresses. Normal constant hold pressures naturally result in this condition because as the viscosity of the cooling molding material increases, the system fails to increase system pressure to maintain constant cavity pressure. The controlled holding portion of the adaptive control system will allow a profiled hold, thus cavity pressure can be varied as required to minimize stress in the part.

Molding experiments performed as part of this program were divided into five phases. Phase One used the monitoring capabilities of the adaptive process control unit to determine the cavity pressure vs. ram position relationship of the molding system without using the flow control during injection. Thirty rotor blade rings were molded at conditions previously determined to yield visually good parts. These rotors were X-ray and visually inspected and judged to be of a quality level comparable to those molded just prior to the beginning of these experiments.

Cavity pressure traces for the rotors molded with no flow control exhibited large variations in curve shape and pressure level attained. An example of curves generated during four successive molding operations are seen in Figure 4.9. Records were kept for each blade ring molded with respect to visual quality and the ease with which the component could be removed from the molding tool. Ease of removal is related to shrinkage prior to tool opening, and therefore may relate to molding stress level in the molded blade ring. A cavity pressure vs. ram position curve which represented those blade rings observed to be best in surface finish and ease of removal from the die was selected for duplication in the Phase Two work. The parameters used in molding are as follows:

Phase I parts were as follows:

Material Temperature (°F)	Zone 1	200
	Zone 2	200
	Zone 3	200
	Nozzle	80
Sequence Times (Seconds)	Inject	3
	Hold	6
	Open die	7
Die Temperature (°F)	Moveable	90
	Stationary	85

The adaptive control unit was in the "monitor only" position.

No X-ray results from the microfocus unit were available at this point because the unit was in the preliminary set-up stage. Microfocus X-ray results became available later and are summarized in Table 4.2. The Microfocus unit revealed more void type defects than previously shown by conventional X-ray. As would be expected and confirmed from previous test data, voids and planar defects in the blade sections near the rotor rim were more critical than those in the lower stressed tip region of the blade. Therefore, elimination of voids in the inner one-third of the blade was given primary effort in this program. The number of voids per blade ring shown in Table 4.2 refers to blade voids in the inner one-third of the blade.

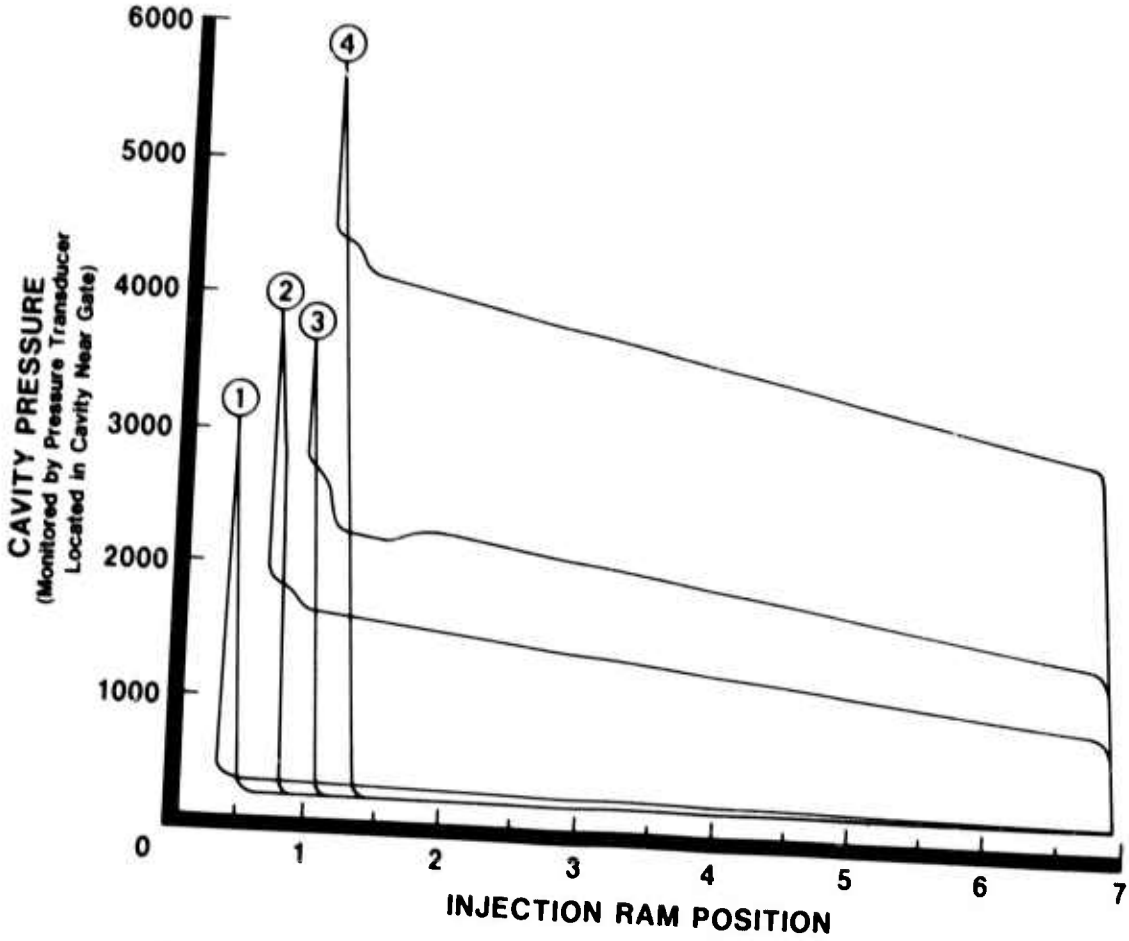

Figure 4.9 Typical Cavity Pressure Profiles During Phase One

TABLE 4.2

X-RAY RESULTS OF PHASE I

Total Number of Blade Rings	Total Number of Voids in Base Sections*	Average Number of Voids per Blade Ring
29	28	0.97

* in lower 1/3 of blades

Phase Two of the program utilized the capabilities of the adaptive process control to duplicate the cavity pressure vs. ram position curve determined to be optimum during Phase One. Once parametric adjustments were complete and the cavity pressure vs. ram position curve closely resembled the one selected, 25 rotor blade rings were molded for evaluation. The adaptive process control unit controlled the shape and magnitude of the cavity pressure curve much more closely than the standard machine controls used in Phase One.

An example of four sequential cavity pressure vs. ram position curves is shown in Figure 4.10. The surface finish and ease of removal for the molded rotors was more consistent during Phase Two controlled molding. Molding parameters used during Phase Two included all those held constant under Phase One and the following adaptive process control unit parameters. Fill stroke was nine inches with a cushion of 0.6 inch. Cavity pressure limit was 1200 psi, this level when achieved shifts the control from the injection mode to the hold mode. Injection profile was a constant 100% of machine capacity for the entire 9" stroke. Hold pressure was ramped from 800 psi to 1300 psi over a 6 second hold time.

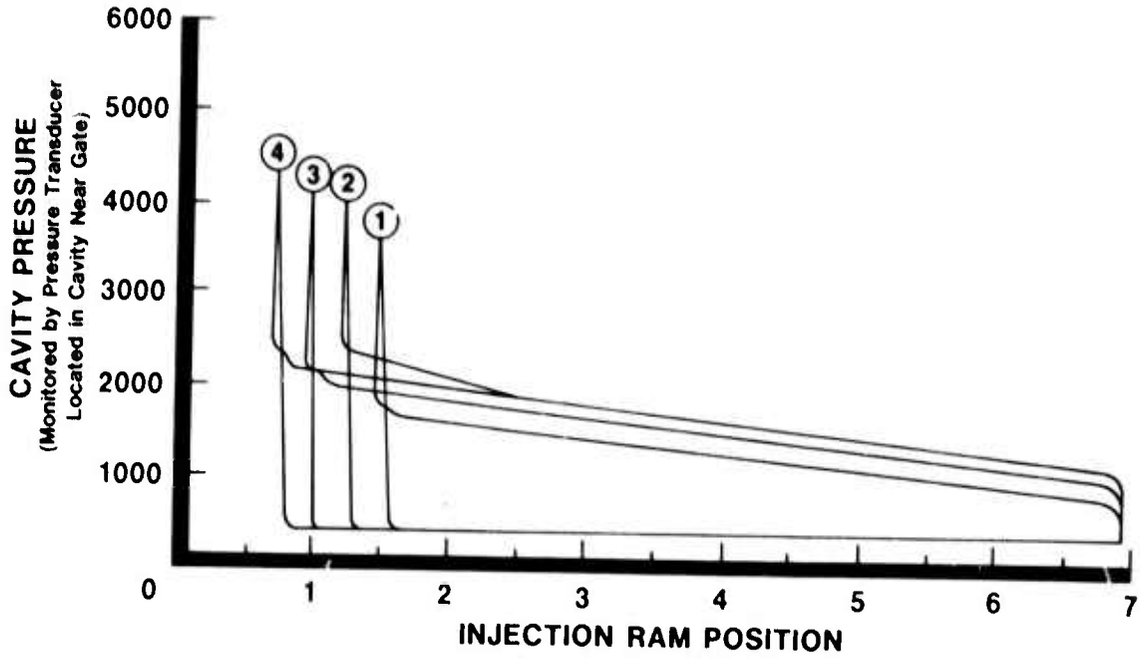

Figure 4.10 Typical Cavity Pressure Profiles During Phase Two

X-ray results for Phase Two blade rings are seen in Table 4.3. The X-ray results from Phase One and Two revealed that those conditions believed to yield best quality blade rings based on visual inspection did not coincide with optimum X-ray results. Although Phase Two parts had more defects, due to the parameters selected, they were more consistent from shot to shot.

TABLE 4.3

X-RAY RESULTS OF PHASE II

Total Number of Blade Rings	Total Number of Voids in Base Sections*	Average Number of Voids per Blade Ring
20	35	1.75

* in lower 1/3 of blades

Phase Three attempted to vary molding flow and hold pressure in an effort to reduce the number and size of void-type defects in the blade base section of the blade rings. The parameters held constant during the Phase Three study were identical to those used in Phase Two with the exception of fill stroke which was reduced to 0.50 inch with a cushion of 0.10 inch. Pressure limit and hold pressure were varied rather than held constant as was injection profile and program (hold) profile. The variable parameters used are shown in Table 4.4. Three rotor blade rings were molded at each point on the matrix. The resultant parts were visually inspected and evaluated by microfocus X-ray evaluation. It was noted from these results that high injection rates and moderate hold pressures resulted in a lower average number of blade base voids.

TABLE 4.4

X-RAY RESULTS OF PHASE III

(Average Number of Voids Per Blade Ring*)

Parameter →	Injection Velocity Profile (100% = 10"/Seconds)	
Parameter	% Machine Capacity	
↓	99%	35%
Hold Pressure (psi)		
2000	1.33	5.67
500	0.67	5.67
300	1.17	5.17
75	1.0	5.67

* in lower 1/3 of blades

The injection and hold profiles used in Phase Three were linear with a slope = 0. For example if injection rate was at 35% of machine capability, it was 35% for the entire fill of the rotor.

In order to vary injection flow in a nonconstant manner (i.e., slope of the control line ‡ 0) the shot size and corresponding region of fill had to be determined for each of the 10 zones of flow control. A study was run at this point to determine this relationship. In addition, control of the material remaining ahead of the plunger when the tool has filled, referred to as cushion, had to be achieved in order to assure the tool fill versus ram position relationship would be valid for each shot. Figure 4.10 shows uncontrolled cushion, while Figure 4.11 illustrates controlled cushion for cavity pressure vs. position curves on four consecutive shots. The varying X displacement shot to shot results from variable cushion. Note that the larger cushion reduces cavity pressure achieved for a given injection setting. Once more sophisticated flow programs are used, variable cushion would result in the wrong velocity of flow in any given die section due to the ram's displacement in relationship to the set points on the flow control curve.

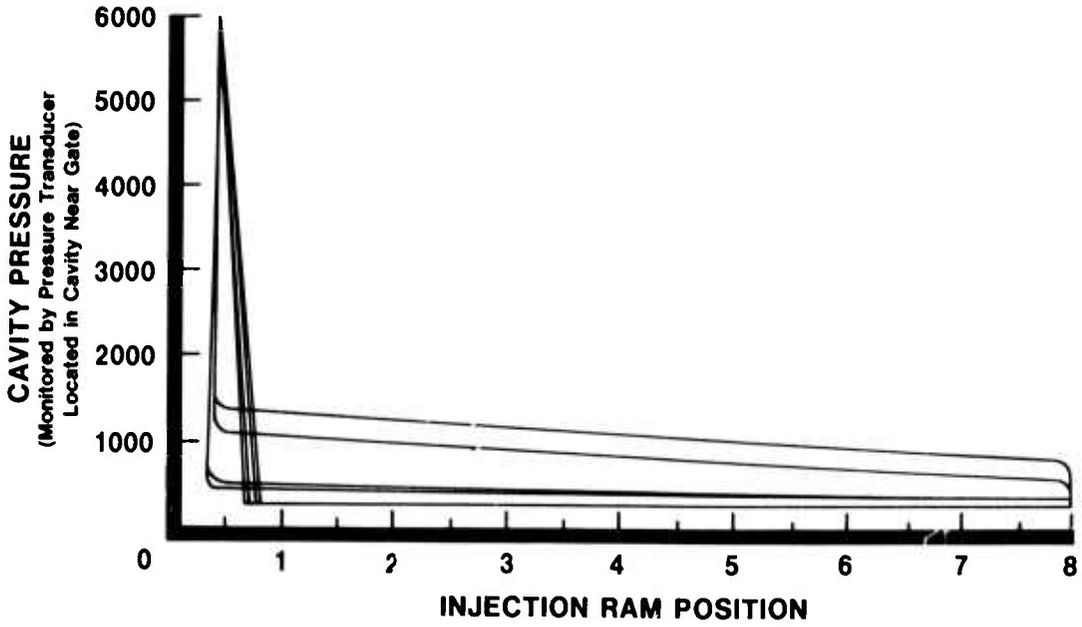

Figure 4.11 Typical Cavity Pressure Profiles with Controlled Cushion

In order to more accurately see the results of changing injection and hold profile values the X-(ram position) scale of the oscilloscope was expanded. The resulting curves were more easily interpreted. This change was needed to discern between subtle variations encountered from shot to shot under adaptive process control. As seen in Figure 4.11, prior to scale expansion, the curves for each shot appeared colinear. The expanded scale as seen in Figure 4.12 allowed differentiation between shots.

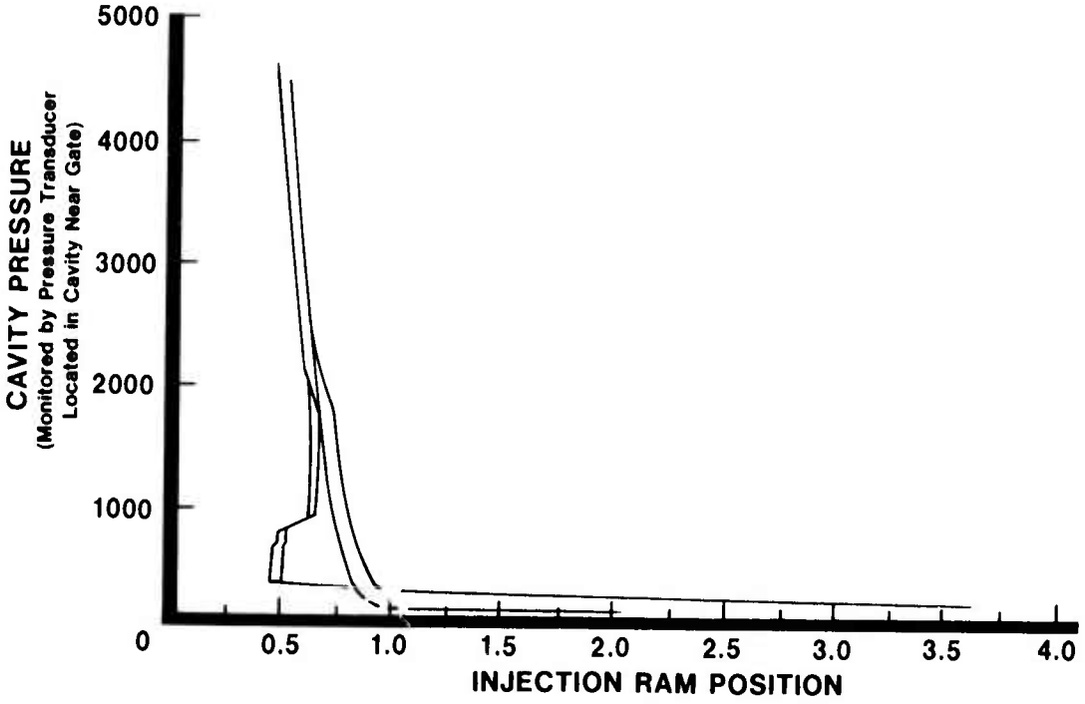

Figure 4.12 Expanded Osciliscope Scale

Based on the results of Phase Three, namely that fewer blade base voids existed at low hold pressures and high injection rates, a Phase Four matrix was developed to concentrate on the high injection and low hold pressure areas. Once again injection and hold profiles were linear with slope = 0. The parameters held constant were identical to those in Phase Three. The injection and hold parameters used in Phase Four are shown in Table 4.5. Cushion control was also utilized for this study as previously explained. As in Phase Three, moderate to low hold pressures and high injection rates yielded a lower level of blade base voids. With the cushion control the absolute level of voids also was decreased in the Phase Four matrix.

TABLE 4.5

X-RAY RESULTS OF PHASE IV

(Average Number of Voids Per Blade Ring*)

Parameter →	**Injection Velocity Profile (100% = 10"/Second)**		
Parameter	**% Machine Capability**		
↓	99%	70%	35%
Hold Pressure (psi)			
2000	0.33	0.67	4.33
1200	0.33	0	5
300	0	4.67	3.33

* in lower 1/3 of blades

To further optimize the relationship between injection rate, hold level and blade ring base voids, a Phase Five study was run based on the results of Phase Four. In an effort to approach the low hold pressure more gradually, a non-linear injection profile was used. The hold profile was retained as linear with slope = 0. The constant parameters for Phase Five were identical to Phases Three and Four. The injection and hold profiles which were varied are shown in Table 4.6. Injection was linear at the indicated level from pin 1 to pin 6 of the injection control patch panel. Injection rate was reduced in a linear form from pin 7 to 10 over the range from the indicated level to 35%. The 35% level was chosen from Phase Three as the minimum injection level required to maintain material flow into the tool.

TABLE 4.6

X-RAY RESULTS OF PHASE V

(Average Number of Voids Per Blade Ring*)

Parameter →	**Injection Velocity Profile (100% = 10"/Second)**		
Parameter	**% Machine Capability**		
↓	95%	75%	70%
Hold Pressure (psi)			
900	1.67	1.0	2.67
600	2.0	0.67	8.67
300	3.33	8.67	4.0

* in lower 1/3 of blade

From the X-ray results shown in Table 4.6, it can be noted that there were less blade base voids at the higher injection rates. The absolute level of voids was higher for Phase Four and the level of hold pressure required to minimize voids was higher. It appears that higher hold pressure compensates somewhat for the reduced injection rate. It was concluded that the reduction in injection velocity prior to hold was too abrupt and should be reduced or eliminated.

Summary/Conclusion

On the basis of these studies it is concluded that injection velocities of 75 to 100% of machine capacity with hold pressure from 300 to 1200 psi, significantly reduce the number of blade base voids in injection molded blade rings. The optimization of flow controlled injection will require much further experimentation. Control over the process afforded by the adaptive process control yields the level of injection uniformity required to carry out significant experiments in regard to material flow and its relation to molding defects.

It was also found that the iteration between molding variations and feedback from the Microfocus X-ray examination of the as-molded parts was indeed a useful method of attacking the problem of molding flaws. The Microfocus X-ray equipment itself was deemed to be considerably better than conventional industrial X- ray equipment for detection of small flaws. Further work iterating further process control variations with Microfocus X-ray examination should yield molded blade rings of significantly higher quality.

4.1.2 NON-DESTRUCTIVE EVALUATION

During previous reporting periods several N.D.E. techniques were assessed for the detection of flaws in complex shaped silicon nitride gas turbine components[11-13]. Table 4.7 shows the current results of this assessment. Infra-red thermography was not successful due to an inability to establish the necessary thermal gradient across the test piece[13]. The electrostatic method would only detect flaws in mechanically stressed regions and only relatively small portions of the rotor blades could be readily stressed by simple blade loading[13]. Both computerized tomography and holosonic N.D.E. techniques would require considerable development time. Ultrasonic inspection is useful for small flaw detection in simple shapes but this technique is currently not employed for the very complex shaped parts such as the airfoils of a gas turbine rotor. The microfocus x-ray technique showed the most promise and the equipment was procured[13].

TABLE 4.7

ASSESSMENT OF NDE TECHNIQUES CONSIDERED FOR FLAW DETECTION IN REACTION BONDED SILICON NITRIDE COMPONENTS

CRITERIA	N.D.E. TECHNIQUE						
	Microfocus X-ray	Infra-red Thermography	X-ray Tomography	Electrostatic Method	Holosonic Method	Mechanical Load Testing	High Frequency Ultrasonic
1. Capability of detecting flaws in complex parts, i.e turbine rotor	Large flaws 200μ	Not Feasible	Expect improved detection capability over conventional x-ray	If flaw is put under load	Feasibility demonstrated only on simple disk and rectangular shapes.	Detects flaws through failure. Not a direct indication of flaw.	Potentially useful for small flaws (25μ) in simple shapes.
2. Provides rapid examination of complex parts	Yes, may be improved with panoramic X-ray tube.	N.D.*	Very attractive. Can store data for pictorial or numerical rapid output.	N.D.*	N.D.*	Yes	Currently not feasible for complex shaped parts.
3. Development time and cost estimates.	Reasonably short time, low development and equipment cost.	N.D.*	Very expensive—particularly equipment costs.	Short development time, potentially inexpensive.	Long development time; high equipment costs.	Inexpensive	High development and equipment costs.
4. Status or recommendation	Proceed to feasiblity and apply as rapidly as possible	Not recommended.	Seek support for funded program.	Additional development required.	Recommend technique for other programs which use hi-frequency equipment	Currently used on stators.	Keep abreast of ongoing development work

* Not Determined

During this reporting period the microfocus x-ray equipment was utilized to detect subsurface defects in blade rings as described in section 4.1.1 of this report. The Magnaflux variable focus x-ray unit is shown in Figure 4.13 along with a lead cabinet having a working area of approximately 35x30x35 inches. Figure 4.14 shows the microfocus x-ray tube and molded blade ring positioned for an oblique radiograph.

One of the important features of the MXK-100m Maganflux x-ray system is the small focal spot (variable from 0.05mm — 0.5mm) which permits film focal distances and direct film enlargements up to 36x with very good geometric sharpness. Another feature of this equipment is the availability of the panoramic accessory tube which can be used for radial x-ray viewing of circular components. This optional tube is shown in Figure 4.15, while the fixture used to obtain panoramic radial views of the rotor blade rim and blades is shown in Figure 4.16.

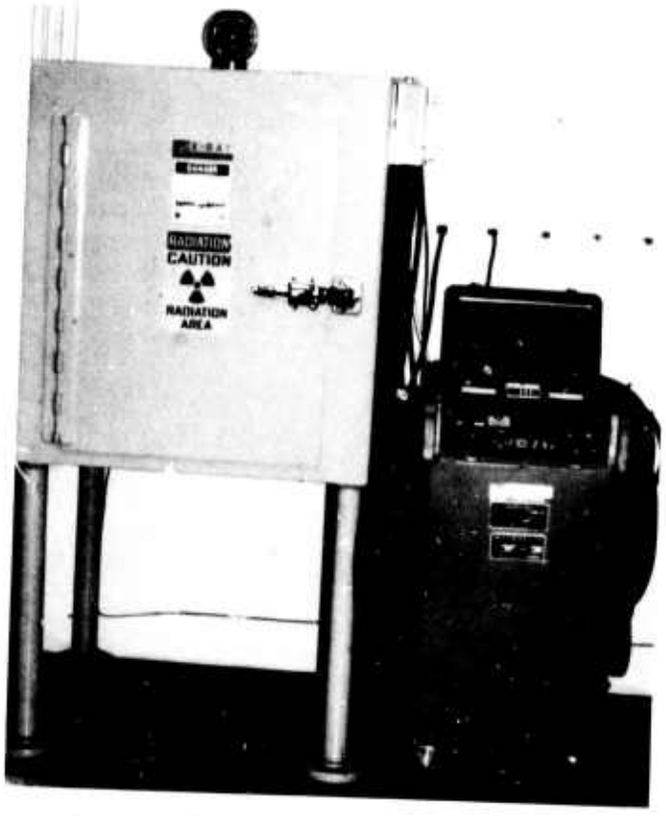

Figure 4.13 Microfocus X-ray Equipment

Figure 4.14 Microfocus X-ray Tube and Molded Blade Ring Positioned for Oblique Radiograph

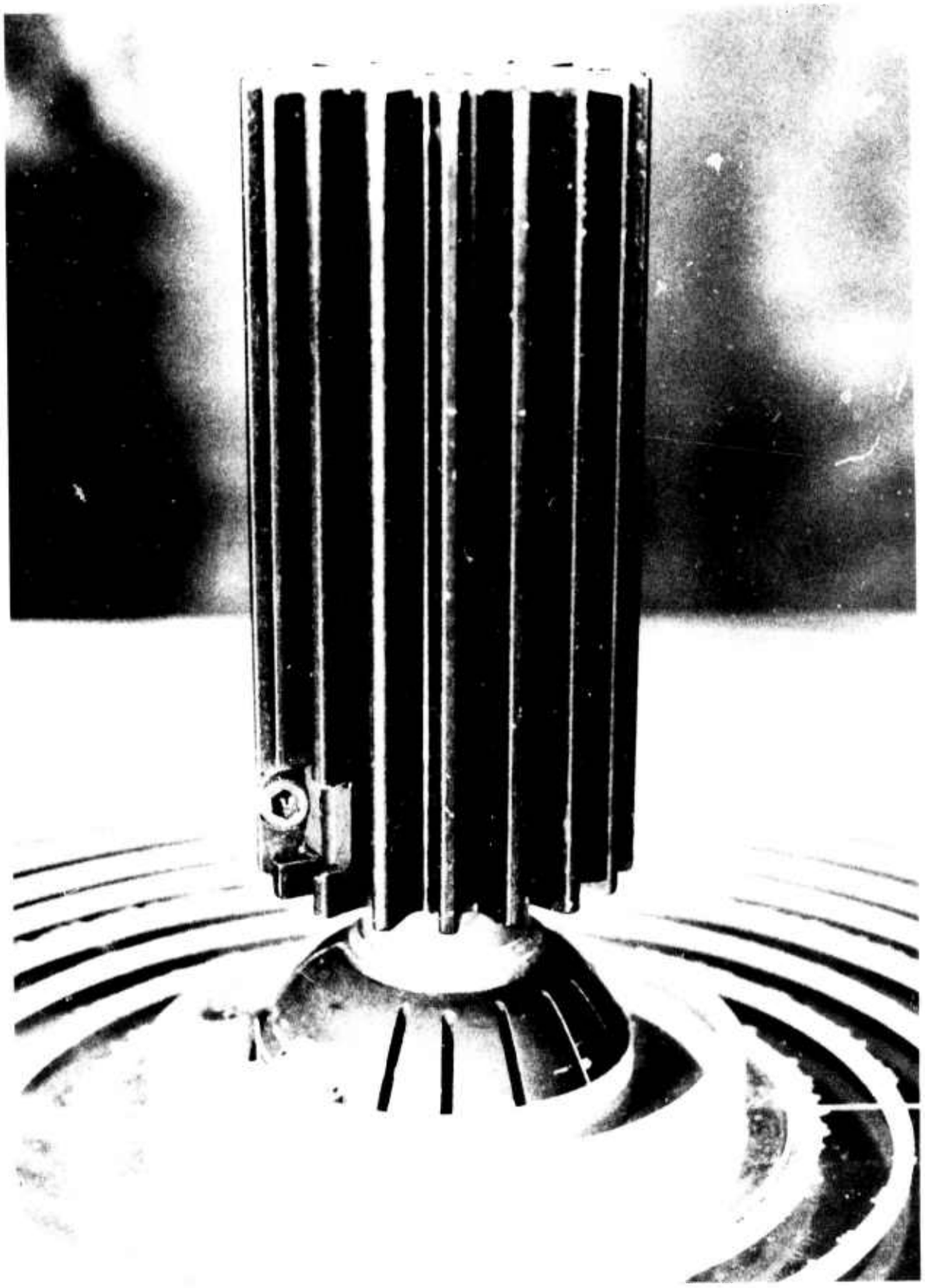

Figure 4.15 Close Up of Panoramic Microfocus Tube Head

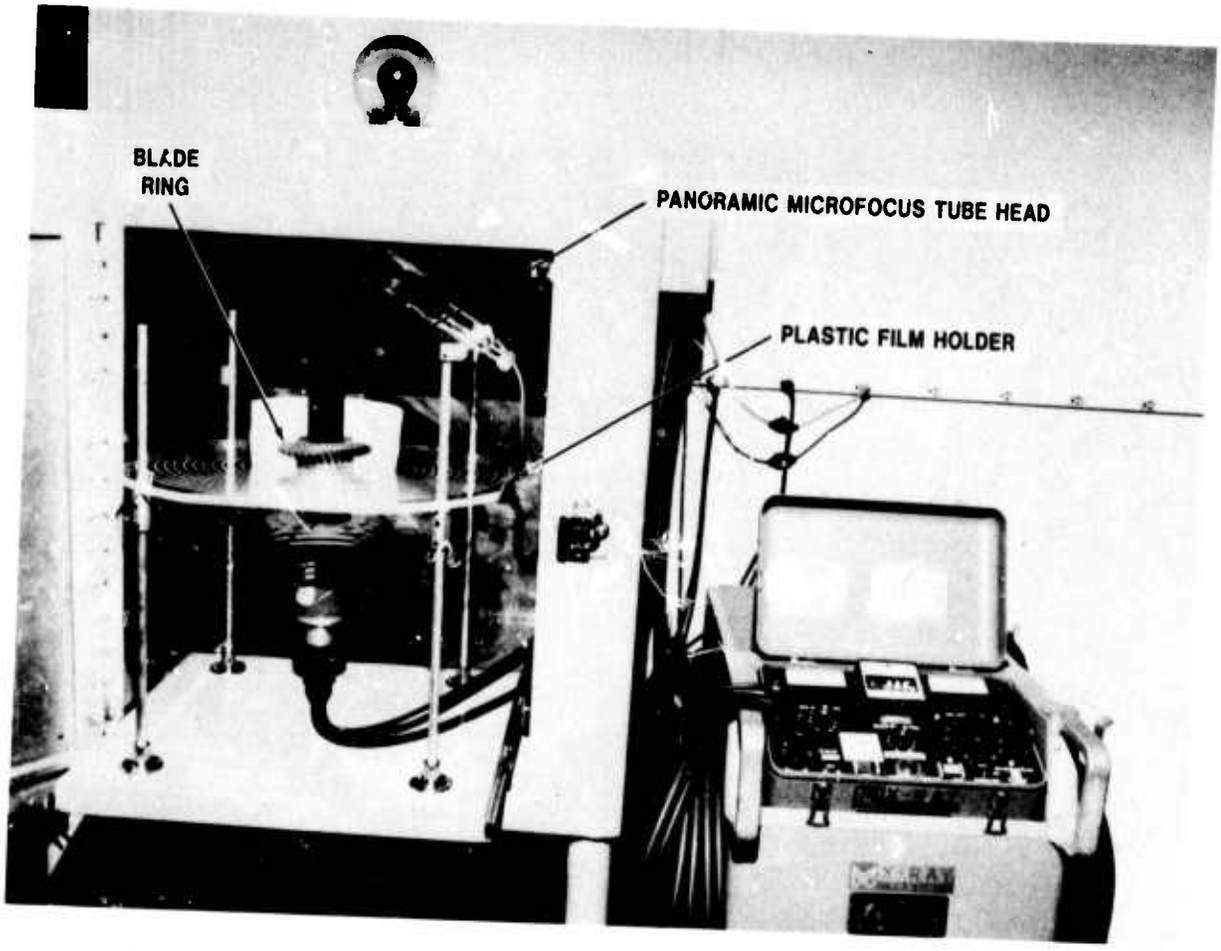

Figure 4.16 Panoramic Microfocus Equipment and Fixture for Radial X-ray

Sensitivity of X-Ray Equipment

The first experiment conducted with the microfocus x-ray was to determine the sensitivity of the equipment. Several penetrameters were fabricated using reaction bonded silicon nitride of 2.7 g/cc density. Figure 4.17 shows radiographic results for a 1/8 inch penetrameter. It can be seen that the 2T hole of 0.010 inch is detectable in the 1/8 inch cross section. This corresponds to a sensitivity of at least 8 percent for sections encountered in molded blade rings.

Most of the NDE effort during this reporting period was directed towards the detection of gross flaws[13] encountered in the molding of silicon nitride blade rings. These defects can be catagorized as one of two basic types: 1) voids and 2) planar type cracks. The planar crack is shown in Figure 4.18. This particular defect is characterized by a large length-to-width ratio. The crack can be detected after nitriding via visual inspection of the surface. However, 100 percent detection is difficult because of part complexity or failure of the crack to surface.

Radiographic and Visual Inspection Results of Molded and Nitrided Blade Rings

A number of x-ray parameters were explored in an effort to produce quality radiographs for oblique and axial viewing of blade rings and individual blades at 1x through 18x magnification. These variables included film speed, focal spot size, voltage setting and x-ray exposure. Best results were obtained with medium film speed, low voltage setting and the small focal spot.

Figure 4.19 and 4.20 are photographs of radiographs made of blade rings molded using flow control. These figures represent the quality extremes of molded parts radiographed during this study. Overall results on all molded components were presented previously.

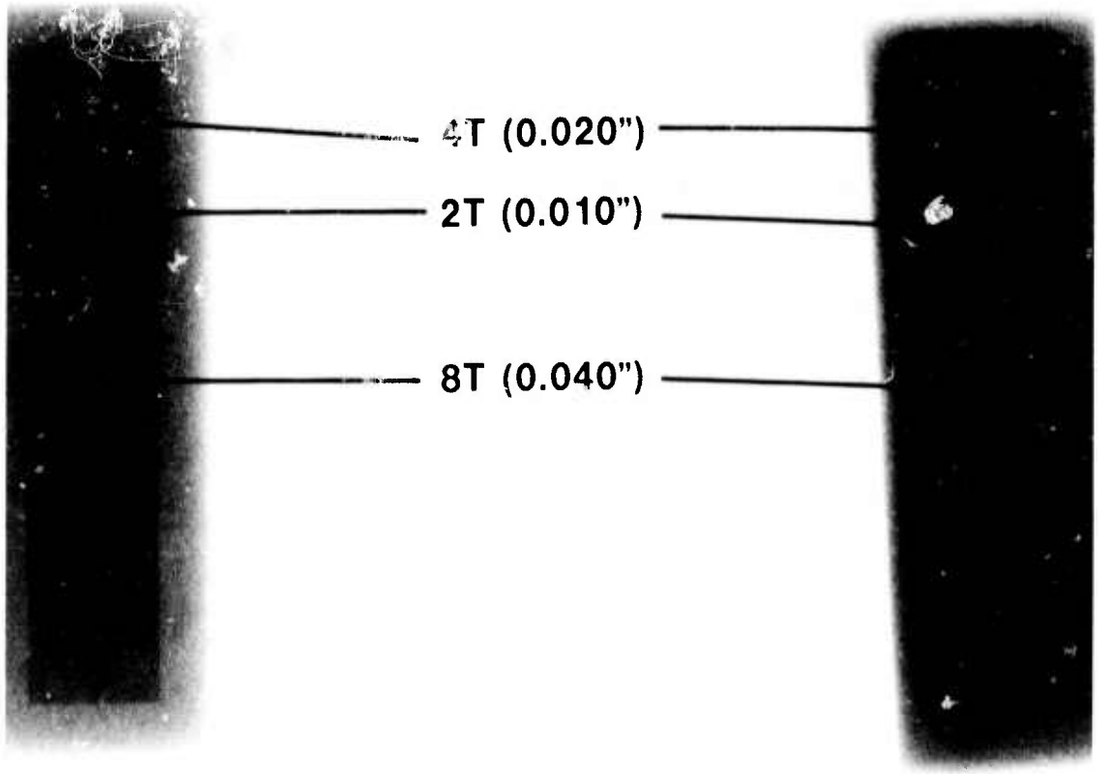

Figure 4.17 Microfocus X-ray of One Eighth Inch Silicon Nitride Penetrameter

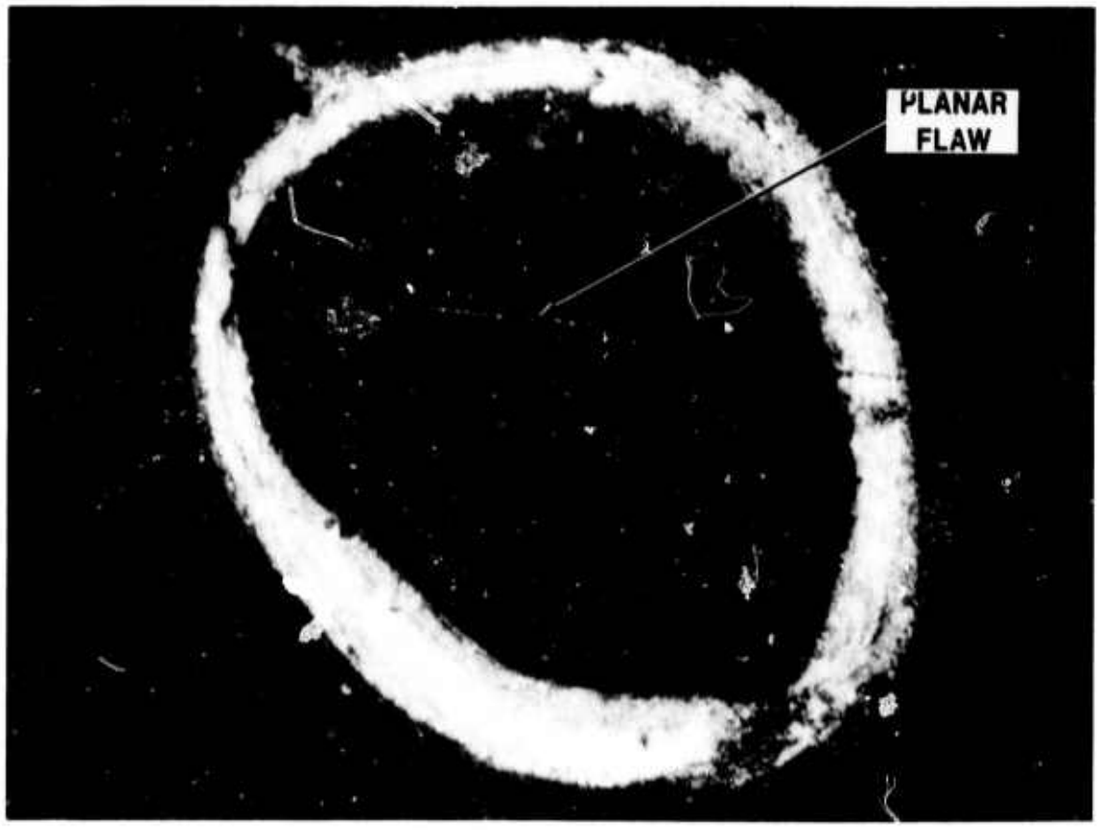

Figure 4.18 Planar Type Defect Detected by Visual Inspection

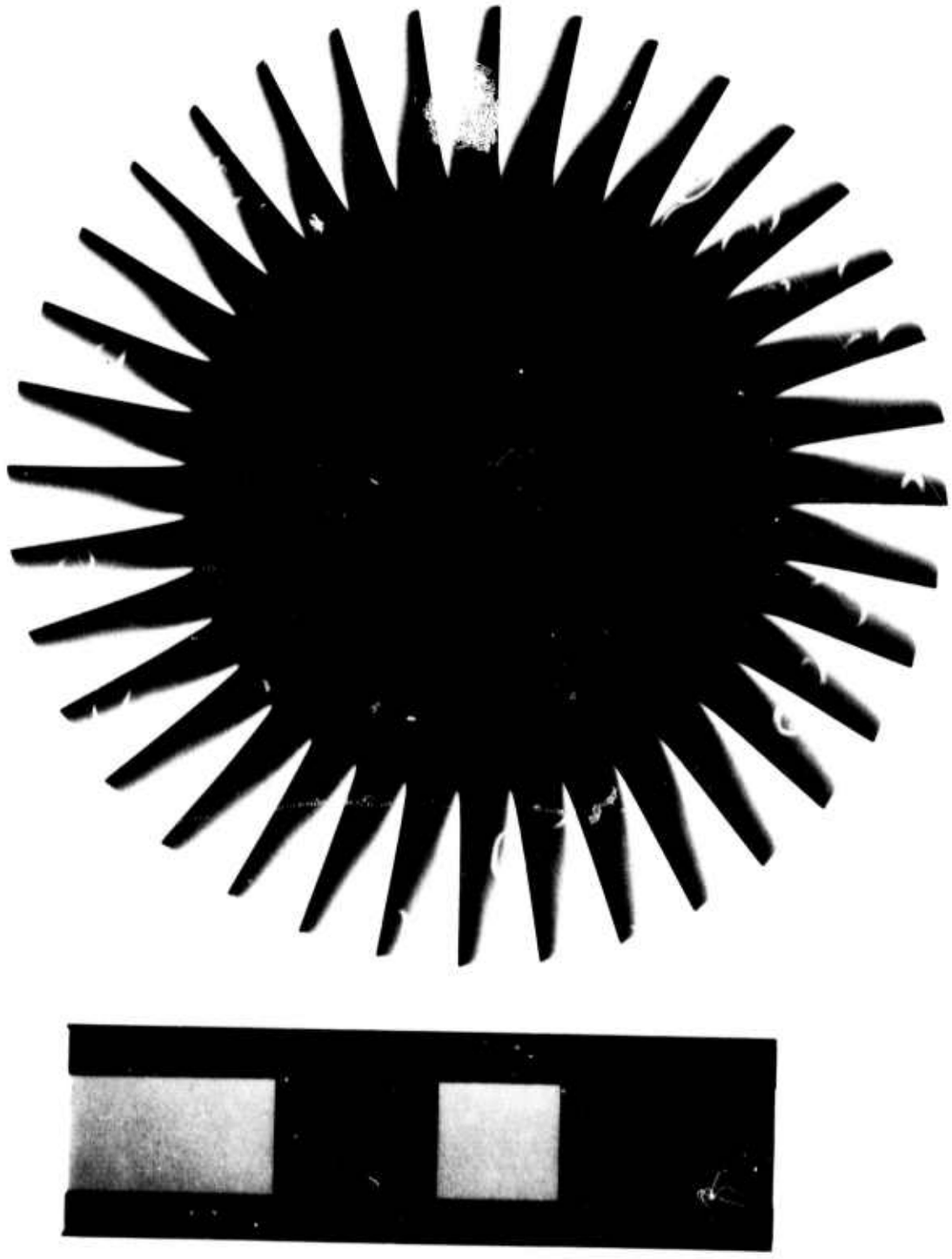

Figure 4.19 Microfocus X-ray Reproduction of Molded Blade Ring with Lower Level of Defects

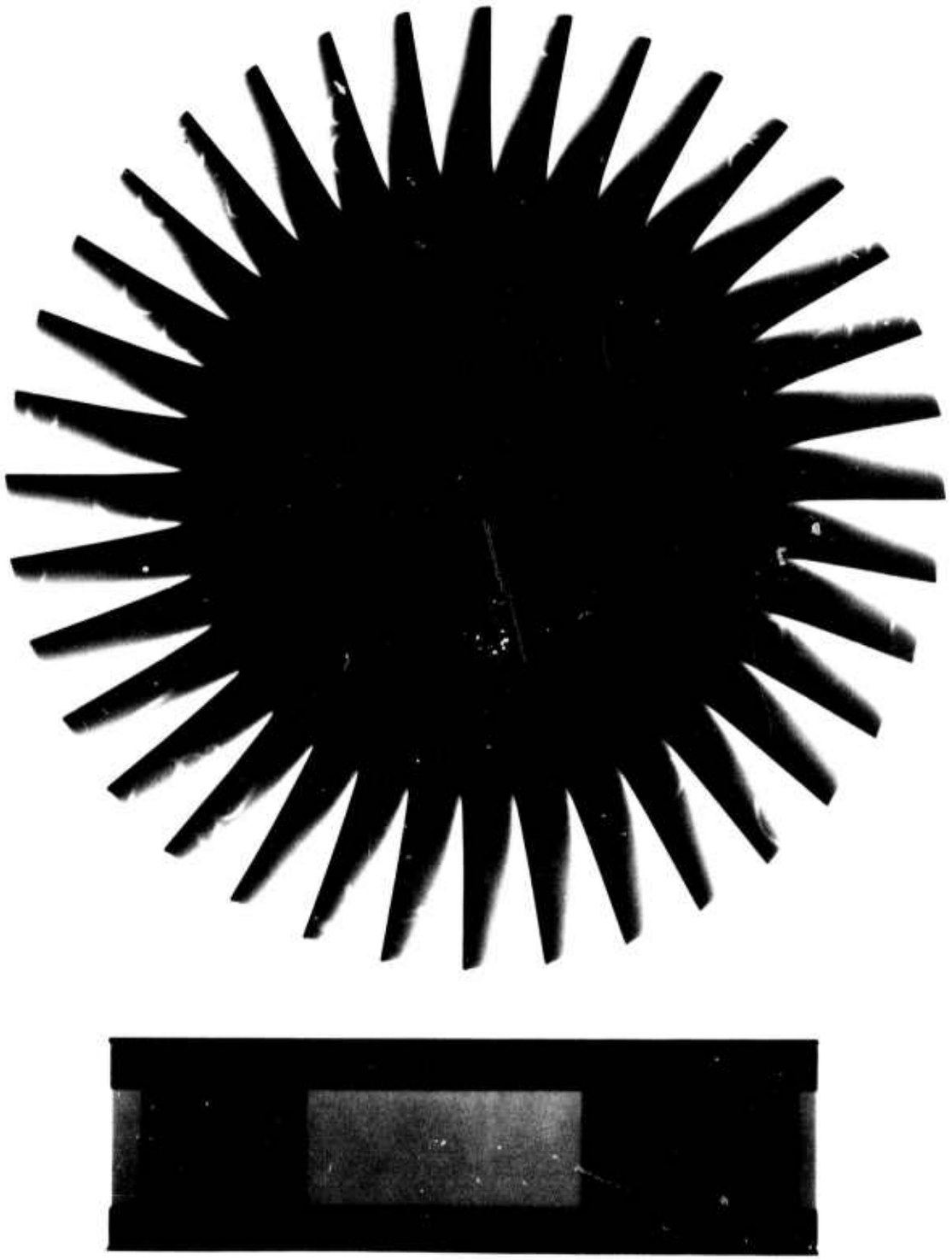

Figure 4.20 Microfocus X-ray Reproduction of Molded Blade Ring with Numerous Defects

In Figures 4.19 and 4.20 two types of flaws are evident, voids and inclusions. In these photographs, the voids, shown as the light indications, are mostly confined to the outer sections of the molded blade ring. This would be expected since this area is the last part of the die to fill during molding.

Several inclusions (dark spots) can also be seen in these figures. Such inclusions were random in location. These inclusions were found in all molded parts and believed to have originated in the mixing of the molding powders or in the incoming raw materials. While detection of this type of defect was not the object of the investigation, it was shown to be within the capability of the microfocus x-ray.

Figure 4.21 illustrates a blade void which was tracked, using x-ray techniques, from molding to nitriding. This void was uncovered by grinding the surface of the part using a small hand grinder. Figure 4.22 is a fractured blade void similarly detected by x-ray. Note the absence of white alpha silicon nitride in Figure 4.21. It was first thought that these flaws were dissimilar in origin, however, repeated grinding and fracturing of other blade voids indicated that grinding of the defective area removed the alpha material and in addition grinding dust tended to mask the presence of alpha silicon nitride.

Figure 4.21 Subsurface Void in Reaction Bonded Silicon Nitride Blade Uncovered by Grinding

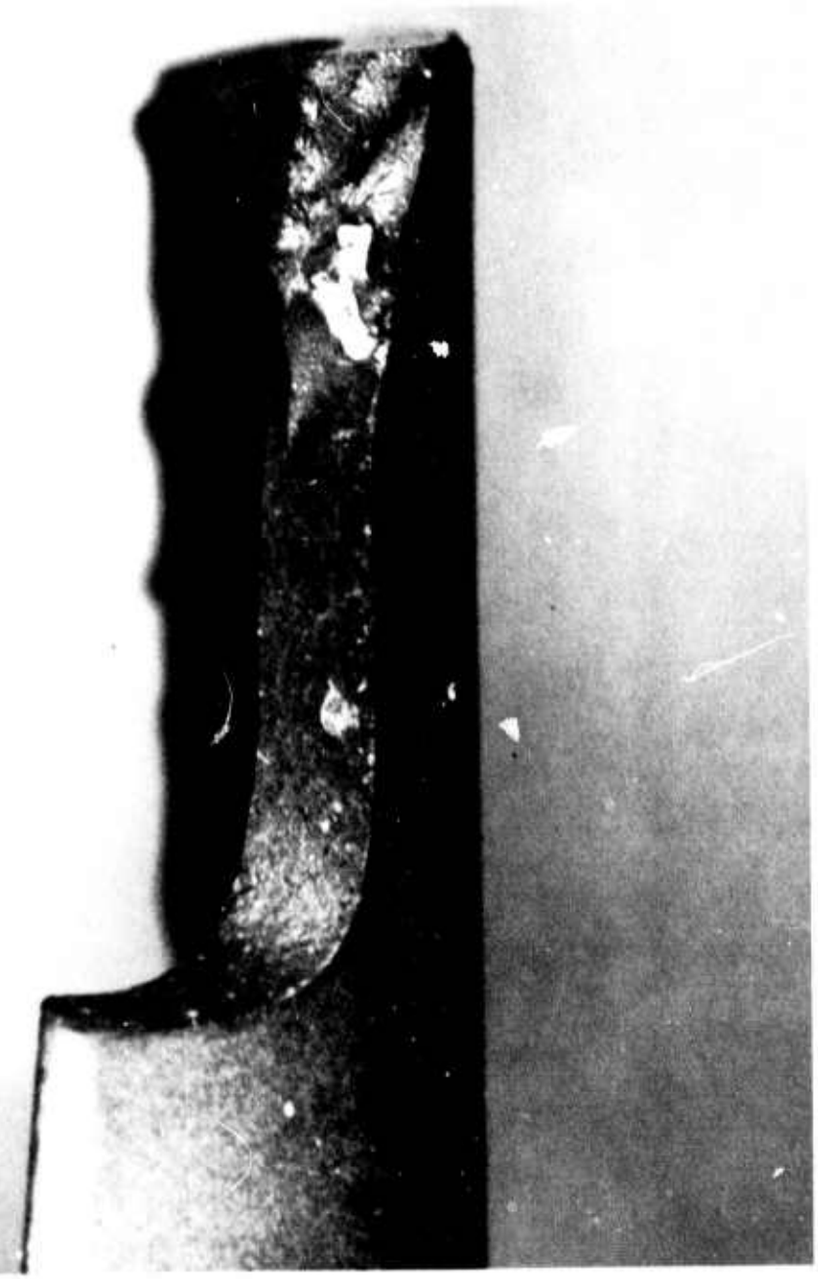

Figure 4.22 Molding Flaw in Reaction Bonded Silicon Nitride Blade — Fractured Surface

Many attempts were made to detect the planar type flaw, Figure 4.18, in as molded blade rings. One experiment consisted of using blade segments cut from the blade rings after molding, and monitoring the parts using visual inspection and x-ray from molding to nitriding. This technique permitted better inspection of the part, and x-ray viewing from several angles not possible with a complete blade ring. The results of this work revealed 1) gross spherical type flaws are detectable in the molded as well as nitrided blades. 2) planar flaws were not seen until after nitriding.

Some of these planar flaws were detected for the first time using x-ray during this program. Figures 4.23 and 4.24 show negative reproductions of x-rays obtained of the same blade (#30) shown in Figure 4.18. These radiographs, taken at 5x and 18x magnification, point out the value of the variable focus x-ray tube at high magnification as evidenced by the sharpness of the x-rays. Of equal significance was the detectability of the planar crack in the nitrided state. This finding coupled with the lack of detection of this defect in the molded state suggests that the actual formation of the defect may occur after molding.

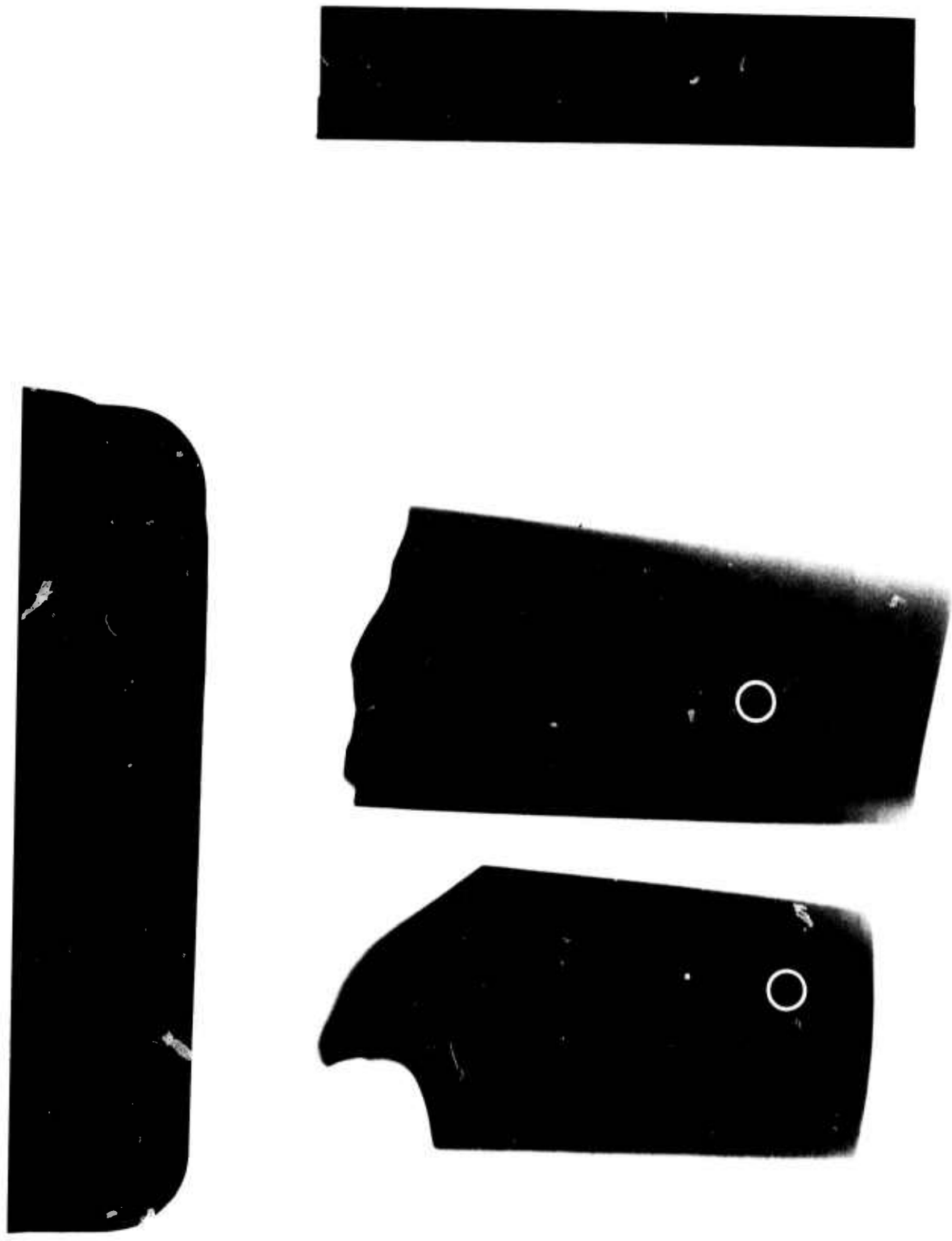

Figure 4.23 Microfocus X-ray Reproductions of Blades Showing Planar Type Flaws

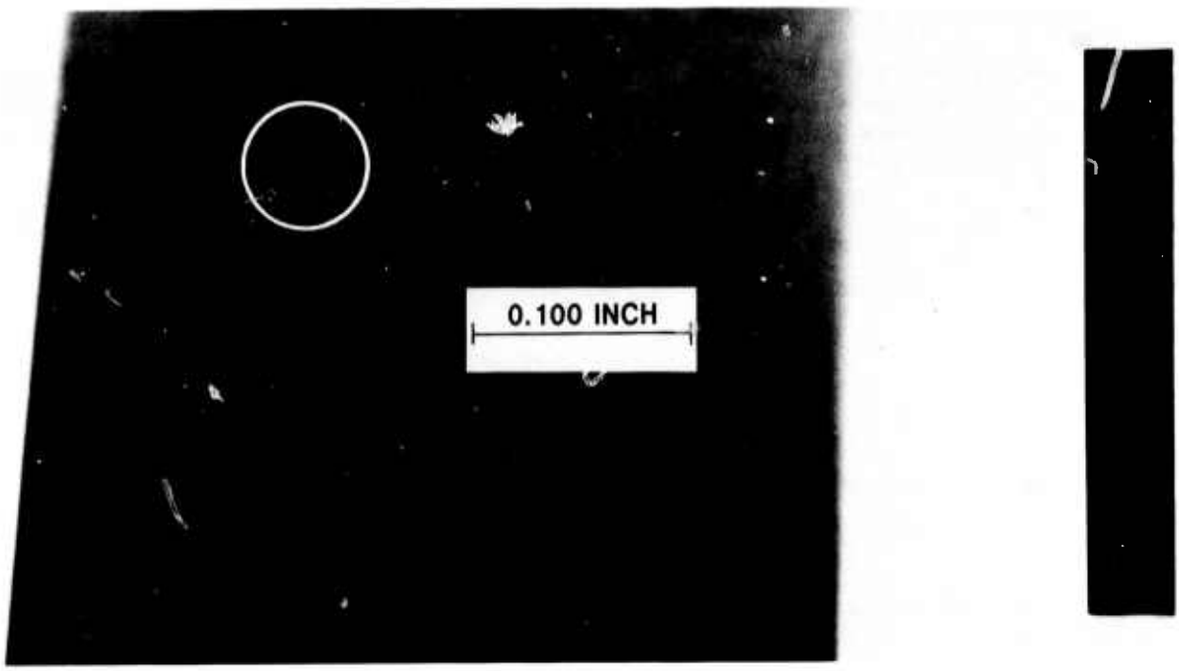

Figure 4.24 Microfocus X-ray Reproduction Showing Planar Type Flaw

Not all planar cracks were detectable using x-ray even with multiple orientation. A reason for this is obvious when one inspects the fractured section of a planar crack previously detected with x-ray. Figure 4.23, blade #31, shows an x-ray of such a flaw, and Figure 4.25 shows the fractured section of blade #31. It can be seen that there is appreciable flaw volume (white material) below the surface of the defect. Only in such cases was the planar defect detectable using x-ray. These results are consistent with flaw sensitivity measurements made using penetrameters.

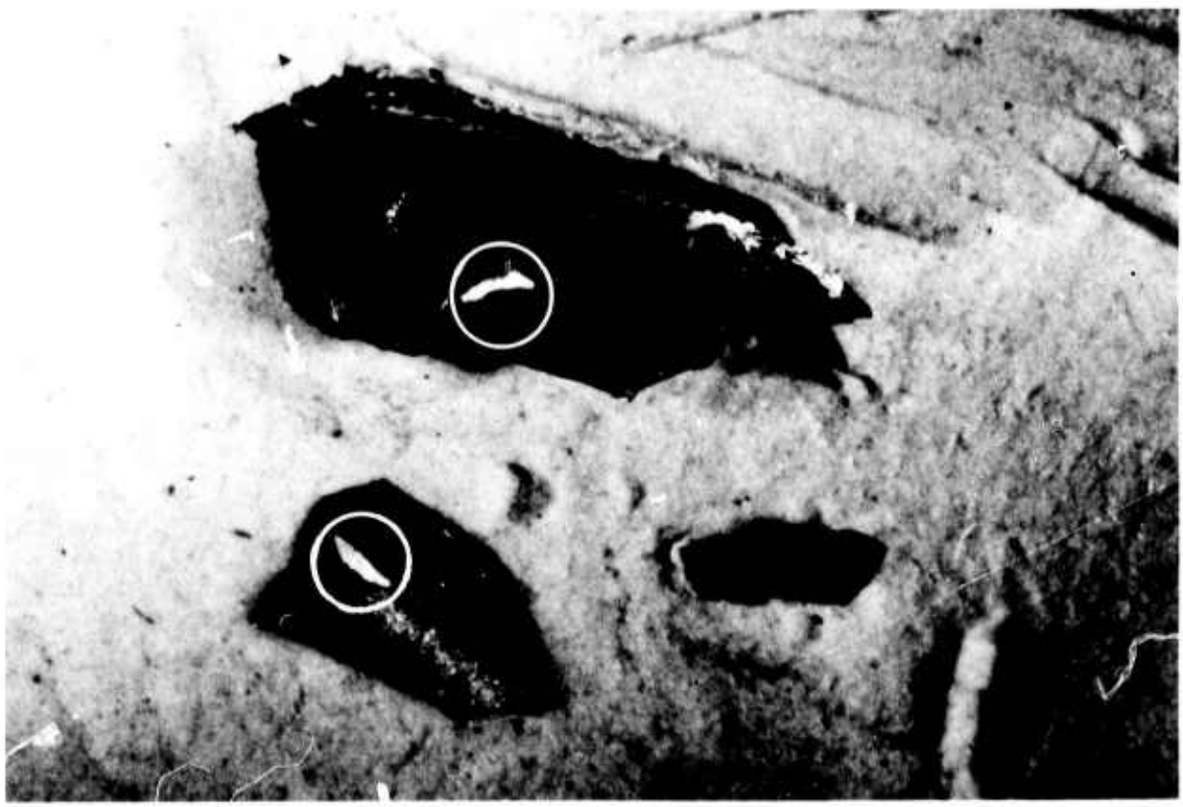

Figure 4.25 View of Planar Flaw After Fracture of Blade

Panoramic Microfocus Tube

The remaining time on the program was utilized assesing blade rim quality. The fixture shown in Figures 4.15 and 4.16 was designed for radial x-ray inspection of the rim in its' circumference along with the entire 36 blades. This illustrates the panoramic tube positioned in the inverted position projecting through the center hole of a plastic disk.

The rotor part is placed over the tube head and positioned for alignment with the radiation pattern of the tube. A series of concentric slots were cut in the plastic disk to hold the x-ray film strip. These grooves, spaced in a pattern of 1-1/2 — 10 inch radius in increments of 1/2 inch, permit magnification up to 10x.

Several voltage and exposure parameters were varied in an effort to obtain quality panoramic radial radiographs of silicon nitride blade rings. Blade ring rim voids were detected using a 10x magnification and medium speed film. Some distortion or unsharpness of the blades was noted and should be minimized with further work.

Summary

Microfocus x-ray equipment has been purchased, installed and utilized for the N.D.E. of reaction bonded silicon nitride components. Flaw size sensitivity of the equipment was established at 8 percent for voids in 1/8 inch cross sections of reaction bonded silicon nitride of 2.7 g/cc density. Both voids and metallic inclusions were detectable in green as-molded components. Planar cracks were only detected in nitrided components and not all planar cracks were detected even with multiple orientation. Void-type flaws were detected in the rim of nitrided blade rings using a panoramic microfocus x-ray technique.

4.2 PSEUDO-ISOSTATIC HOT PRESSING

Introduction

A process to produce improved duo-density turbine rotors was developed under the sponsorship of DOE. It utilized a blade fill and graphite wedge system to apply a radially inwards restraining load to support the blade ring while the hot pressed hub was being formed and bonded to the blade ring[13]. Because this approach limits the hot pressing pressure and is time consuming, an alternate approach was conceived which replaced the wedge/blade-fill system with an isostatic media. Successful development of this approach would result in simplified tooling, reduced manufacturing time, and increased hot pressing pressure over that allowable with the graphite wedge system.

Initial psendo-isostatic pressing trials with blade rings revealed a number of difficult problem areas[13]. During hot pressing the glass escaped through the clearance between the piston and bucket and prevented piston retraction. The glass also permeated the silicon nitride powder and damaged the reaction bonded blade ring. Solutions for these problem areas were established as the goals of this development effort and they are as follows:

a) Design simplified graphite test tooling.

b) Develop a system for sealing the isostatic fluid in a changing volume cavity for a period of four hours (one hour to reach temperature, three hours at 1700°C).

c) Find a suitable isostatic fluid and determine fluid compatibility with silicon nitride and gas environment in hot press cavity.

d) Develop suitable barrier layers for isolating the reaction bonded silicon nitride from the isopress media.

Experiments

Approximately 30 hot press runs were made using the psendo-isostatic approach to evaluate different isostatic fluids and sealing systems. The fluids examined were oxide glasses (Table 4.8) and metals. The seals employed were Grafoil supplemented in some cases with glass.

TABLE 4.8

PROPERTIES OF GLASSES USED IN ISOPRESS EXPERIMENTS

Glass	Density gm/cm^3	Softening Point °C	Working Point °C	Annealing Point °C	Thermal Exp. 25°C to Set Pt. 10^{-7}cm/cm/°C
Corning #7740 Pyrex	2.233	821	1,252	560	35
Corning #7913 Vycor (96% SiO_2)	2.179	1,530	—	1,020	5.5
Corning #1723 Aluminosilicate	2.64	908	1,168	710	54
Corning #9458 LAS	Not Available				

The glass systems investigated were borosilicates (pyrex and vycor), alumino-silicates, and lithium alumino-silicates. Soda lime glass and fused silica were eliminated based on viscosity considerations and on a possible chemical reactivity with silicon nitride.

Experimental graphite tooling was designed to produce a 2:1 pressure relationship between seal cavity and isopress cavity (See Figure 4.26). Therefore, when 1000 psi was introduced to the seal cavity, 500 psi was generated in the isopress cavity. Several experiments were also performed using tooling designed to produce 3:1 and 4 1 pressure relationships. The seals used in the glass isopress runs were either Grafoil laminated preformed rings or a wound Grafoil ribbon pack.

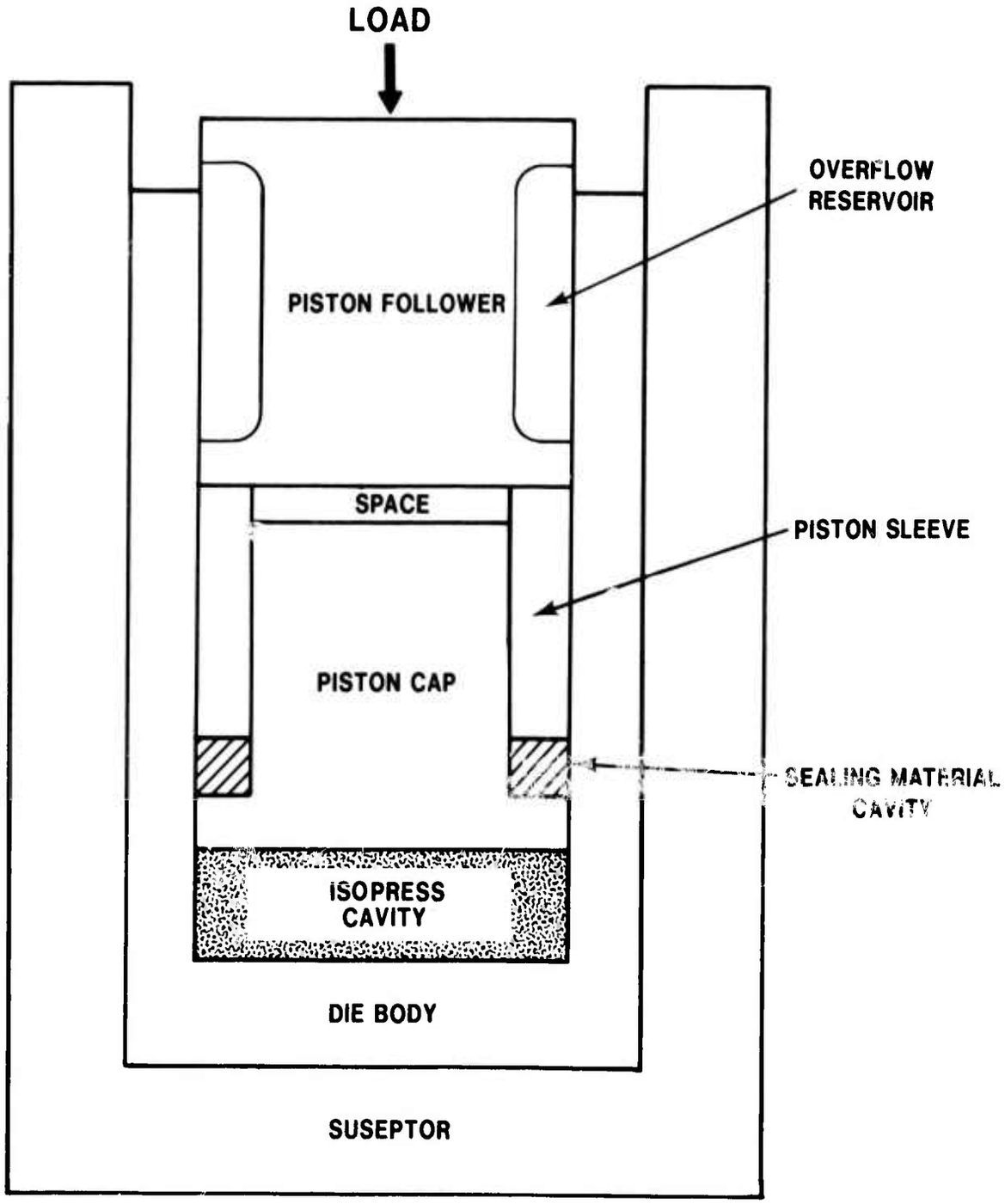

Figure 4.26 Graphite Tooling

The pyrex system was first investigated using the grafoil laminated or ribbon pack seals. From compaction measurements, the pyrex was found to soften at a hot press susceptor wall temperature of 1200°C. These runs were made to 1700°C for hold times of 30 and 60 minutes and an isopress cavity pressure of 500 psi. A seal pressure of 1000 psi (2:1 ratio tooling) was used in all but one case where 3:1 tooling gave a seal pressure of 1500 psi. Both sealing systems showed no leakage of pyrex, but did show a substantial glass weight loss (18% weight loss after 30 minutes and 36% weight loss after 60 minutes). This was attributed to the pyrex (SiO_2) being reduced by the carbonaceous hot-press atmosphere. Evidence of this was also observed when smoke was noted coming from the furnace at about 1700°C (susceptor temperature). Coating the isopress cavity with boron nitride prior to pressing only slightly reduced the weight loss even though no smoke was noted during the run. The reaction of pyrex with silicon nitride was examined by drilling holes in the piston head and connecting these to the isopress cavity. Examination of reaction bonded silicon nitride bars placed in these holes during a run showed no reaction or penetration of the glass with the silicon nitride when boron nitride (BN) was employed as a barrier layer and the glass was easily removed from the bars. Without the barrier material the glass bonded to the silicon nitride test bars. Figure 4.27 shows the difference between a boron nitride coated test bar and an uncoated test bar after pseudo-isostatic pressing in a glass media.

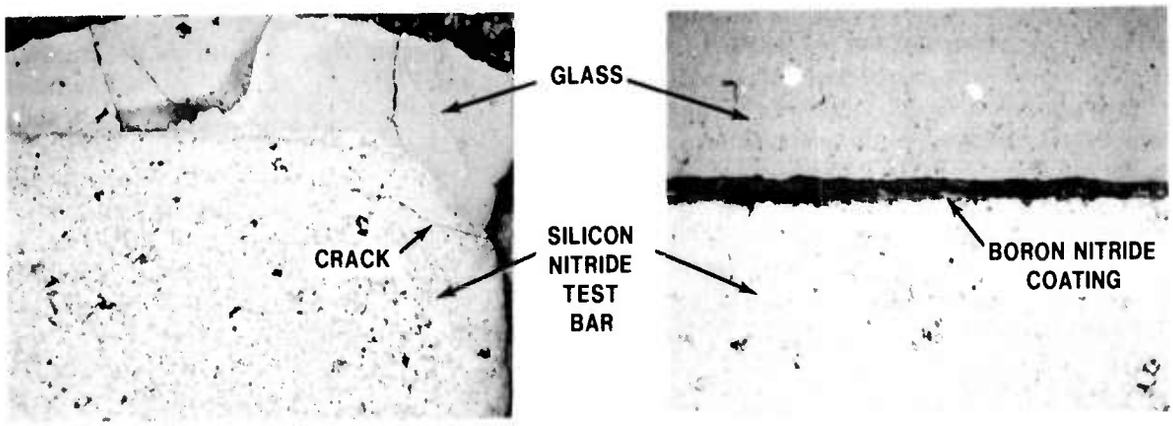

Figure 4.27 Coated and Uncoated Test Bars

Due to the high volatility of pyrex in a carbonaceous environment, it was eliminated as a candidate isopress material. The above results have demonstrated that the attrition rate of pyrex is such that after four hours in the hot press there would be no glass remaining. As a note of interest, the highly volatile character (high vapor pressure) of pyrex was also demonstrated by the piston raising approximately one inch when the load was released at the end of the test run.

Alumino-Silicate glass was evaluated in an attempt to find a more stable glass system. This glass proved to be very stable under a carbonaceous environment but very difficult to seal. Using the standard 2:1 pressure ratio tooling resulted in leakage in one case and a graphite bucket failure in the other. A pressure ratio of 4:1 tooling at a 500 psi cavity pressure failed to stop the leak problem. Increasing cavity pressure to 1000 psi again using 4:1 tooling resulted in a cracked bucket during the run. This glass remains as a candidate due to its stability, however, the seal problem must still be overcome.

Lithium-alumino-silicate glass was also evaluated. This glass showed a severe volatilization problem greater than that demonstrated by the pyrex system and, therefore, was eliminated.

Vycor appeared to be the most promising of the glass materials investigated. This glass does volatilize under hot pesss conditions; however, the volatilization rate is considered acceptable. For example, after a 4-hour hot press run (3 hours at 1700°C) with the isopress cavity coated with BN, approximately 15 w/o loss was experienced. The BN barrier layer between the graphite and the glass cavity was very effective in this case. Without BN barriers, the glass loss rate approximates that experienced

with pyrex. The BN was also an effective barrier for silicon nitride. No deleterious reactions were noted on test specimens examined. In all cases, vycor was easily sealed using grafoil as the sealing material. It should also be noted that the bucket cracked in each instance upon cool down due to the thermal expansion differences between the graphite and the vycor.

The use of liquid metals in the isopress cavity was seen as a way to circumvent the dissociation problem of the oxide glasses. Reviewing the possible candidates, it was decided to begin experimentation with tin which has a very low melting point (232°C) and which would allow easy removal from a rotor. Tin also has a high boiling point and low vapor pressure in the hot pressing temperature range.

An initial run was made for 50 minutes at 1700°C and 500 psi cavity pressure. Upon opening, no tin was found in the cavity with some being in the overflow reservoir (Figure 4.26), and the remaining tin was in the base of the susceptor. Leaking through the seal accounted for the reservoir tin, but that under the susceptor was more difficult to explain. Immersion density measurements on graphite from various bucket locations showed that the tin was forced through the pores of the ATJ graphite (75% TD). Test bars of RBSN in this run showed a BN barrier layer to be effective for stopping Sn - Si_3N_4 reaction. Of note was the observation that the tin showed no reaction and did not wet the graphite. This indicates the viscosity of the molten tin must have been very low to be forced through the graphite pores.

Further tests were carried out with a higher melting metal — copper. Again, Cu did not wet graphite and BN proved to be a good barrier layer between molten Cu and RBSN. The melted Cu also exhibited a low viscosity and grafoil laminated or ribbon seals consistently leaked. Combination grafoil and glass seals were developed of the general form shown in Figure 4.28. Pyrex and vycor were tried as the sealing glasses with pyrex superior since it is soft at the melting point of copper (1083°C). When a pyrex floating seal is used with copper, the pyrex takes on a distinct copper color. This seal uses the density difference between Cu and the glass to keep the seal in position. With these combination seals, volatilization of the glass still occurs but the quantity of glass required is small. The grafoil-glass seal worked well but the copper was forced through the pores in the graphite bucket. This problem might be solved by employing high-density graphite or high-density graphite liners.

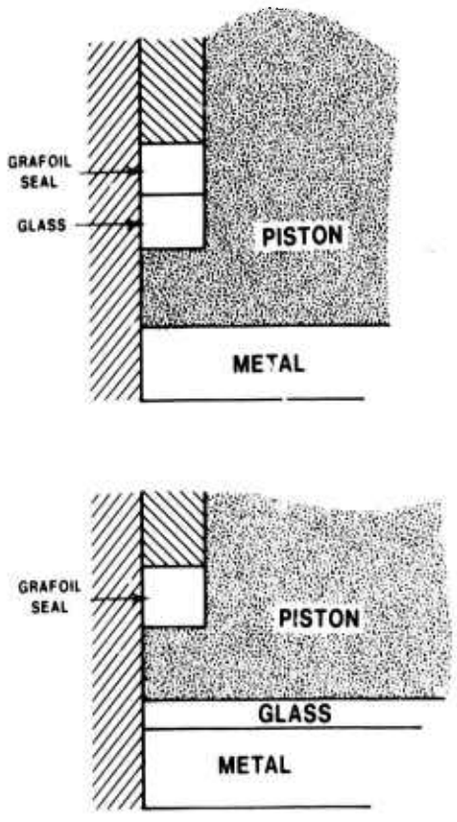

Figure 4.28 Sealing Systems for Metallic Isopress Fluids

Summary

In summary, the major problems approached involved the development of a sealing system, selecting a suitable isostatic media, and the development of an effective barrier layer between the reaction bonded silicon nitride and the media. It was found that the oxide glasses could generally be contained by a simple grafoil seal. The major problem with glass proved to be its susceptibility to decomposition under a hot-press environment. Of the glasses investigated, vycor appeared to be the most promising isopress media material. Although some vycor loss will be experienced, this loss is acceptable.

Results also show that boron nitride appears to be an effective barrier layer material between the vycor and silicon nitride.

Tin and Copper metals, as the isostatic media, were found to be very stable in the hot press environment but were difficult to contain without employing a more complicated grafoil-glass hybrid seal. The chief difficulty was extrusion of the molten metal through the porosity of the graphite.

The reaction bonded silicon nitride test bars recovered from the isostatic media were not checked for densification but considering the short times and low pressures employed and from examination of the microstructures it is believed that little if any densification occurred.

5.0 ANALYTICAL CODES

The development of analytical design codes and the application of these analytical techniques to the duo-density silicon nitride turbine rotor were ongoing activities in the Ford/DARPA Brittle Materials Design Program since its' inception. This technology is an important part of the systems approach employed in this project for the development of high temperature gas turbine engines. DOE funded work concentrated on development of analytical tools and limited analysis to clarify a few issues identified during the DARPA portion of the program.

During previous reporting periods[11,13] several analytical tools and procedures were developed. The maximum-likelihood method was selected as the procedure for the estimation of the parameters of Weibull distributions[11]. Analytical procedures were developed for computing time-dependent reliability for ceramic structures which exhibit the phenomenon of delayed fracture or static fatigue[11]. A "Hypothesis Testing" procedure was prepared for determining whether statistically significant differences exist between two sets of data[13]. This test was applied to the turbine rotor and showed that blade strength does deteriorate after the press-bonding operation. Use of proof-testing as a potential means of enhancing the accuracy of life predictions was theoretically investigated[13]. The turbine rotor hub contour was modified based on a life prediction analysis which indicated a thicker throat was beneficial[13].

During this reporting period a reliability analysis was performed for the off-design operating conditions of rotor 1195 which had been tested previously[12]. This analysis, presented in Section 5.1, was conducted to determine the time dependent reliability for the duration of the testing and determine if the reliability estimate agreed with the successful engine test. Section 5.2 presents the reliability estimates for thicker throat rotors (0.40 and 0.48 inches) operating in the hot spin rig.

5.1 RELIABILITY ANALYSIS OF ROTOR 1195 TESTING

Rotor 1195 was tested in a modified engine for ten hours of steady state operation at 45,000 rpm and 2200°F turbine inlet temperature (T.I.T). Following a successful shutdown and examination of the parts a second run was made comprising of 25 hours at an average T.I.T. of 2250°F and 1-1/2 hours at an average T.I.T. of 2530°F, all 26-1/2 hours at 50,000 rpm. At this time an engine shutdown was started to reduce the excessively high air temperatures (~1900°F) in the vicinity of the metal curvic adapter, but was unsuccessful when the rotor system abruptly failed[12]. The speed selected for the second test, 50,000 rpm, was 100% design speed for a three stage turbine discussed in a previous report[11].

During this reporting period a reliability analysis was conducted for the individual loading conditions and the cumulative reliability estimated for the entire test cycle of rotor 1195. The average turbine inlet temperature was taken to be 2200°F for both the 10 hour and 25 hour portions of the test and 2500°F for the remaining 1-1/2 hours. Thermal loadings used in the analysis were obtained from separate heat transfer analyses modified to simulate the conditions prevailing in the modified engine and defined from measurements taken during the test runs.

As shown in Figure 5.1 four thermocouples were placed in the vicinity of the first stage rotor (1195) so the air temperatures on the forward and aft surfaces of the disk could be measured during the test run of Engine 6-14C. Using these test temperatures as a guide, two dimensional (axisymmetric) thermal analyses were made for the turbine end of the modified engine rotor system at turbine inlet temperatures of 2200°F and 2500°F.

The heat flow into the rim of the disk was simulated by using film coefficients (h) and adiabatic wall temperatures on that edge of the disk model. Two and three dimensional analytical techniques have previously been used to define the thermal boundaries at the rim of the disk for full power loading (2500°F TIT and 64,240 rpm)[8].

With this data as a baseline, the film coefficients corresponding to the 2500°F TIT portion of the modified engine run were obtained by using a ratio of the mass flow rates to the 0.8 power, while the adiabatic wall temperatures were left unaltered. For the 2200°F TIT condition both thermal parameters were adjusted to reflect measured engine data (mass flow rate and turbine inlet temperature).

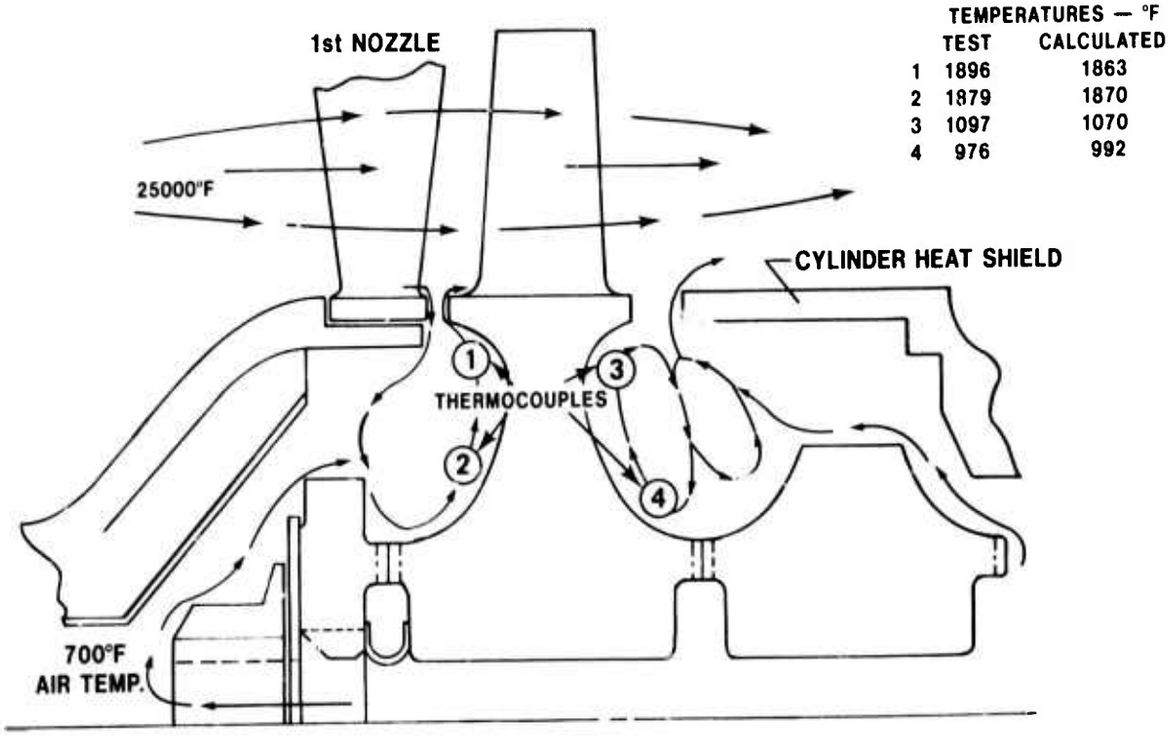

	TEMPERATURES — °F	
	TEST	CALCULATED
1	1896	1863
2	1879	1870
3	1097	1070
4	976	992

Figure 5.1 Assumed Air Flow Around Rotor 1195

To duplicate the measured air temperatures at the forward face of the disk (Points 1 and 2 in Figure 5.1) turbine gases were assumed to leak inboard at the axial clearance between the first stage nozzle and disk and then mix with the turbine bolt cooling air. This air mixture was then assumed to flow up the forward contour of the disk from the curvic to the rim. For the aft side of the disk (Points 3 and 4) the flow of labyrinth seal air was assumed to create vortices, which caused recirculation to heat up the air along the back face of the rotor. Figure 5.1 shows the assumed air flows, and the test and calculated air temperatures at the forward and aft sides of Rotor 1195 for a turbine inlet temperature of 2500°F. As shown in the figure the thermal analysis closely simulated the temperature environment in the modified engine.

Using the thermal boundaries in Figure 5.1 the temperature distributions in the rotor disk at 50,000 rpm and for turbine inlet temperatures of 2200°F and 2500°F were calculated and are shown in Figures 5.2 and 5.3, respectively. Using the material properties in Table 5.1, the maximum principle tensile stresses in the disk for the two engine loading conditions were calculated and are shown in Figures 5.4 and 5.5. In these calculations it was assumed that the rotor was fully bladed (36), while actually Rotor 1195 had 28 blades. Thus, the computed stresses will be approximately 2% higher than the actual stresses developed in the disk making the reliability estimates on the conservative side. Since the recorded test data from the 10 hours of running in Engine 6-14B were similar to the 25 hours in 6-14C it was assumed that the temperature distributions in the disk for these two engine runs at 2200°F TIT were the same. Therefore, using the temperatures shown in Figure 5.2, the disk stresses at 2200°F TIT and 45,000 rpm were calculated and are presented in Figure 5.6.

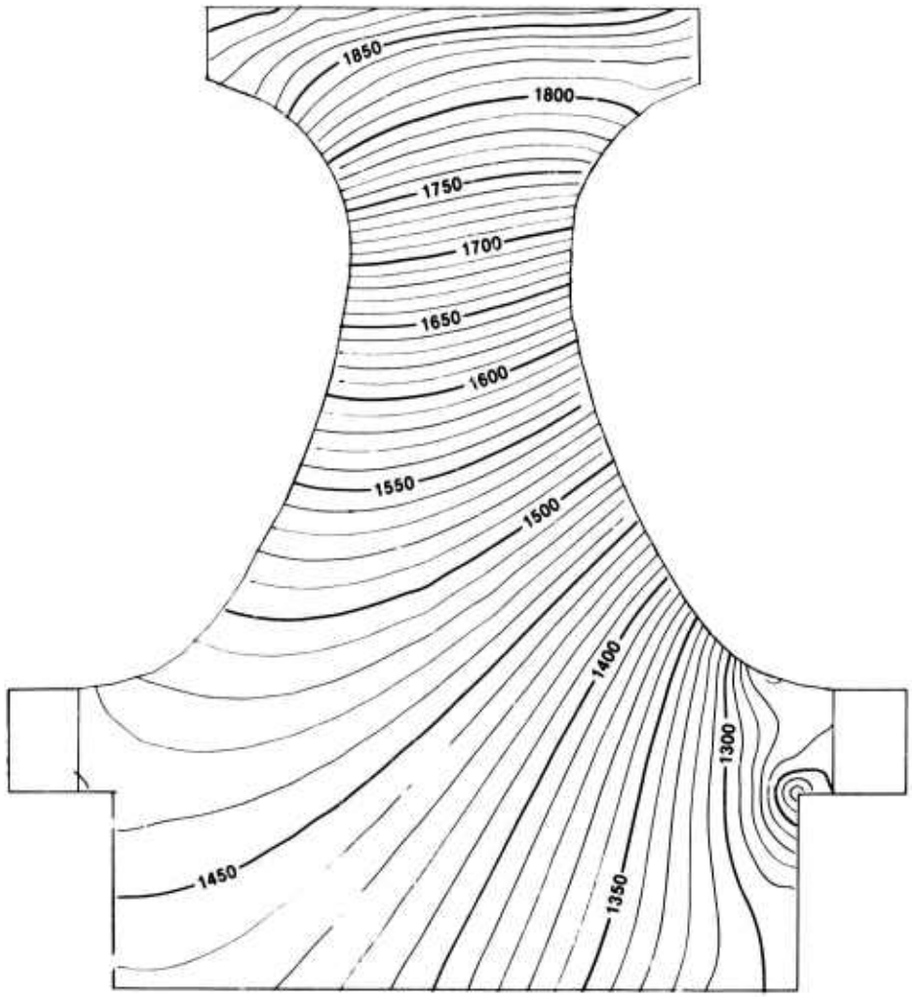

Figure 5.2 Temperature Distribution (°F) for Rotor 1195 in Engine 6-14c at 2200°F TIT and 50,000 rpm

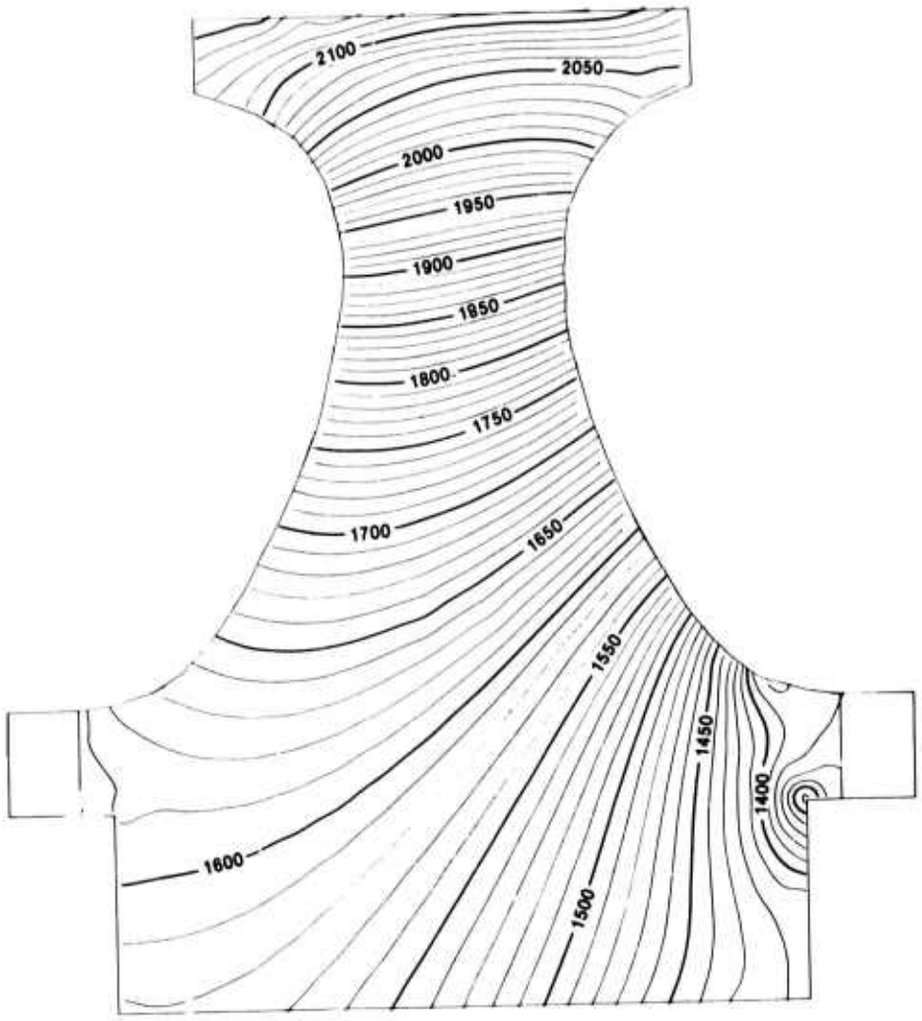

Figure 5.3 Temperature Distribution (°F) for Rotor 1195 in Engine 6-14c at 2500°F TIT and 50,000 rpm

TABLE 5.1
MATERIAL PROPERTIES

	Temp. °F	Young's Modulus x10^6 psi	Poisson's Ratio	Shear Modulus x10^6 psi	Coefficient of Thermal Expansion in/in/°F x 10^{-6}	Thermal Conductivity Btu/hr-ft-°F	Specific Heat Btu/lb-°F
3.5% MgO Hot-Pressed Si_3N_4 (Hub)	78	43.5	.272	17.1	0.95	17.0	.178
	500	44.1	.260	17.5	1.23	15.0	.227
	1000	44.3	.251	17.7	1.54	13.0	.263
Density = 3.18 gm/cm^3	1500	43.5	.250	17.4	1.74	11.0	.289
	2000	42.6	.246	17.1	1.89	9.2	.328
	2500	41.3	.237	16.7	2.01	8.0	.325
Injection Molded Si_3N_4	78	25.0	.187	10.5	.82	11.4	.150
	500	24.7	.178	10.5	1.07	10.4	.230
Density = 2.70 gm/cm^3	1000	24.1	.164	10.3	1.46	8.1	.270
	1500	23.3	.152	10.1	1.62	6.6	.280
	2000	22.2	.140	9.8	1.70	5.5	.290
	2500	21.5	.128	9.5	1.73	4.6	.300

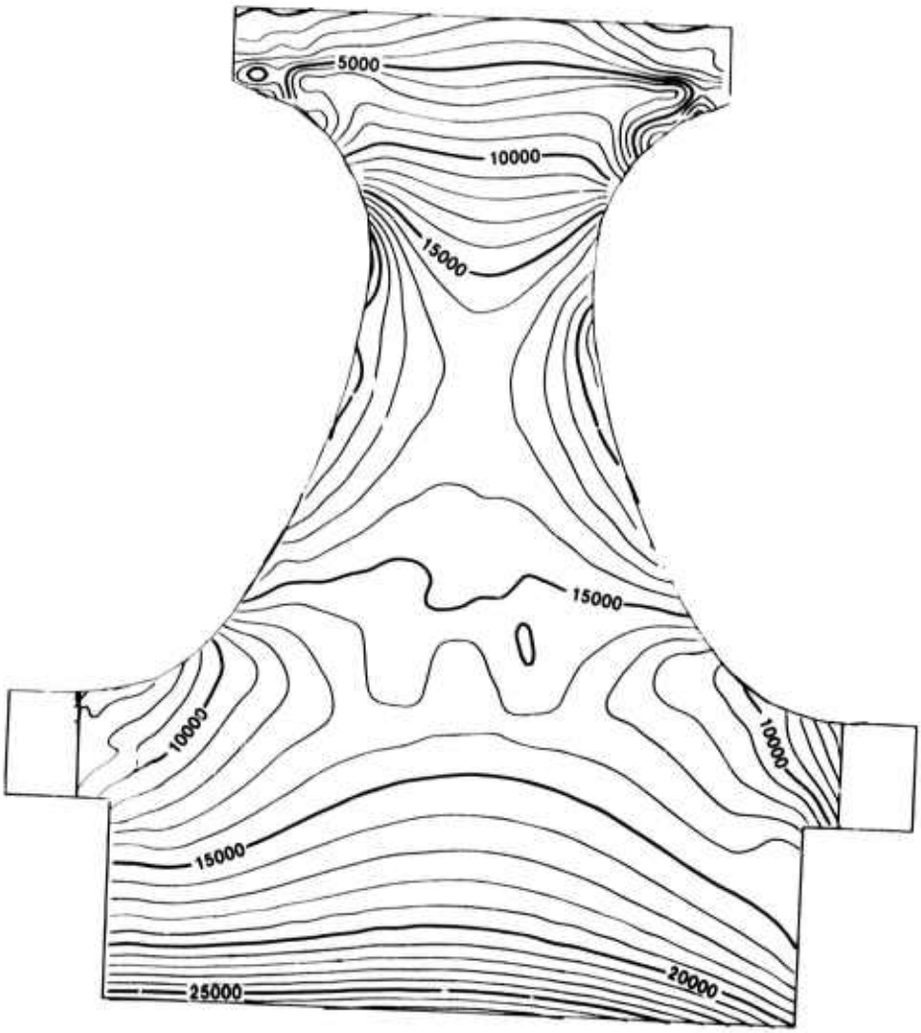

Figure 5.4 Maximum Principal Tensile Stresses (psi) for Rotor 1195 in Engine 6-14c at 2200°F TIT and 50,000 rpm

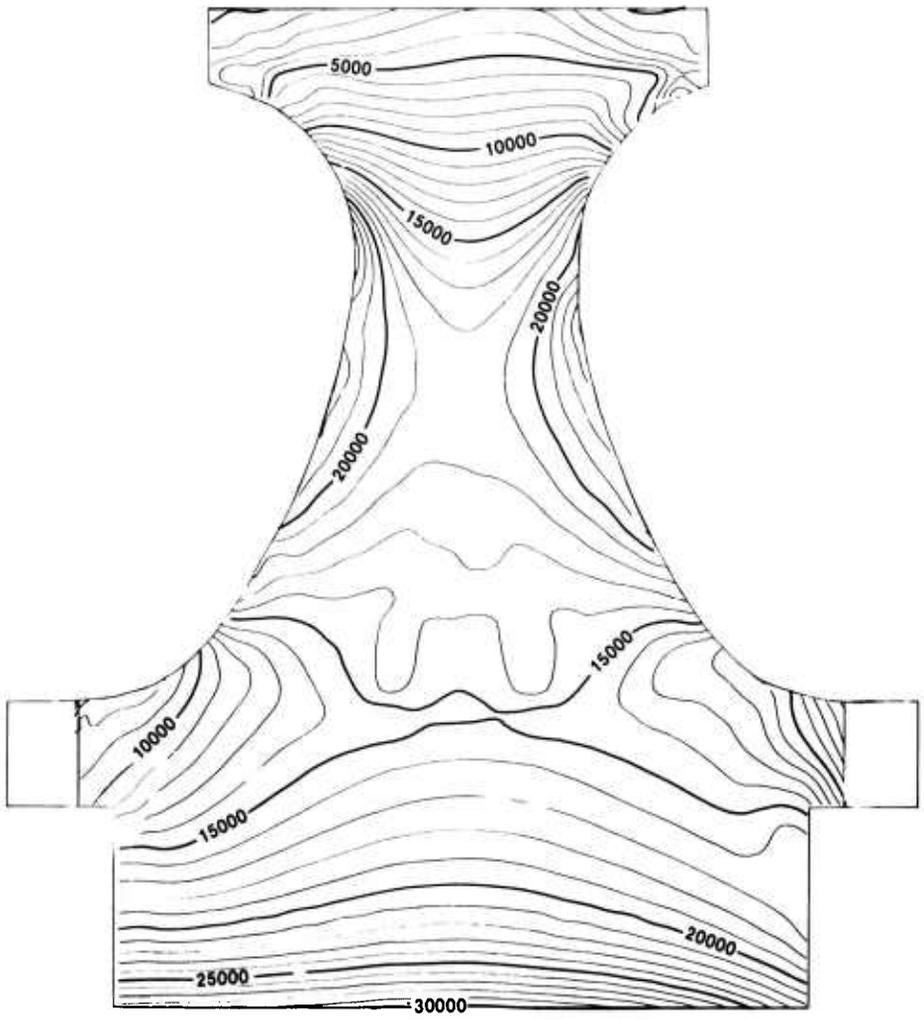

Figure 5.5 Maximum Principal Tensile Stresses (psi) for Rotor 1195 in Engine 6-14c at 2500°F TIT and 50,000 rpm

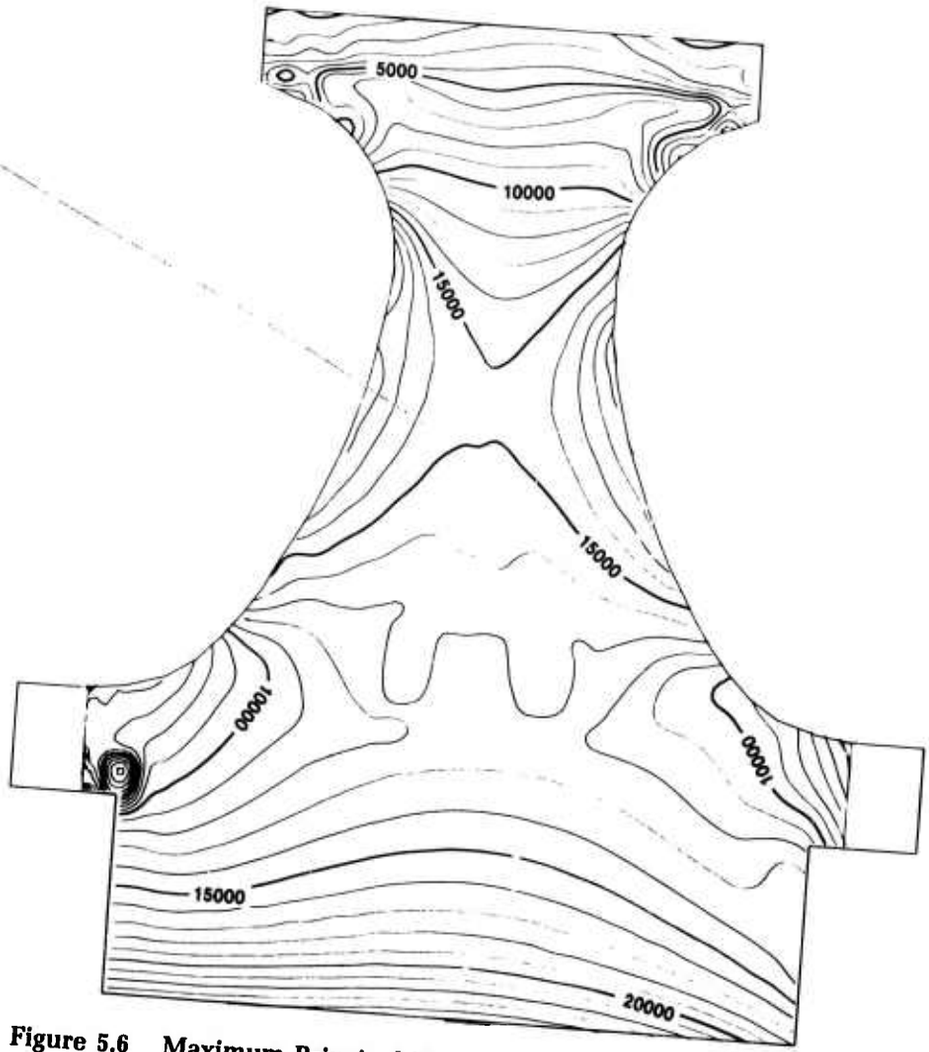

Figure 5.6 Maximum Principal Tensile Stresses (psi) for Rotor 1195 in Engine 6-14b at 2200°F TIT and 45,000 rpm

Table 5.2 lists the temperatures and the stresses in the disk at the bore, throat, and rim for the 2500°F TIT and 50,000 rpm operating condition of engine 6-14C. Also shown in this table is the temperature and stress gradient between the disk and rim.

TABLE 5.2

Temperature and Maximum Principle Tensile Stresses of Rotor 1195

	Bore		Throat		Rim		Gradient (Bore-Rim)	
	Temp. (°F)	Stress (psi)	Temp. (°F)	Stress (psi)	Temp. (°F)	Stress (psi)	Temp. (°F)	Stress (psi)
Modified Engine (6-14C) 2500°F TIT & 50,000 rpm	1530	30,000	1900	23,000	2110	7,000	580	23,000

Estimated Weibull strength parameters presented in Figure 6.9 of report[13] were used to make the fast and time dependent reliability point estimates for rotor 1195 which are presented in Table 5.3.In all the reliability estimates presented, the reliablility of the proof tested blade ring was excluded on the assumption that reaction bonded silicon nitride does not exhibit subcritical crack growth at the temperatures experienced in the engine tests.

TABLE 5.3

Fast Fracture and Time-Dependent Reliabilities for Rotor 1195

Loading	Time (Hours)	Fast Fracture Reliability		Time Dependent Reliability (2)	
		m = 7	m = 10	m = 7	m = 10
2200°F TIT & 45,000 rpm	10	.98113	.99981	.97443	.99972
2200°F TIT & 50,000 rpm	25	.96145	.99947	.91667	.99845
2500°F TIT & 50,000 rpm	1.5	.89500	.99766	.85830	.99623

1. Point estimates of disk hub material Weibull slope: 7 and 10
2. Assuming individual loading on the rotor disk.
3. Cumulative time dependent reliability for the total 36.5 hours of running time:
   .83843 ($m = 7$, $\overline{m} = 8.5$, $n = 15.9$)
   .99547 ($m = 10$, $\overline{m} = 12.2$, $n = 15.9$)
4. The reliability of the blades is 1 since they were proof-tested by cold-spinning to 50,000 rpm.

where m = Weibull slope for fast fracture
$\overline{m}$ = Weibull slope in presence of slow crack growth
n = crack propagation velocity exponent

As mentioned earlier all analyses were made for a 36-bladed rotor, and since Rotor 1195 had only 28 blades, the reliability estimates are conservative. The time dependent reliabilities at each loading mode were calculated assuming no previous load history. They provide a measure of the relative severity of the individual loading mode. Using an estimated Weibull modulus, m, of 7, the calculated cumulative time dependent reliability for the total 36.5 hours of running time is 0.83843. For an m of 10, this cumulative reliability increases to 0.99547. These cumulative estimates tend to corroborate the engine testing, since an evaluation of the failed parts shows that Rotor 1195 material quality was not the direct cause of the shutdown failure.

5.2 ANALYSIS OF ROTOR DISK CONTOUR MODIFICATIONS

Hot spin rig testing is being used to evaluate the quality of Ford's duo-density rotors under the DARPA program and eventually will serve to verify analytically predicted failure distributions of test rotors. Before the axisymmetric thermal analysis of the hot spin rig rotor system could be made, the existing 2-D model[11] had to be altered to represent the geometry of the test hardware. This included the change from a conical piloting system to curvic couplings and modifying the configuration of the disk from the original designed 0.300 inch throat to the recontoured 0.400 inch throat configuration. The 0.400 inch disk shape was chosen since this alteration to the model would require the least amount of time. No significant difference in disk temperature is expected between the 0.480 and the recontoured 0.400 inch throat rotors since there is not a major difference in the disk geometries.

For the thermal environment, it was assumed that the rim of the disk from the leading to the trailing edge had a uniform temperature of 1800°F. Next, two modes of air flow were assumed to occur around the disk. For the first, shop supplied bolt cooling air was assumed to flow up the forward disk face, while labyrinth seal air was assumed to cool the aft disk surface. Figure 5.7 shows the temperature distribution in the disk for this condition. For the second mode, hot recirculated air was assumed to bathe both disk surfaces. This assumption was based on optical pyrometer readings, taken during rig testing of hub 988, which showed higher disk temperatures, Figure 5.8, than those presented in Figure 5.7. Figure 5.9 shows the calculated disk temperatures for this hotter condition. As expected, these two assumed operating conditions produce vastly different temperature levels and gradients in the disk.

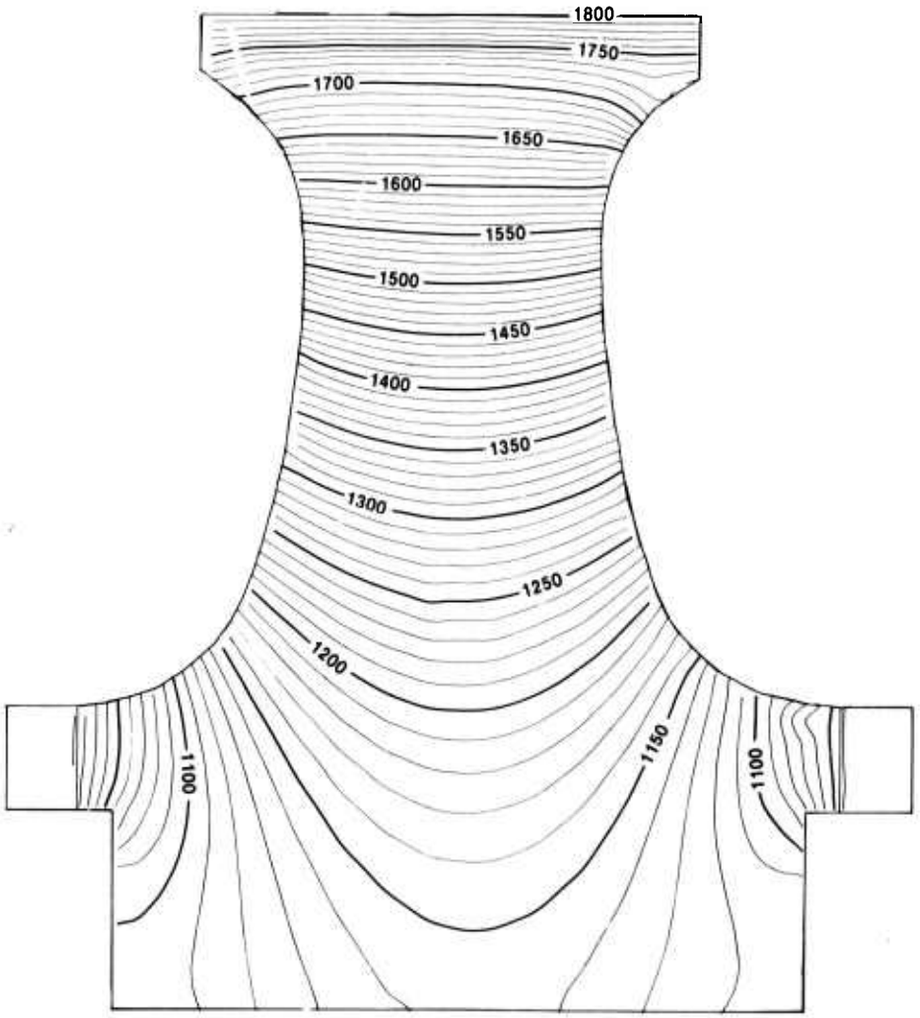

Figure 5.7 Temperatures (°F) of Recontoured 0.400 Inch Throat Disk in Hot Spin Rig at 1800°F Rim Temperature and 50,000 rpm. Cooling Air Along Both Forward and Aft Disk Surfaces

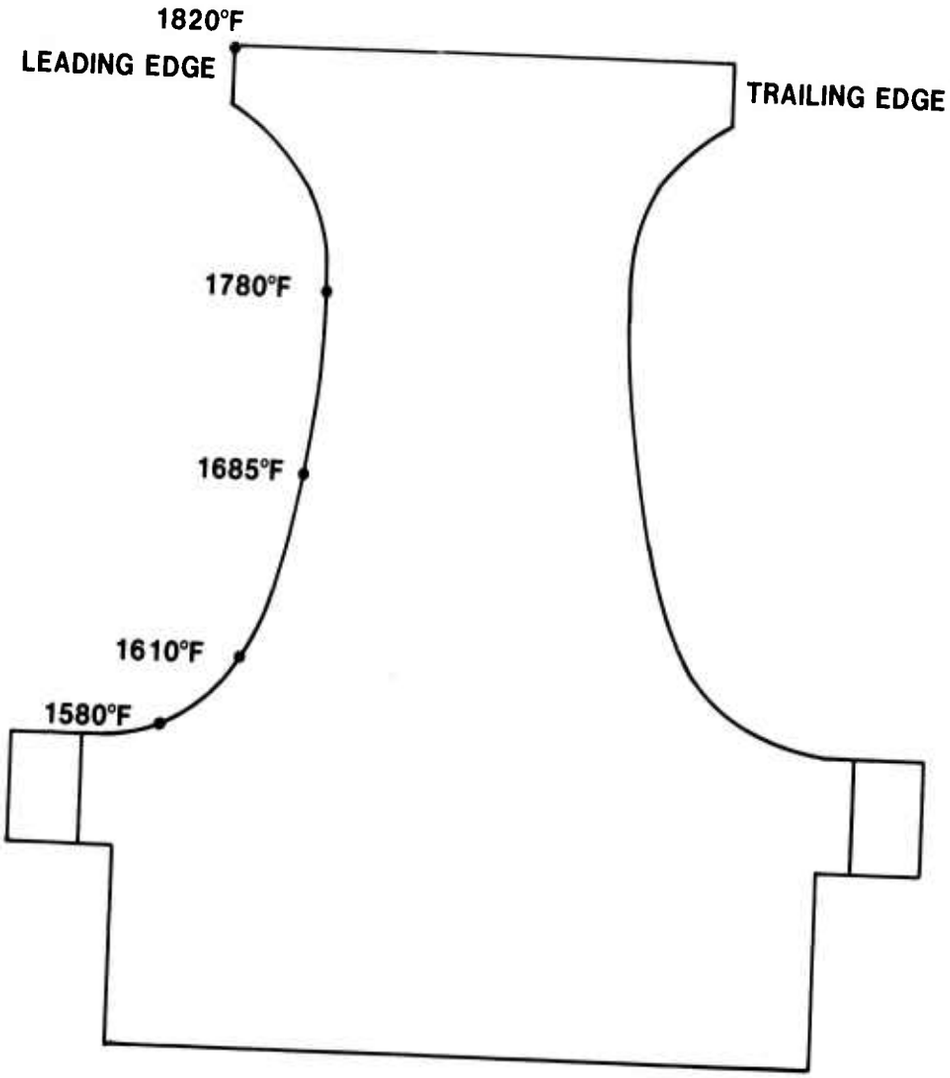

Figure 5.8 Measured Disk Temperatures (°F) on Hub 988 in Hot Spin Rig at 1800°F Rim Temperature at 50,000 rpm

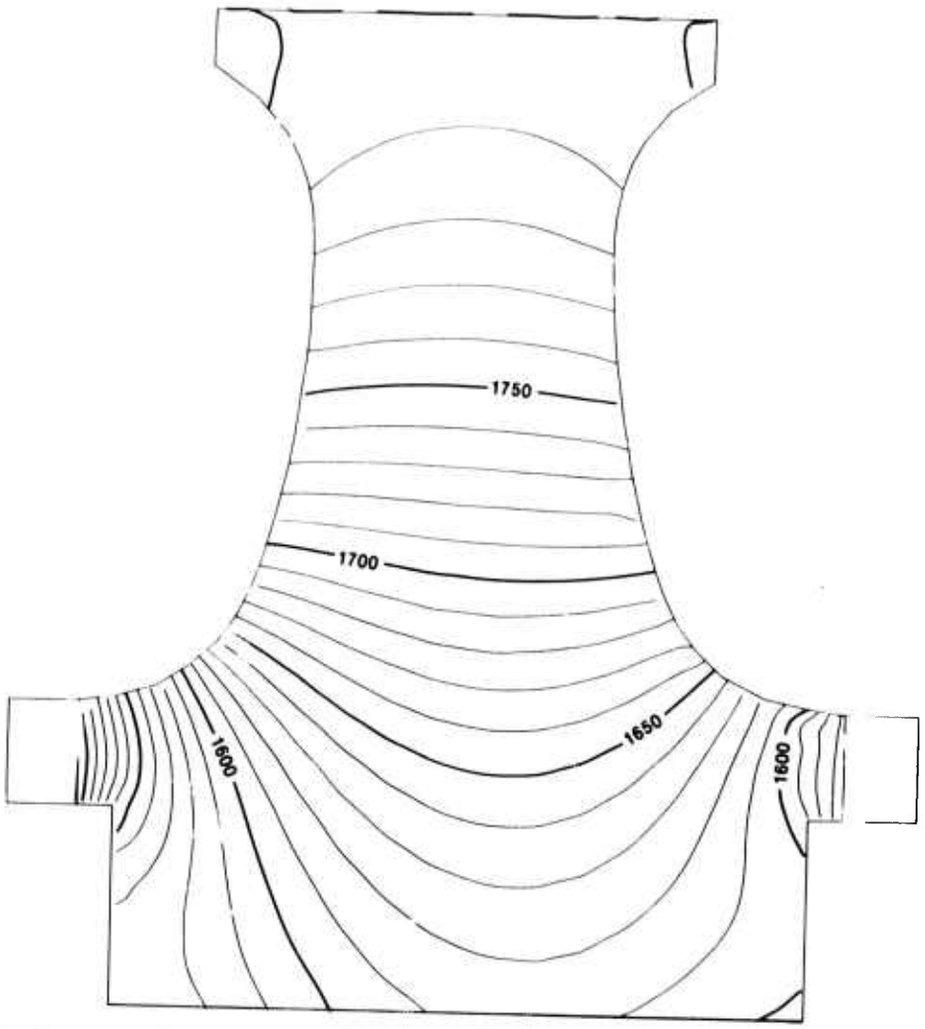

Figure 5.9 Temperatures (°F) of Recontoured 0.400 Inch Throat Disk in Hot Spin at 1800°F Rim Temperature and 50,000 rpm. Hot Recirculated Air on Both Forward and Aft Disk Surfaces

Using the two sets of disk temperatures and the material properties in Table 5.1, the maximum principle tensile stresses in the disks at 50,000 rpm (78% of Design D or 100% for a three stage design) were calculated and are shown in Figures 5.10 and 5.11 for the recontoured 0.400 inch profile and in Figures 5.12 and 5.13 for the 0.480 inch configuration. A comparison of these figures show that the bore stresses in the cooler running disks (higher thermal gradients) are approximately 10,000 psi greater than those in the hotter rotors.

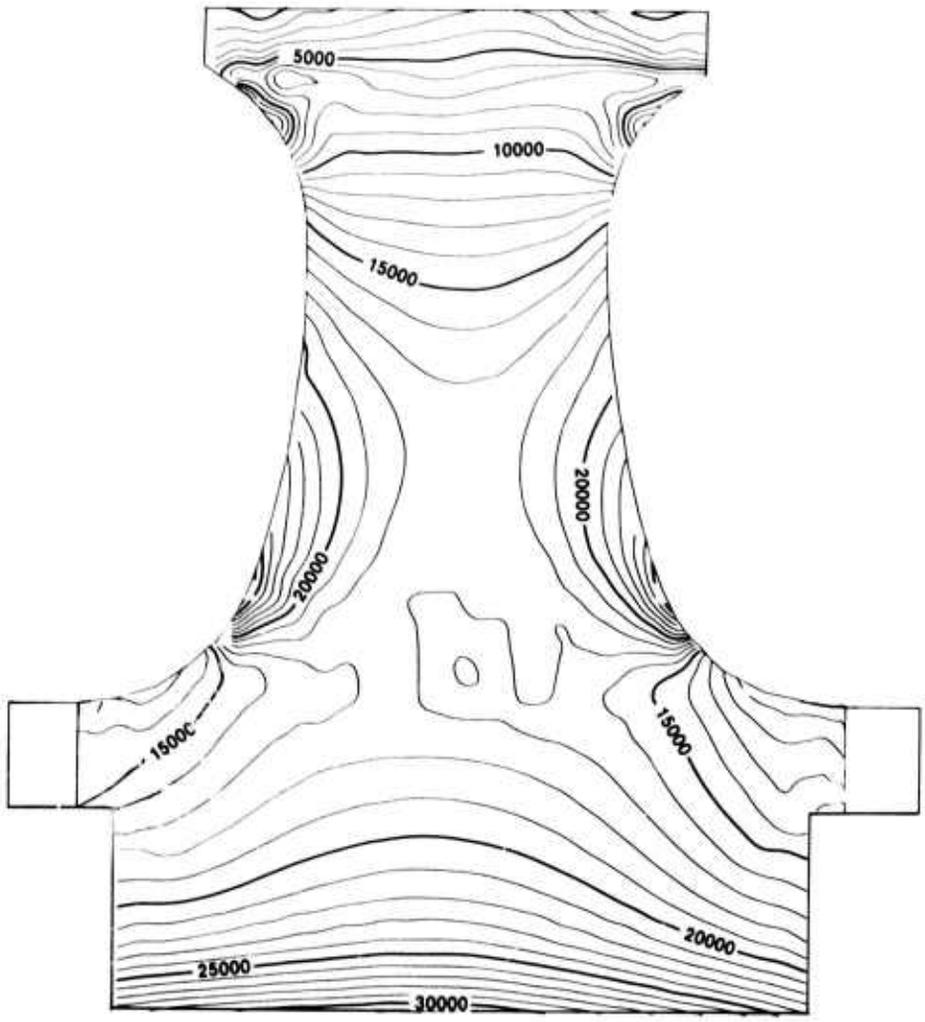

Figure 5.10 Maximum Principal Tensile Stresses (psi) for Recontoured 0.400 Inch Throat Disk in Hot Spin Rig at 1800°F Rim Temperature and 50,000 rpm. Cooling Air Along Both Forward and Aft Disk Surfaces

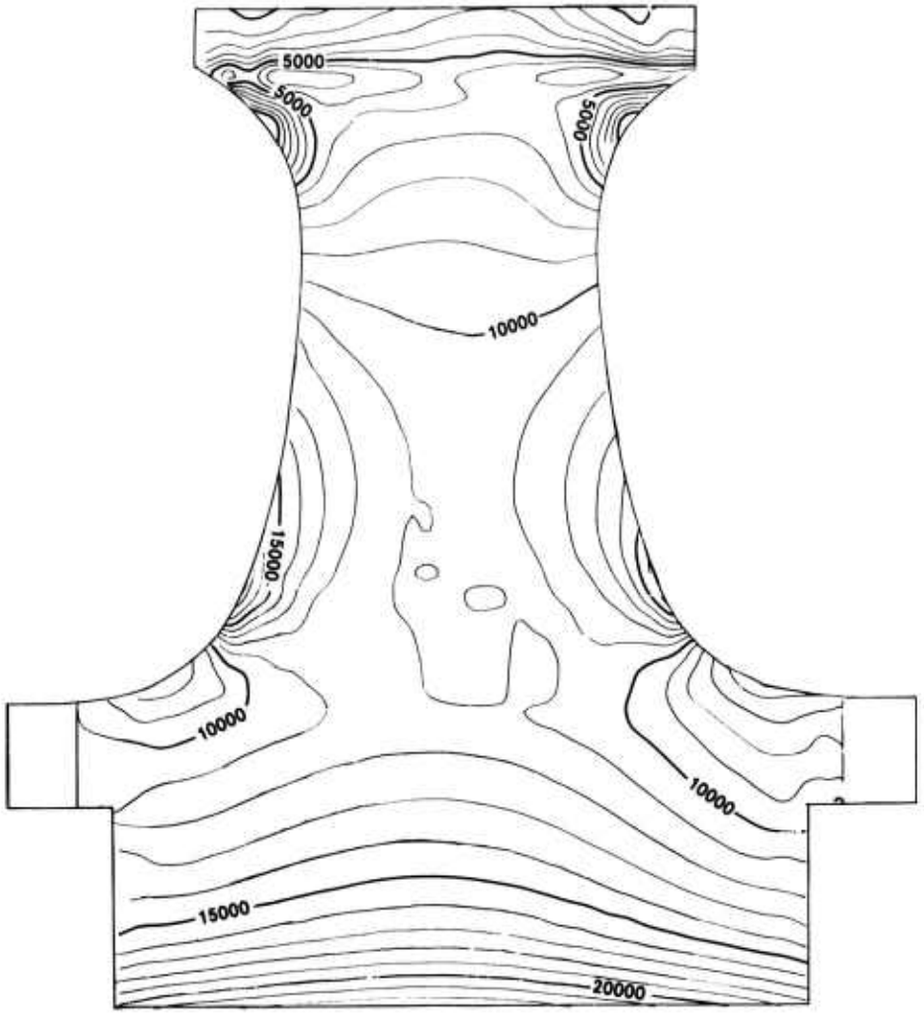

Figure 5.11 Maximum Principal Tensile Stresses (psi) for Recontoured 0.400 Inch Throat Disk in Hot Spin Rig at 1800°F Rim Temperature and 50,000 rpm. Hot Recirculated Air on Both Forward and Aft Disk Surfaces

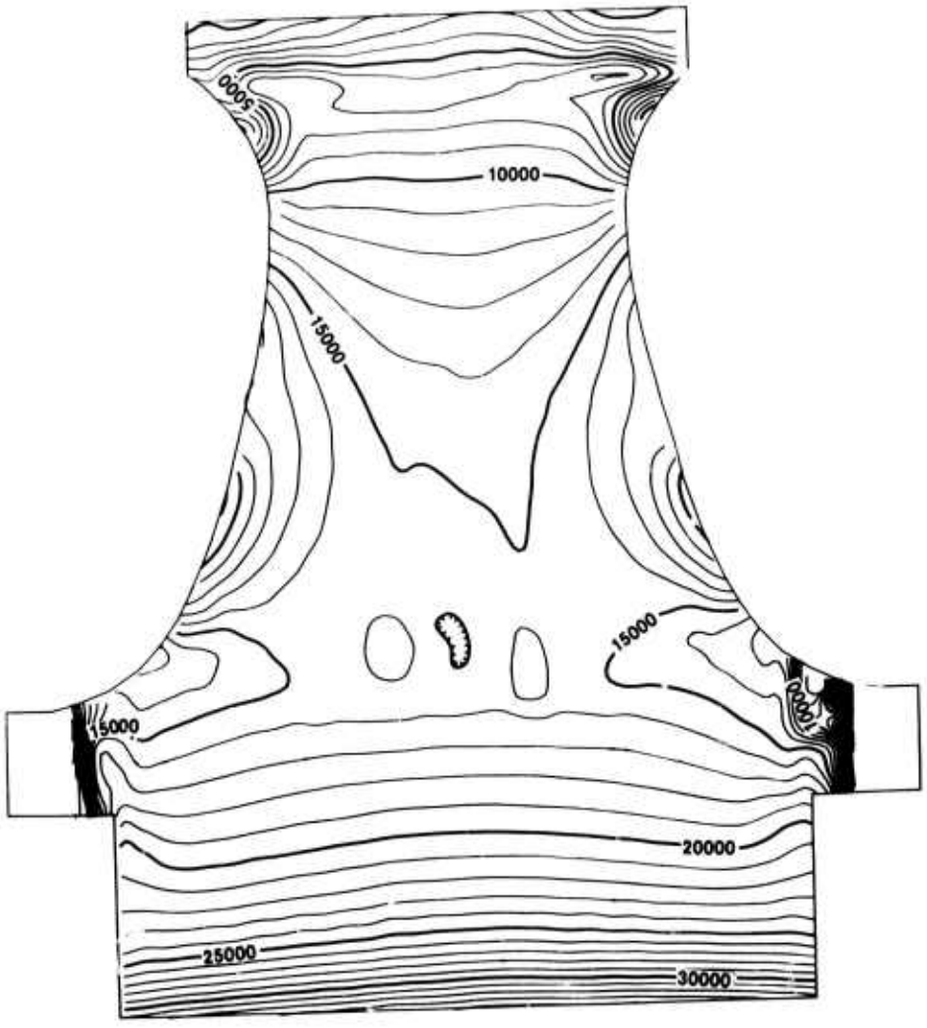

Figure 5.12 Maximum Principal Tensile Stresses (psi) for 0.480 Inch Throat Disk in Hot Spin Rig at 1800°F Rim Temperature and 50,000 rpm. Cooling Air Along Both Forward and Aft Disk Surfaces

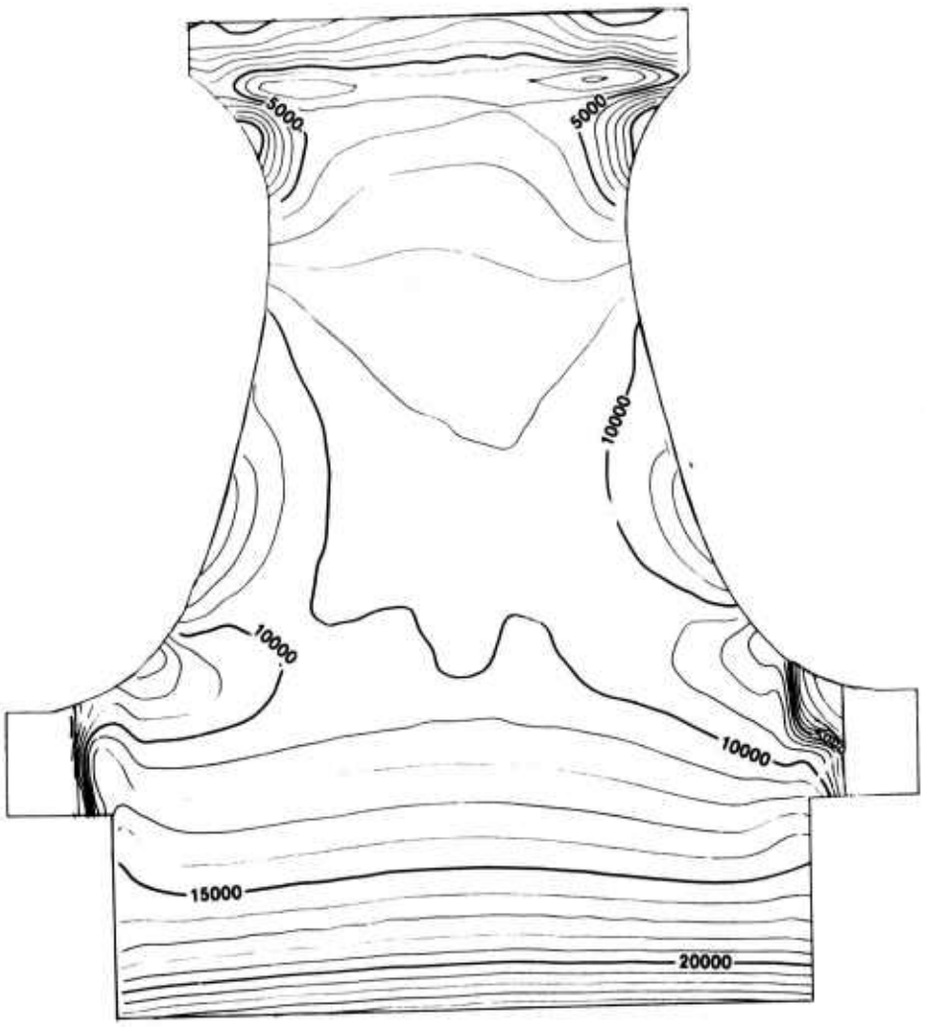

Figure 5.13 Maximum Principal Tensile Stresses (psi) for 0.480 Inch Throat Disk in Hot Spin Rig at 1800°F Rim Temperature and 50,000 rpm. Hot Recirculated Air on Both Forward and Aft Disk Surfaces

Using estimated Weibull parameters from Figure 6.9 of the last report[13], the fast fracture and the 25 hour time dependent reliability estimates of the rotors were calculated and are shown in Table 5.4. In these computations the blade reliability is assumed to be 1.0, based on the rotor being proof-tested up to maximum operating speed prior to hot testing. The steeper temperature gradient, shown in Figure 5.7, approximates closely in severity the loading conditions of the modified engine at 2200°F turbine inlet and 50,000 RPM. The temperature distribution in Figure 5.9, which approximates closer the temperature distribution observed in tests, is less severe as reflected in higher reliability estimates. Both temperature distributions show very little degration in the reliability with time as evident from fast fracture reliabilities. This is not unexpected as the operating temperatures are relatively low (1800°F and less) and therefore not as conducive to subcritical crack growth.

TABLE 5.4

Fast Fracture and 25 Hour Time Dependent Reliability Estimates for Rotors in the Hot Spin Rig with a Rim Temperature of 1800°F and 50,000 rpm (m = 7)

Throat Thickness (Inches)	Cooling Air		Hot Recirculated Air	
	Fast Fracture	25 Hour Time Dependent	Fast Fracture	25 Hour Time Dependent
Recontoured				
.400	.93263	.93078	.98961	.96970
.480	.92226	.92162	.98549	.95525

6.0 RECOMMENDATIONS

Work during this reporting period under the DOE-sponsored portion of the program and reported herein focused on development of ceramic materials and process technology used to fabricate duo-density silicon nitride turbine rotors. Hot press bonding process parameters were defined to eliminate microstructural and strength degradation of blade rings. Improvements were also made in the injection molding of rotor blade rings though more work is required to eliminate subsurface void-type blade flaws. It is recommended that a program be initiated to fabricate and test such improved all-ceramic turbine rotors to demonstrate the improvement.

Development of practical NDE techniques is also recommended to detect subsurface flaws of 100 microns or less in compiex shapes; this would be extremely useful to assess and confirm anticipated improvements in blade ring quality.

Recommendations would not be complete without the cali for continued programs on materials, processing and ceramic rotor testing. In particular, improved reaction bonded and hot pressed silicon nitride, along with a simplified process to fabricate highly-stressed ceramic turbine rotors, is required to produce large quantities of reliable parts at low cost. More ceramic rotor testing is required to validate or modify life prediction analyses and substantiate the reliability of ceramics in such a demanding high-temperature application.

While a methodology basis has been established, support should continue toward further development of this energy efficient turbine technology. An all-inclusive program is recommended, encompassing materials research, process research, ceramic design and testing under realistic conditions of environment, temperature and stress. Such an inter-disciplinary, all-inclusive approach is recommended to provide for cross fertilization of ideas and to facilitate emphasis on different aspects of the research program as required.

7.0 REFERENCES

1. McLean, A. F., Fisher, E. A., Harrison, D. E., "Brittle Materials Design, High Temperature Gas Turbine", AMMRC-CTR-72-3, Interim Report, March, 1972.

2. McLean, A. F., Fisher, E. A., Bratton, R. J., "Brittle Materials Design, High Temperature Gas Turbine", AMMRC-CTR-72-19, Interim Report, September, 1972.

3. McLean, A. F., Fisher, E. A., Bratton, R. J., "Brittle Materials Design, High Temperature Gas Turbine", AMMRC-CTR-73-9, Interim Report, March, 1973.

4. McLean, A. F., Fisher, E. A., Bratton, R. J., "Brittle Materials Design, High Temperature Gas Turbine", AMMRC-CTR-73-32, Interim Report, September, 1973.

5. McLean, A F. Fisher, E. A., Bratton, R. J., "Brittle Materials Design, High Temperature Gas Turbine", AMMRC-CTR-74-26, Interim Report, April, 1974.

6. McLean, A. F., Fisher, E. A., Bratton, R. J., "Brittle Materials Design, High Temperature Gas Turbine", AMMRC-CTR-74-59, Interim Report, September, 1974.

7. McLean, A. F., Fisher, E. A., Bratton, R. J., "Brittle Materials Design, High Temperature Gas Turbine", AMMRC-CTR-75-8, Interim Report, April, 1975.

8. McLean, A. F., Fisher, E. A., Bratton, R. J., Miller, D. G., "Brittle Materials Design, High Temperature Gas Turbine", AMMRC-CTR-75-28, Interim Report, September, 1975.
9. McLean, A. F., Baker, R. R., Bratton, R. J., Miller, D. G., "Brittle Materials Design, High Temperature Gas Turbine", AMMRC-CTR-76-12, Interim Report, April, 1976.

10. McLean, A. F., Baker, R. R., "Brittle Materials Design, High Temperature Gas Turbine", AMMRC-CTR-76-31, Interim Report, October, 1976.

11. McLean, A. F., Fisher, E. A., "Brittle Materials Design, High Temperature Gas Turbine", AMMRC-CTR-77-20, Interim Report, June, 1977.

12. McLean, A. F., Baker, R. R., "Brittle Materials Design, High Temperature Gas Turbine, Volume 1, Ceramic Component Fabrication and Demonstration", AMMRC-TR78-14, Interim Report, March, 1978.

13. McLean, A. F., Baker, R. R., "Brittle Materials Design, High Temperature Gas Turbine, Volume 2, Ceramic Turbine Rotor Technology", AMMRC-TR 78-14, Interim Report, March, 1978.
14. Baker, R. R., DeBell, G. C., Hartsock, D. L., "Processing Technology and Evaluation of Duo-Density Ceramic Turbine Rotors", DOE Highway Vehicle System Contractors' Coordination Meeting, Troy, Michigan, May 10, 1978.
15. Bowen, L. J., Carrathers, T. G., "Development of Mechanical Strength in Hot Pressed Silicon Nitride", Journal of Material Science, Volume 13, 1978.
16. Godfrey, D. J., Pitman, K. C., "Mechanical Properties of Silicon Nitride Ceramics", Ceramics for High Performance Applications-2, J. J. Burke et al. editors, Brook Hill Publishing Company.

17. Mencik, Z., Short, M. A., "Quantitative Phase Analysis of Synthetic Silicon Nitride by X-ray Diffraction: An Improved Procedure" Ford Scientific Staff Technical Report No. SR 72-98, 1972.

18. Spencer, R. S., Gilmore, G. D., "Equation of State for Polystyrene", Journal of Applied Physics, Volume 20, page 502, 1949.

Army Materials and Mechanics Research Center
Watertown, Massachusetts 02172

AD_____

BRITTLE MATERIALS DESIGN
HIGH TEMPERATURE GAS TURBINE

Arthur F. McLean, Robert R. Baker,
Ford Motor Company, Dearborn, Michigan 48121

Technical Report AMMRC TR-79-11, February, 1979
94 pages, 65 illus., 19 tables, 18 references
Contract DAAG 46-71 C-0162, ARPA Order Number
1849, Thirteenth Report, October 1, 1977 to March 31, 1978

Key Words
Gas Turbine Engine
Brittle Design
Ceramics
High Temperature Materials
Silicon Nitride
Silicon Carbide
Non-Destructive Tests
Mechanical Properties

ABSTRACT

This report contains progress during the last six months and a summary of earlier progress on the DOE supported programs within the joint DARPA/DOE "Brittle Materials Design, High Temperature Gas Turbine" Program and constitutes the final report of work under DOE funds. A separate report will cover the progress on the DARPA supported Ceramic Turbine Testing Program.

The summary of previous work supported by DOE includes progress on reaction bonded and hot pressed silicon nitride materials technology. Several NDE techniques were considered for the detection of flaws in complex-shaped silicon nitride components. Improvements to the hot press bonding process resulted in a significant improvement in the yield of flaw-free hot press bonded rotors. M.O.R. and cold spin tests of rotor blade rings revealed the presence of undetected subsurface flaws in both the blades and the rim. Blade bend testing indicated that blade strength degraded during hot press bonding.

During this reporting period, an investigation of hot press bonding temperatures and time at temperature defined a region of zero microstructural and strength degradation. This study involved 19 hot press bondings from which curves were generated defining the changes in color, porosity, hardness, phase and strength as a function of time and temperature.

Improvements in injection molding of rotor blade rings were made utilizing an adaptive process control unit which controlled and monitored the injection velocity and die cavity pressure during the injection and hold portions of the molding cycle. Five parametric studies were conducted with systematically varied injection profiles and hold pressures. Microfocus X-ray results indicated that high injection flow rates combined with low holding pressures in the die cavity reduced the number of subsurface void-type blade flaws.

The detection of planar flaws in both green as-molded and nitrided blade rings revealed that this type flaw was only detectable after nitriding, indicating that it may only occur after burn out and/or nitriding. Void-type flaws were detected in the rim of blade rings using a panoramic microfocus X-ray technique.

Approximately 30 experiments were conducted utilizing glass and/or metals as isostatic hot pressing media. A profoil seal system was developed which contained the molten pressurized glasses. Decomposition of the glass was minimized with vycor utilizing boron nitride as a barrier material. A sliding seal for molten metals employed a grafoil-glass hybrid system; however, the metals were extruded through the porosity of the graphite.

A reliability analysis was conducted for individual loading conditions and the cumulative reliability estimated for Rotor #1195 which was previously engine tested. The cumulative time-dependent reliability for the 38.5 hour run was 0.838. Reliability estimates were also made for 0.40 and 0.48 inch thick throat rotors operating in the hot spin rig at a rim temperature of 1800°F at 50,000 rpm.

An assessment of where the technologies addressed in this report now stand and recommendations for follow on work are presented.

Army Materials and Mechanics Research Center
Watertown, Massachusetts 02172

AD_____

BRITTLE MATERIALS DESIGN
HIGH TEMPERATURE GAS TURBINE

Arthur F. McLean, Robert R. Baker,
Ford Motor Company, Dearborn, Michigan 48121

Technical Report AMMRC TR-79-11, February, 1979
94 pages, 65 illus., 19 tables, 18 references
Contract DAAG 46-71 C-0162, ARPA Order Number
1849, Thirteenth Report, October 1, 1977 to March 31, 1978

Key Words
Gas Turbine Engine
Brittle Design
Ceramics
High Temperature Materials
Silicon Nitride
Silicon Carbide
Non-Destructive Tests
Mechanical Properties

ABSTRACT

This report contains progress during the last six months and a summary of earlier progress on the DOE supported programs within the joint DARPA/DOE "Brittle Materials Design, High Temperature Gas Turbine" Program and constitutes the final report of work under DOE funds. A separate report will cover the progress on the DARPA supported Ceramic Turbine Testing Program.

The summary of previous work supported by DOE includes progress on reaction bonded and hot pressed silicon nitride materials technology. Several NDE techniques were considered for the detection of flaws in complex-shaped silicon nitride components. Improvements to the hot press bonding process resulted in a significant improvement in the yield of flaw-free hot press bonded rotors. M.O.R. and cold spin tests of rotor blade rings revealed the presence of undetected subsurface flaws in both the blades and the rim. Blade bend testing indicated that blade strength degraded during hot press bonding.

During this reporting period, an investigation of hot press bonding temperatures and time at temperature defined a region of zero microstructural and strength degradation. This study involved 19 hot press bondings from which curves were generated defining the changes in color, porosity, hardness, phase and strength as a function of time and temperature.

Improvements in injection molding of rotor blade rings were made utilizing an adaptive process control unit which controlled and monitored the injection velocity and die cavity pressure during the injection and hold portions of the molding cycle. Five parametric studies were conducted with systematically varied injection profiles and hold pressures. Microfocus X-ray results indicated that high injection flow rates combined with low holding pressures in the die cavity reduced the number of subsurface void-type blade flaws.

The detection of planar flaws in both green as-molded and nitrided blade rings revealed that this type flaw was only detectable after nitriding, indicating that it may only occur after burn out and/or nitriding. Void-type flaws were detected in the rim of blade rings using a panoramic microfocus X-ray technique.

Approximately 30 experiments were conducted utilizing glass and/or metals as isostatic hot pressing media. A profoil seal system was developed which contained the molten pressurized glasses. Decomposition of the glass was minimized with vycor utilizing boron nitride as a barrier material. A sliding seal for molten metals employed a grafoil-glass hybrid system; however, the metals were extruded through the porosity of the graphite.

A reliability analysis was conducted for individual loading conditions and the cumulative reliability estimated for Rotor #1195 which was previously engine tested. The cumulative time-dependent reliability for the 38.5 hour run was 0.838. Reliability estimates were also made for 0.40 and 0.48 inch thick throat rotors operating in the hot spin rig at a rim temperature of 1800°F at 50,000 rpm.

An assessment of where the technologies addressed in this report now stand and recommendations for follow on work are presented.

Army Materials and Mechanics Research Center
Watertown, Massachusetts 02172

AD_____

BRITTLE MATERIALS DESIGN
HIGH TEMPERATURE GAS TURBINE

Arthur F. McLean, Robert R. Baker
Ford Motor Company, Dearborn, Michigan 48121

Technical Report AMMRC TR-79 11, February 1979
94 pages, 65 illus., 19 tables, 16 references
Contract DAAG 46-71 C-0162, ARPA Order Number
1849, Thirteenth Report, October 1, 1977 to March 31, 1978

Key Words
Gas Turbine Engine
Brittle Design
Ceramics
High Temperature Materials
Silicon Nitride
Silicon Carbide
Non-Destructive Tests
Mechanical Properties

ABSTRACT

This report contains progress during the last six months and a summary of earlier progress on the DOE supported programs within the joint DARPA/DOE "Brittle Materials Design, High Temperature Gas Turbine" Program and constitutes the final report of work under DOE funds. A separate report will cover the progress on the DARPA supported Ceramic Turbine Testing Program.

The summary of previous work supported by DOE includes progress on reaction bonded and hot pressed silicon nitride materials technology. Several NDE techniques were considered for the detection of flaws in complex shaped silicon nitride components. Improvements in the hot press bonding process resulted in a significant improvement in the yield of flaw-free hot press bonded rotors. M.O.R. and cold spin tests of rotor blade rings revealed the presence of undetected subsurface flaws in both the blades and the rim. Blade bend testing indicated that blade strength degraded during hot press bonding.

During the reporting period, an investigation of hot press bonding temperatures and time at temperature defined a region of zero microstructural and strength degradation. This study involved 19 hot press bondings from which curves were generated defining the changes in color, porosity, hardness, phase and strength as a function of time and temperature.

Improvements in injection molding of rotor blade rings were made utilizing an adaptive process control unit which controlled and monitored the injection velocity and die cavity pressure during the injection and hold portions of the molding cycle. Five parametric studies were conducted with systematically varied injection profiles and hold pressures. Microfocus X-ray results indicated that high injection flow rates combined with low holding pressures in the die cavity reduced the number of subsurface void-type blade flaws.

The detection of planer flaws in both green as-molded and nitrided blade rings revealed that this type flaw was only detectable after nitriding, indicating that it may only occur after burn out and/or nitriding. Void-type flaws were detected in the rim of blade rings using a panoramic microfocus X-ray technique.

Approximately 30 experiments were conducted utilizing glass and/or metals as isostatic hot pressing media. A grafoil seal system was developed which contained the molten pressurized glasses. Decomposition of the glass was minimized with vycor utilizing boron nitride as a barrier material. A sliding seal for molten metals employed a grafoil-glass hybrid system, however, the metals were extruded through the porosity of the graphite.

A reliability analysis was conducted for individual loading conditions and the cumulative reliability estimated for Rotor #1195 which was previously engine tested. The cumulative time-dependent reliability for the 36.5 hour run was 0.838. Reliability estimates were also made for 0.40 and 0.48 inch thick throat rotors operating in the hot spin rig at a rim temperature of 1800°F at 50,000 rpm.

An assessment of where the technologies addressed in this report now stand and recommendations for follow on work are presented.

Army Materials and Mechanics Research Center
Watertown, Massachusetts 02172

AD_____

BRITTLE MATERIALS DESIGN
HIGH TEMPERATURE GAS TURBINE

Arthur F. McLean, Robert R. Baker
Ford Motor Company, Dearborn, Michigan 48121

Technical Report AMMRC TR-79 11, February 1979
94 pages, 65 illus., 19 tables, 16 references
Contract DAAG 46-71 C-0162, ARPA Order Number
1849, Thirteenth Report, October 1, 1977 to March 31, 1978

Key Words
Gas Turbine Engine
Brittle Design
Ceramics
High Temperature Materials
Silicon Nitride
Silicon Carbide
Non-Destructive Tests
Mechanical Properties

ABSTRACT

This report contains progress during the last six months and a summary of earlier progress on the DOE supported programs within the joint DARPA/DOE "Brittle Materials Design, High Temperature Gas Turbine" Program and constitutes the final report of work under DOE funds. A separate report will cover the progress on the DARPA supported Ceramic Turbine Testing Program.

The summary of previous work supported by DOE includes progress on reaction bonded and hot pressed silicon nitride materials technology. Several NDE techniques were considered for the detection of flaws in complex shaped silicon nitride components. Improvements in the hot press bonding process resulted in a significant improvement in the yield of flaw-free hot press bonded rotors. M.O.R. and cold spin tests of rotor blade rings revealed the presence of undetected subsurface flaws in both the blades and the rim. Blade bend testing indicated that blade strength degraded during hot press bonding.

During this reporting period, an investigation of hot press bonding temperatures and time at temperature defined a region of zero microstructural and strength degradation. This study involved 19 hot press bondings from which curves were generated defining the changes in color, porosity, hardness, phase and strength as a function of time and temperature.

Improvements in injection molding of rotor blade rings were made utilizing an adaptive process control unit which controlled and monitored the injection velocity and die cavity pressure during the injection and hold portions of the molding cycle. Five parametric studies were conducted with systematically varied injection profiles and hold pressures. Microfocus X-ray results indicated that high injection flow rates combined with low holding pressures in the die cavity reduced the number of subsurface void-type blade flaws.

The detection of planer flaws in both green as-molded and nitrided blade rings revealed that this type flaw was only detectable after nitriding, indicating that it may only occur after burn out and/or nitriding. Void-type flaws were detected in the rim of blade rings using a panoramic microfocus X-ray technique.

Approximately 30 experiments were conducted utilizing glass and/or metals as isostatic hot pressing media. A grafoil seal system was developed which contained the molten pressurized glasses. Decomposition of the glass was minimized with vycor utilizing boron nitride as a barrier material. A sliding seal for molten metals employed a grafoil-glass hybrid system, however, the metals were extruded through the porosity of the graphite.

A reliability analysis was conducted for individual loading conditions and the cumulative reliability estimated for Rotor #1195 which was previously engine tested. The cumulative time-dependent reliability for the 36.5 hour run was 0.838. Reliability estimates were also made for 0.40 and 0.48 inch thick throat rotors operating in the hot spin rig at a rim temperature of 1800°F at 50,000 rpm.

An assessment of where the technologies addressed in this report now stand and recommendations for follow on work are presented.